Modeling level alignment at interfaces in molecular junctions

Celis Gil, Jose

DOI
10.4233/uuid:792fc17c-d68f-480a-b797-e7750879f4a2

Publication date
2017

Document Version
Final published version

Citation (APA)
Celis Gil, J. (2017). *Modeling level alignment at interfaces in molecular junctions*. [Dissertation (TU Delft), Delft University of Technology]. https://doi.org/10.4233/uuid:792fc17c-d68f-480a-b797-e7750879f4a2

MODELING LEVEL ALIGNMENT AT INTERFACES IN MOLECULAR JUNCTIONS

MODELING LEVEL ALIGNMENT AT INTERFACES IN MOLECULAR JUNCTIONS

Proefschrift

ter verkrijging van de graad van doctor
aan de Technische Universiteit Delft,
op gezag van de Rector Magnificus prof. ir. K.C.A.M. Luyben,
voorzitter van het College voor Promoties,
in het openbaar te verdedigen op donderdag 2 november 2017 om 15:00 uur

door

Jose Arturo CELIS GIL

Master of Science in Physics
van Universidad Nacional de Colombia, Bogotá, Colombia,
geboren te Bogotá, Colombia.

Dit proefschrift is goedgekeurd door de

promotor: prof. dr. ir. H. S. J. van der Zant
copromotor: dr. J. M. Thijssen

Samenstelling promotiecommissie:

Rector Magnificus,	voorzitter
Prof. dr. ir. H. S. J. van der Zant,	Technische Universiteit Delft (promotor)
Dr. J. M. Thijssen,	Technische Universiteit Delft (copromotor)
Onafhankelijke leden:	
Prof. dr. F. Evers,	Universität Regensburg
Prof. dr. S.J. Picken,	Technische Universiteit Delft
Prof. dr. Yaroslav Blanter,	Technische Universiteit Delft
Dr. S. J. van der Molen,	Universiteit Leiden
Dr. P. H. T. Philipsen,	Vrije Universiteit Amsterdam

Keywords: Molecular Electronics, Single-Molecule Junction, Green's Function, DFT, level alignment.

Printed by: Gildeprint - Enschede

Front & Back: Cover art designed by J.A. Celis Gil showing the miniaturization tendency of electronic devices.

Casimir PhD series, Delft-Leiden 2017-38

ISBN 978-90-8593-322-9

An electronic version of this dissertation is available at
http://repository.tudelft.nl/.

To my beloved saurios.

Thanks for being with me all these years.

CONTENTS

SUMMARY

Molecular devices are planned as alternative solutions for heat dissipation problems and reliable fabrication of nano-scale devices. However, it also opens up possibilities of combining many other degrees of freedom into functional device design. While they introduce interesting opportunities for study, they also demand a versatile, scalable toolset. In this thesis we calculate the electronic transport through molecular devices using the DFT+NEGF technique. We model the interaction of the molecule with the electrodes surfaces taking into account different facts such as the gap reduction produced by the charge polarization on metallic surfaces, the spin states of the molecule and the hydrophilicity of the leads. We hope our contribution helps to improve the functional single molecule devices design.

In the first chapter we briefly introduces molecular electronic devices from experimental and theoretical points of view. Then, in chapter 2 we describe the well known Hartree Fock and Density Functional Theory methods to introduce the DFT+NEGF (non-equilibrium Green's function) technique a method which is extensively used for the molecular junctions calculations. We then, introduce some simple models to describe molecular junctions.

We calculate the HOMO-LUMO gap reduction of a molecule in between two metallic leads. In chapter 3 we propose a classical model to explain this reduction and we contrast our results with experimental measurements. Similarly, in chapter 4 we present a method for predicting one-particle energies for a molecule in a junction using fully ab-initio calculations. With these methods it is possible to correct the molecular orbitals energies and calculate the corrected transmission through the junction. As a result we obtain better agreement between calculations and experiments for the low bias conductance.

The chapter 5 is an outlook for the DFT+NEGF calculations. Here we propose to use hybrid functionals to improve the agreement between transport calculations and measurements. For our calculations we use molecules of the OPE family which are molecules that have been widely studied and we show an improvement in the zero bias conductance.

In chapters 6 and 7 we model two interesting systems that provide the ability to create molecular switches and rectifiers. In Chapter 6 we investigate transport via a mechanically activated single molecule switch. This molecule has two stable configurations, one with total spin equal to zero and the other with total spin +2. Our calculations indicate that the spin transition can be triggered by stretching the molecule and a larger conductance is found for the high-spin state. In Chapter 7 we investigate electronic transport through a molecular device that combines rectification with switchability. Water molecules play an important role in this system as they are the main responsible for changes in the molecular orbitals moving the system from resonance to out of resonance.

SAMENVATTING

Moleculaire elektronica biedt perspectief als alternatieve oplossing voor warmtedissipatieproblemen en maakt betrouwbare fabricage van nano-schaalapparaten mogelijk. Daarnaast kunnen veel vrijheidsgraden gecombineerd worden met functioneel apparaatontwerp. Dit gebied opent interessante paden voor onderzoek, maar vraagt ook om een veelzijdige, schaalbare gereedschapsset. In dit proefschrift berekenen we het elektronisch transport door moleculaire apparaten met behulp van de DFT + NEGF techniek. Wij modelleren de interactie van het molecuul met de elektrodenoppervlakken, waarbij rekening wordt gehouden met verschillende effecten, zoals de kloofvermindering die wordt geproduceerd door de ladingpolarisatie op metaaloppervlakken, de spinstanden van het molecuul en de hydrofiliciteit van de leidingen. Wij hopen dat onze bijdrage helpt bij het verbeteren van het functionele design van 'single molecule devices'.

In het eerste hoofdstuk introduceren we moleculaire elektronische apparaten vanuit experimentele en theoretische standpunten. Vervolgens beschrijven we de bekende Hartree Fock en Density Functional Theory methoden om de DFT + NEGF (non-equilibrium Green's functie) techniek te introduceren, een methode die extensief gebruikt wordt voor de moleculaire apparaten. In hoofdstuk 2 introduceren we enkele eenvoudige modellen om moleculaire verbinding te beschrijven.

We berekenen de HOMO-LUMO kloofvermindering van een molecuul tussen twee metallische elektroden. In hoofdstuk 3 stellen we een klassiek model voor om deze reductie uit te leggen en vergelijken we onze resultaten met experimentele metingen. Evenzo presenteren we in hoofdstuk 4 een methode voor het voorspellen van deeltjesenergieën voor een molecuul in een verbinding met behulp van volledig ab initio berekeningen. Met deze methoden kunnen we de moleculaire orbitale energie corrigeren en de gecorrigeerde transmissie via het apparaat berekenen. Als gevolg hiervan krijgen we betere overeenstemming tussen berekeningen en experimenten voor lage biasconductie.

Het hoofdstuk 5 is een vooruitzicht voor de DFT + NEGF berekeningen. Hier stellen we voor om hybride functionaliteit te gebruiken om de overeenkomst tussen transportberekeningen en metingen te verbeteren. Voor onze berekeningen gebruiken we de OPE moleculen, die veelal zijn onderzocht en we tonen een verbetering in de nulbiasconductie.

In hoofdstukken 6 en 7 modelleren we twee interessante systemen die de mogelijkheid bieden om moleculaire schakelaars en gelijkrichters te creëren. In hoofdstuk 6 onderzoeken we transport via een mechanisch geactiveerde single molecule switch. Dit molecuul heeft twee stabiele configuraties, één met totale spin gelijk aan nul en de andere met totale spin +2. Onze berekeningen wijzen erop dat de spinovergang geactiveerd kan worden door het molecuul te strengen en er wordt een grotere geleidbaarheid gevonden voor de high-spin toestand. In hoofdstuk 7 onderzoeken we elektronisch transport door middel van een molecuul apparaat dat rectificatie combineert met switchabi-

lity. Watermoleculen spelen een belangrijke rol in dit systeem, omdat ze de belangrijkste verantwoordelijk zijn voor veranderingen in de moleculaire orbitalen die het systeem verplaatsen van resonantie tot uit resonantie.

PREFACE

Since the beginning I knew that to do a Phd would be difficult and now that i am finishing mine I can say that it really was. Sometimes I was sad, sometimes happy, sometimes I was relaxed and sometimes stressed. To do a Phd was not a fairly tale, it was pushing, trying, failing, struggling, dealing and fighting to show others that my ideas were valuable, but I have to say "I enjoyed this experience". It was like a roll playing game (RPG), I learned new abilities, I got new tools and I met new friends and altogether helped me to achieve the goals.

In this short preface, I would like to share the story of some of my ideas during the PhD. These projects will be described in more detail along this thesis, but now I want to summarize the story behind them.

A few moths after I started, I listened one suggestion –let us surround a cluster of gold atoms with a perfect dielectric surface, that would make the system believe that the cluster is infinite–, given the fact that electrostatically a perfect conductor has an infinite dipole moment, the idea was brilliant. I performed DFT calculations and I made some changes to the source code, after many tries I finally managed to surround the atoms with a dielectric, unfortunately the gold atoms do not feel the dielectric, maybe due to restrictions in the potentials in DFT. Probably, it would sound sad if I say that I lost the first battle, but despite the loss I learned a new ability, I fought against a huge Fortran code and I survived. *"At first I was afraid, I was petrified, Kept thinking I could not go out without checking a huge Fortran code, but I have survived."*.

After this point, I continued with the project started by the former PhD., Chris Verzijl, in his work he analyzed the image-charge effect on a molecular junction. I worked together with Chris on his project, when we submitted the paper *"I saw trees of green, red roses too, I saw them bloom for me and you, And I though to myself, what a wonderful world"*. When apparently everything was going well, one of the referees touched a sensitive point, something that we could not answer with the procedures that we were doing. Neither Jos, Chris or me knew the answer, then one idea appeared, I made some calculations and I obtained the spin resolved occupation of the molecule in the junction. Honestly, I did not know how this could help us, but fortunately Jos did. We answered the referee and submitted the paper and this time it was accepted. Despite the fact that I did not understand what I was doing, that was the fist paper. After it was published, I finally understood the procedure and I got a new idea, a project that took me two years to finish it, later I will come back to this.

Every Monday at 13:00, I attended to the MED meeting. One day one pos-doc, Julien Dugay, gave a presentation about transport properties on spin cross-over nanoparticles, at that point I though that it would be nice to compare his results with numeric calculations. The size of the nanoparticles which is close to 10 nm would be a problem, if I was lucky and DFT converged, they would take a lot of time. Running calculations, I noticed that I was intended to study systems with two spin states and transport cal-

culations in the ADF/BAND version that I was using did not resolved these kind of systems. After some weeks of reading the source code, I created some functions to perform spin resolved transport calculations. Although I had tested the functions before, with the nanoparticles I struggled with long calculations and non-converging processes, giving me no clue about the accuracy of my functions. Some months later, I listened that Riccardo Frisenda (a brilliant experimental physicist) was doing conductance measurements on spin cross-over molecules using mechanically controlled break junctions (that was the perfect system to test the spin resolved implementation). A few calculations were enough to see how my results fit so well with his measurements. From this work together with Riccardo we got a nice publication, this was the second step on my ladder to the Phd.

Now, let me return to the idea that I got after the paper with Chris was published. In that paper, we were using classical mechanics to calculate the energy levels shift, one question was in my mind, Can I do it using ab-initio calculations only?. The answer was yes, but this project was done before by other authors. The amount of literature and the fact that similar ideas were proposed before guided me to do something new. I tested the method with different electrodes materials and different molecules, in both cases I got good results, but the real contribution came with the full self consistent scissors-operator, a correction that improves significantly the agreement between calculations and measurements. At this point, I want to make a small break, because I am very proud of this paper, I do not know if it is because of the effort or the time that I invested, but I feel this paper like one of the biggest goals that I have achieved.

There are two more projects to mention. The first one, done in collaboration with colleagues in Leiden, was the humidity dependence of transport properties through Ru complexes, this project tries to explain the drastic change in the electric current through molecular junctions induced by presence of water molecules. This is probably one of the projects with more potential were I have participated. Bhadra and Huseyin: after three years of obstacles our results were accepted in a high impact journal. The second project, in collaboration with my colleague Jobbe in Delft, was about using hybrid functionals for transport properties calculations using DFT-NEGF. Definitely we should write a paper about this.

Finally there is still one last project that I would like to talk, but unfortunately I could not work more on it. It was single molecular junctions immersed in water. While everything in theory and calculations guide me to predict one behavior, experiments showed the opposite one. Thanks to this project I learned new computational techniques as REAX-FF and QMMM, and I think I was in the right track to find possible explanations to the phenomenon, but due to the amount of calculations required to support it I could not finish it. I want to make a parenthesis here because I developed this project when I was working with Huseyin, and actually I got good ideas working in parallel for both projects. I proudly pass the flag to the next generation, Nikolas and Davide, for sure you will get nice results.

So that is it, the story behind the results, what do you think?.

Jose Arturo Celis Gil
Delft, October 2017

1

INTRODUCTION

In this chapter we introduce the field of molecular electronics, and link it to the discipline of quantum transport. We also introduce the molecular level alignment concept show its importance for the design of molecular electronic devices.

1

1.1. MOLECULAR ELECTRONICS

In the recent years, the fast developments in the field of semiconductor technology have proved that the efforts to miniaturize transistors will reach physical limits [1]. Thermal dissipation and a lack of reliability in fabrication are the main problems that appear in the miniaturization trend. Following this route, at some point in this race, electrical circuits will include active elements based on molecules, which are the smallest entities occurring in nature that can perform a specific function. Whereas in semiconductors the main functionality comes from their crystal structure and tuning the concentration of dopants, in molecules the functionality can be based on the structure of a single molecule, which is often only a few nanometers long. This therefore makes single-molecule electronics a promising route in creating even smaller electronic devices than the ones that are used currently.

In molecular electronic devices, it is possible to experiment with resonant vs. off-resonant transport [2–4], mechanical and electrical switching [5–7], spin as an information carrier [8–11], molecular magnetism [12], absorption and emission of light [13] and interplay between all of the above. Together with the wide range in functionality, molecules offer possibilities like lower cost, compatibility with flexible substrates and simpler packaging when compared to conventional electronics. Despite the advantages, it also introduce new complications, specially from the point of view of fabrication, given that until now it is not really clear whether individual molecular devices can be integrated into larger-scale computing circuits.

A fundamental understanding of molecular devices, based on quantum mechanics is vital to increase the advantages and reduce the disadvantages. It is our hope that a better understanding of the origins of molecular-device functionality and the role of the metal-molecule interface will contribute to the solution of problems in the (near) future.

1.2. MOLECULAR DEVICES

The idea of molecular devices was initially proposed by Aviram and Ratner in 1974 [14]. In the next decades molecular electronics measurements were done using thin molecular films [5]. The first single-molecule junction was measured in 1997 [15]; since that many different molecules have been measured on the single molecule scale with a wide variety of techniques.

The scanning tunneling microscope break junction (STM) is a technique where the height of a metallic tip above a surface can be controlled. The tip is moved into the surface and then slowly retracted until a gap is formed which can be bridged by a single molecule. This setup is very sensitive, versatile and has the advantage that it can, at low temperature, image the surface beforehand to identify molecules. A drawback is that the sensitivity results in limited stability in junction formation at room temperature.

Another method is the mechanically controlled break junction technique (MCBJ). A wire is on top of a substrate that can bend. The bending results in a stretching of the top surface of the substrate. If a suspended wire is placed on top of this surface it can be broken and form a nano-gap. The advantage of the MCBJ technique is that it is more stable than the STM technique. It is also possible to include a gate electrode[10] to investigate transport as a function of Fermi energy.

Similarly to the MCBJ, the electromigrated break junction technique form a nanogap in a wire, but instead of pulling a wire apart, the metallic wire is electromigrated by applying a voltage over the wire [16]. When the momentum transfer from the conduction electrons to an atom is large enough, the atom will move, if enough atoms are moved, a gap may form and continuing this process results in breakage of the wire.

1.3. QUANTUM TRANSPORT

A practical starting point to discuss the transport through nano-structures is the Landauer scattering approach. This approach is a non-interacting particle approach and can be used to describe a single site connected to electrodes [17–19], resulting in basic features in transport which are also observed in transport through single molecules.

In the Landauer scattering approach all the complex interactions in the electrodes are captured in two quantities of interest, a generally bias dependent transmission $T(E,V)$ and the steady state current $I(V)$.

We can treat electrons in the electrodes as coherent waves that have an energy dependent probability to be transmitted though the molecule to the other electrode. If he electron-electron interaction is weak (which in nano-structures of the scale of the Fermi-wavelength is often the case), the current is given by the Landauer formula:

$$I(V) = \frac{2e}{h}\int_{-\infty}^{\infty} dE\left[f_L(E) - f_R(E)\right]T(E,V), \tag{1.1}$$

with e the charge of an electron, h the Planck's constant and $f_{L,R}$ the Fermi distribution function of electrodes. $\frac{2e^2}{h}$ is the conductance quantum.

Using this approach, determining the current through a molecule connected to metallic electrodes is reduced to calculating the transmission through the molecule. To calculate the transmission through a molecule we use the non-equilibrium Green's functions approach described in the next chapter.

1.4. LEVEL ALIGNMENT

A molecule in gas has well defined orbitals, called molecular orbitals (MOs), at discrete energies. The density of states of the molecule can be seen as a series of narrow peaks separated in energy. When the molecule starts to approach a metal surface, the first interactions that play a role are due to long-range forces. The energy of the MOs is renormalized and the energy gap between the highest occupied molecular orbital (HOMO) and the lowest unoccupied molecular orbital (LUMO) decreases as the interaction between molecule and metal increases (when the molecule gets closer to the surface).

The increased screening from the electrons in the metal is the main reason for the reduction of the HOMO-LUMO gap. When the molecule is close enough to the surface, the wave-function of the metal overlaps with the molecule wave-function and chemical bonds between molecule and metal can be formed. An important consequence of the hybridization of the wave-functions is the substantial broadening introduced in the MOs density of states.

1.5. THESIS OUTLINE

In this thesis, charge transport through molecules is investigated. Calculations based on the combination of density functional theory (DFT) with the non-equilibrium Green's function (NEGF) formalism for transport, developed within the Landauer formalism are perform to describe different systems.

We have implemented different functions in the ADF/BAND quantum-chemistry package [20–22]. The thesis is organized as follows:

After this introductory chapter, chapter 2 introduces the theoretical framework for describing transport calculations, focusing on the combination of density functional theory calculations with the non-equilibrium Green's function formalism. We also introduce some simple models for studying possible interactions inside the molecules. The two subsequent chapters (3 and 4) are dedicated to study metal-molecule interfaces and how molecules are affected by the presence of the electrodes. Chapter 5 explores DFT hybrid functionals to improve the long range interactions description in single molecule junctions transport calculations. Chapter 6 presents spin resolved transport calculations on a spin cross-over molecule where a spin transition is triggered by the electrodes being moved apart. Chapter 7 presents a model to explain the mechanism of a humidity dependent switchable molecular rectifier recently measured.

REFERENCES

[1] D. Goldhaber-Gordon, M. S. Montemerlo, J. C. Love, G. J. Opiteck, and J. C. Ellenbogen, *Overview of nanoelectronic devices,* Proceedings of the IEEE **85**, 521 (1997).

[2] S. Y. Quek, H. J. Choi, S. G. Louie, and J. B. Neaton, *Length dependence of conductance in aromatic single-molecule junctions,* Nano Lett. **9**, 3949 (2009).

[3] I. V. Krive, A. Palevski, R. I. Shekhter, and M. Jonson, *Resonant tunneling of electrons in quantum wires (review),* Low Temperature Physics **36**, 119 (2010).

[4] Z.-L. Cheng, R. Skouta, H. Vazquez, J. R., Widawsky, S. Schneebeli, W. Chen, M. S., Hybertsen, R. Breslow, and L. Venkataraman, *In situ formation of highly conducting covalent au-c contacts for single-molecule junctions,* Nat. Nano , (2011).

[5] A. C. Whalley, M. L. Steigerwald, X. Guo, and C. Nuckolls, *Reversible switching in molecular electronic devices,* J. Am. Chem. Soc. **129**, 12590 (2007).

[6] F. Pistolesi, Y. M. Blanter, and I. Martin, *Self-consistent theory of molecular switching,* Phys. Rev. B **78**, 085127 (2008).

[7] S. J. van der Molen and P. Liljeroth, *Charge transport through molecular switches,* J. Phys.: Condens. Matter **22**, 133001 (2010).

[8] S. A. Wolf, D. D. Awschalom, R. A. Buhrman, J. M. Daughton, S. von Molnár, M. L. Roukes, A. Y. Chtchelkanova, and D. M. Treger, *Spintronics: A spin-based electronics vision for the future,* Science **294**, 1488 (2001).

[9] J. R. Petta, S. K. Slater, and D. C. Ralph, *Spin-dependent transport in molecular tunnel junctions,* Phys. Rev. Lett. **93**, 136601 (2004).

[10] A. R. Rocha, V. M. Garcia-suarez, S. W. Bailey, C. J. Lambert, J. Ferrer, and S. Sanvito, *Towards molecular spintronics,* Nat. Mater. **4**, 335 (2005).

[11] S. Sanvito, *Molecular spintronics,* Chem. Soc. Rev. **40**, 3336 (2011).

[12] C. J. Milios, A. Vinslava, W. Wernsdorfer, S. Moggach, S. Parsons, S. P. Perlepes, G. Christou, and E. K. Brechin, *A record anisotropy barrier for a single-molecule magnet,* J. Am. Chem. Soc. **129**, 2754 (2007).

[13] D. Li, R. Clérac, O. Roubeau, E. Harté, C. Mathonière, R. Le Bris, and S. M. Holmes, *Magnetic and optical bistability driven by thermally and photoinduced intramolecular electron transfer in a molecular cobalt-iron prussian blue analogue,* J. Am. Chem. Soc. **130**, 252 (2008).

[14] A. Aviram and M. A. Ratner, *Molecular rectifiers,* Chem. Phys. Lett. **29**, 277 (1974).

[15] M. A. Reed, C. Zhou, C. J. Muller, T. P. Burgin, and J. M. Tour, *Conductance of a molecular junction,* Science **278**, 252 (1997).

[16] H. Park, A. K. L. Lim, A. P. Alivisatos, J. Park, and P. L. McEuen, *Fabrication of metallic electrodes with nanometer separation by electromigration,* Appl. Phys. Lett. **75**, 301 (1999).

[17] S. Datta, *Electronic Transport in Mesoscopic Systems*, 1st ed. (Cambridge University Press, 1997).

[18] M. Di Ventra, *Electrical Transport in Nanoscale Systems*, 1st ed. (Cambridge University Press, 2008).

[19] Y. V. Nazarov and Y. M. Blanter, *Quantum Transport: Introduction to Nanoscience*, 1st ed. (Cambridge University Press, 2009).

[20] C. Fonseca Guerra, J. G. Snijders, G. te Velde, and E. J. Baerends, *Towards an order-n dft method,* Theoretical Chemistry Accounts **99**, 391 (1998).

[21] G. te Velde and E. J. Baerends, *Precise density-functional method for periodic structures,* Phys. Rev. B **44**, 7888 (1991).

[22] G. te Velde, F. Bickelhaupt, S. van Gisbergen, C. Fonseca Guerra, E. Baerends, J. Snijders, and T. Ziegler, *Chemistry with ADF,* J. Comput. Chem. **22**, 931 (2001).

2

THEORETICAL FRAMEWORK

The purpose of this chapter is to give the reader a introduction to the theory for the description of many-electron wave functions, the standard procedures used to obtain energies and wave functions, and the role of one-electron wave functions (orbitals) in the scheme. We provide the theory behind the most non-empirical quantum chemistry computer codes.

2.1. ELECTRONIC HAMILTONIAN

A molecule can be viewed as a collection of charged particles interacting through electrostatic forces that obey quantum mechanics and Coulomb's law. The potential energy of interaction between any two electrons is e^2/r_{ij}, where r_{ij} is the separation between the electrons i and j and e is the electron charge. For any two nuclei I and J with atomic numbers Z_I and Z_J separated by a distance R_{IJ}, the interaction potential is $Z_I Z_J e^2/R_{IJ}$. The potential energy of an electron i with a nucleus I is $Z_I e^2/r_{Ii}$. The kinetic energies of the ith electron and the Ith nucleus in momentum formulation are $p_i^2/2m_e$ and $P_I^2/2M_I$, respectively, where the electron mass m_e and the nuclear mass M_I are constants [1]. We use the convention that lowercase letters refer to electrons and capital letters refer to nuclei. For an isolated system of N nuclei and n electrons, the classical non-relativistic total energy can be written as the sum of the kinetic energies of the individual particles and the sum of all pair potentials:

$$\hat{H} = \sum_{i=1}^{n} \frac{\hat{p}_i^2}{2m_e} + \sum_{I=1}^{N} \frac{\hat{P}_I^2}{2M_I} - \sum_{i=1}^{n}\sum_{I=1}^{N} \frac{Z_I e^2}{r_{iI}} + \frac{1}{2}\sum_{i=1}^{n}\sum_{j=1,j\neq i}^{n} \frac{e^2}{r_{ij}} + \frac{1}{2}\sum_{I=1}^{N-1}\sum_{J=1,J\neq I}^{N} \frac{Z_I Z_J e^2}{R_{IJ}}. \tag{2.1}$$

The first two terms of equation 2.1 describe the kinetic energy of the electrons and nuclei respectively. The last three terms describe the Coulomb potential of electron-nuclei attraction, electron-electron repulsion, and nuclear-nuclear repulsion respectively. The energy is zero when the particles are infinitely far apart and not moving.

Since the electron-nuclear masses ratio is close to 1/2000, electronic velocities are much higher than nuclear velocities. Making use of the Born-Oppenheimer (BO) approximation, the wave function is separated into an electronic part and a nuclear part, where the electronic wave function depends on the instantaneous positions of the nuclei [2]. Then, the second term on the right hand side of equation 2.1 is zero and the last term is a constant since the nuclear coordinates are known and fixed. The total energy depends on the nuclear coordinates, which we will represent collectively as R:

The electronic Hamiltonian operator $\hat{H}^e$ can be written in the Born-Oppenheimer form is:

$$\begin{aligned} \hat{H}^e &= -\sum_{i=1}^{n} \frac{\hbar^2}{2m_e}\nabla_i^2 - \sum_{i=1}^{n}\sum_{I=1}^{N} \frac{Z_I e^2}{r_{iI}} + \frac{1}{2}\sum_{i=1}^{n}\sum_{j=1,j\neq i}^{n} \frac{e^2}{r_{ij}}, \\ &= \sum_{i=1}^{n} \hat{h}(i) + \sum_{i=1}^{n-1}\sum_{j=i+1}^{n} e^2 \hat{g}(i,j) \end{aligned} \tag{2.2}$$

Where $\hat{h}(i)$ is the one electron Hamiltonian for the ith electron and $\hat{g}(i,j)$ is the electron-electron interaction

$$\hat{h}(i) = -\frac{\hbar^2}{2m_e}\nabla(i)^2 - \sum_{I=1}^{N} \frac{Z_I e^2}{r_{iI}}, \tag{2.3}$$

$$\hat{g}(i,j) = \frac{1}{r_{ij}} \tag{2.4}$$

The electronic Hamiltonian 2.2 does not depend explicitly on R. This is a the consequence of the BO approximation [3].

2.2. HARTREE-FOCK

The total energy of the molecule is the sum of the electronic energy and the nuclear energy. The electronic energy E^e must be obtained by solving the electronic Schrödinger equation.

$$\hat{H}^e |\Phi\rangle = E^e |\Phi\rangle , \tag{2.5}$$

where Φ is the wave function for this many-electron hamiltonian. Unfortunately, no exact solution for this equation exists.

The Hartree-Fock method is a many-body technique, with a single-particle picture, which means that every electron is considered a single-particle and all single particles orbitals together build up the wave function. Each electron feels the presence of the others indirectly through an effective potential, such that, every orbital is affected by the presence of electrons in other orbitals [4].

The starting point of the Hartree-Fock method is to write a variational wave function, which is built from these single-particle orbitals [5]. It is possible to build an antisymmetric solution by introducing the following Slater determinant:

$$\Phi_{AS}(\mathbf{r}_1, \mathbf{r}_2, ..., \mathbf{r}_n,) = \frac{1}{\sqrt{N!}} \begin{vmatrix} \phi_1(\mathbf{r}_1) & \phi_2(\mathbf{r}_1) & \cdots & \phi_n(\mathbf{r}_1) \\ \phi_1(\mathbf{r}_2) & \phi_2(\mathbf{r}_2) & \cdots & \phi_n(\mathbf{r}_2) \\ \cdots & \cdots & \ddots & \vdots \\ \phi_1(\mathbf{r}_n) & \phi_2(\mathbf{r}_n) & \cdots & \phi_n(\mathbf{r}_n) \end{vmatrix} . \tag{2.6}$$

The single-electron orbitals ϕ_i are assumed to be orthogonal:

$$\langle \phi_i | \phi_j \rangle = \int \phi_i^*(\mathbf{r}) \phi_j(\mathbf{r}) d\mathbf{r} = \delta_{ij} . \tag{2.7}$$

It is possible to obtain an estimate for the energy even if one does not know the exact wave function but only an approximate one, Φ, that is,

$$E = \frac{\int \Phi^* H \Phi d\mathbf{r}}{\int \Phi^* \Phi d\mathbf{r}} . \tag{2.8}$$

Writing the Slater determinant Φ_{AS} as a sum of products of spin-orbitals and using the orthonormality of ϕ_i, we obtain for the expectation value of the energy:

$$\begin{aligned} \langle \Phi_{AS} | \hat{H}^e | \Phi_{AS} \rangle =& \langle \Phi_{AS} \left| \sum_i \hat{h}(i) \right| \Phi_{AS} \rangle + \frac{1}{2} \langle \Phi_{AS} \left| \sum_{i,j} \hat{g}(i,j) \right| \Phi_{AS} \rangle \\ =& N \frac{(N-1)}{N} \sum_k \langle \phi_k \left| \hat{h} \right| \phi_k \rangle + \\ & \frac{1}{2} \sum_{k,l} \langle \phi_k \phi_l \left| \hat{g} \right| \phi_k \phi_l \rangle - \langle \phi_k \phi_l \left| \hat{g} \right| \phi_l \phi_k \rangle , \end{aligned} \tag{2.9}$$

where

$$\langle \Phi_{AS} \left| \sum_{i,j} \hat{g}(i,j) \right| \Phi_{AS} \rangle = \sum_{k,l} \langle \phi_k \phi_l \left| \hat{g} \right| \phi_k \phi_l \rangle - \langle \phi_k \phi_l \left| \hat{g} \right| \phi_l \phi_k \rangle,$$

and we have used the notation

$$\langle \phi_k \phi_l \left| \hat{g} \right| \phi_m \phi_n \rangle = \int d\mathbf{r}_1 d\mathbf{r}_2 \phi_k^*(\mathbf{r}_1) \phi_l^*(\mathbf{r}_2) \frac{1}{r_{ij}} \phi_m(\mathbf{r}_1) \phi_n(\mathbf{r}_2).$$

It can be proved that for the ground state, the calculated E is always greater than or equal to the exact energy E_0. The two energies are equal only if $\Phi = \Phi_0$.

For simplicity, lets define the operators

$$J_k(\mathbf{r})\phi(\mathbf{r}) = \int \phi_k^*(\mathbf{r}') \frac{1}{r_{12}} \phi_k(\mathbf{r}') \phi(\mathbf{r}) d\mathbf{r}',$$
$$K_k(\mathbf{r})\phi(\mathbf{r}) = \int \phi_k^*(\mathbf{r}') \frac{1}{r_{12}} \phi(\mathbf{r}') \phi_k(\mathbf{r}) d\mathbf{r}'. \tag{2.10}$$

J is called the Coulomb operator and K the exchange operator. In terms of them, the energy can be written as

$$E = \sum_k \langle \phi_k \left| \hat{h} + \frac{1}{2} \sum_k (\hat{J}_k - \hat{K}_k) \right| \phi_k \rangle. \tag{2.11}$$

This is the energy-functional for a Slater determinant. Once the orbitals have been optimized (see 2.2.1) to yield the lowest possible value of the energy, the energy will be the Hartree-Fock energy E_{HF}.

2.2.1. THE HARTREE-FOCK EQUATIONS

Now, we will determine the minimum of the E functional as a function of the orbitals ϕ_k. It means, any change in the expectation value of E due to an infinitesimal change in any of the orbitals ϕ_k should be zero. However the variation in the orbitals ϕ_k is not completely arbitrary, given that the orthonormality relation should be respected. This can be solved using the Lagrange method of undetermined multipliers.

Defining the functional $\mathscr{L}$ as

$$\mathscr{L} = E - \sum_{k,l} \Lambda_{k,l} (\langle \phi_k | \phi_l \rangle - \delta_{k,l}), \tag{2.12}$$

where $\Lambda_{k,l}$ are the undetermined Lagrange multipliers. Setting the variation $\delta \mathscr{L} = 0$

$$\delta E - \sum_{k,l} \Lambda_{k,l} \left[\langle \delta\phi_k | \phi_l \rangle - \langle \phi_k | \delta\phi_l \rangle \right] = 0. \tag{2.13}$$

The Fock operator is defined as:

$$\hat{F} = \hat{h} + \sum_l (\hat{J}_l - \hat{K}_l), \tag{2.14}$$

Since $\delta\phi$ is arbitrary we get

$$\hat{F}\phi_k = \sum_l \Lambda_{k,l} \phi_l. \tag{2.15}$$

Taking ϕ_k as the eigenvector of the the Fock operator with eigenvalues ϵ_k and $\Lambda_{k,l} = \epsilon_k \delta_{k,l}$.

Koopmans' theorem establishes that each eigenvalue of the Fock operator gives the energy required to remove an electron from the corresponding single-electron state. Similarly the energy required to add an electron to an orbital. In this way, this equation can be written as a traditional eigenvalues equation [6],

$$\hat{F}\phi_k = \epsilon_k \phi_k. \tag{2.16}$$

2.2.2. MOLECULAR ORBITALS THEORY

The concept of the molecular orbital was introduced by Hund to explain the electronic states of molecules [7]. Mulliken summarized this concept [8]. In 1929, Lennard-Jones suggested an Ansatz that molecular eigenfunctions can be represented as the linear combination of atomic eigenfunctions. This was the beginning of the linear combination of atomic orbitals-molecular orbitals (LCAO-MO) approximation for describing molecular orbitals in terms of the atomic orbitals [9].

$$\phi_i = \sum_{j=1} C_{ji} \chi_i. \tag{2.17}$$

Equation 2.16 then takes the matrix form [10]

$$FC_k = \epsilon_k S C_k, \tag{2.18}$$

with

$$S_{i,j} = \langle \chi_i | \chi_j \rangle = \int \chi_i^*(\mathbf{r}) \chi_j(\mathbf{r}) d\mathbf{r}, \tag{2.19}$$

the overlap for the basis used.

2.3. DENSITY FUNCTIONAL THEORY

In the previous section we saw how to use the Hartree-Fock approximation to solve the many-electron problem. However, the nonlocal potentials 2.10 involved in Hartree-Fock are difficult to apply in extended systems [11].

Another way to threat the many-electron problem is by using an approach where the electronic orbitals are solutions of a Schrödinger equation that depends on the electron density rather than on the individual electron orbitals. This approach, called density functional theory (DFT), is the result of the work by Hohenberg, Kohn and Sham [12, 13] and has proven to be an efficient and rather reliable method for a wide range of applications in solid state physics and chemistry.

The Hohenberg and Kohn theorems establish

- For any system of interacting particles in an external potential $V_{ext}(\mathbf{r})$, this potential (and so the Hamiltonian) is determined uniquely (up to a constant) by the ground state density $n_0(\mathbf{r})$. Consequently, as all properties of the system are governed by the Hamiltonian, they are completely determined given only this ground-state density.

- A functional $E[n(\mathbf{r})]$ can be defined for the energy, which is valid for any such potential $V_{ext}(\mathbf{r})$, such that the global minimum of the functional is the ground-state energy of the system. Consequently, the density $n(\mathbf{r})$ which minimizes this functional is the ground-state density $n_0(\mathbf{r})$, and minimization of $E[n(\mathbf{r})]$ alone is enough to fully determine the exact ground-state energy and density.

These two theorems can be summarized in the next equation

$$E[n] = F[n] + \int n(\mathbf{r}) V_{ext}(\mathbf{r}) d\mathbf{r}, \tag{2.20}$$

where F is a universal functional of n and

$$n(\mathbf{r}) = \sum_k |\phi_k(\mathbf{r})|^2. \tag{2.21}$$

It can be proved that the minimum value of the functional E is E_0, the exact ground-state electronic energy [14].

The Coulomb interaction between the electrons and the static nuclei acts as an external potential V_{ext}.

2.3.1. THE KOHN-SHAM EQUATIONS

Let us consider the energy functional $E[n(\mathbf{r})]$ for a many-electron system with density $n(\mathbf{r})$

$$E[n(\mathbf{r})] = T_s[n(\mathbf{r})] + \frac{1}{2}\int\int \frac{n(\mathbf{r})n(\mathbf{r}')}{|\mathbf{r}-\mathbf{r}'|} d\mathbf{r}d\mathbf{r}' + E_{XC}[n(\mathbf{r})] + \int n(\mathbf{r}) V_{\text{ext}}(\mathbf{r}) d\mathbf{r}, \tag{2.22}$$

E_{XC} is a term where we have moved all the terms we do not have under control, and $T_s[n(\mathbf{r})]$ is the kinetic energy. The form of $T_s[n(\mathbf{r})]$ is unknown, but we know that the ground state of the system can be written as a Slater determinant.

We define a functional $\mathscr{L}$

$$\mathscr{L} = E[n(\mathbf{r})] - \Lambda\left(\int n(\mathbf{r}) d\mathbf{r} - N\right), \tag{2.23}$$

where we have introduced the normalization constraint on the electron density, $\int n(\mathbf{r}) d\mathbf{r} = N$.

To find the ground state energy, E_0, and the ground state density, n_0, the one electron Schrödinger equation should be solved

$$\left(-\frac{\hbar}{2m_e}\nabla_i^2 + \frac{\delta E_{XC}[n(\mathbf{r})]}{\delta n(\mathbf{r})} + \int \frac{n(\mathbf{r}')}{\mathbf{r}-\mathbf{r}'} d\mathbf{r}' + V_{ext}(\mathbf{r}) - \epsilon_i\right)\psi_i(\mathbf{r}) = 0, \tag{2.24}$$

where

$$V_{XC}(\mathbf{r}) = \frac{\delta E_{XC}[n(\mathbf{r})]}{\delta n(\mathbf{r})}, \tag{2.25}$$

is the exchange correlation potential and its exact form is not known. In practice we have to use approximations for E_{XC}, some approximations might be better for some materials than for others.

2.3.2. JACOB'S LADDER

The main difference between the HF and DFT is the replacement of the HF exchange term by the exchange correlation energy E_{XC} which is a functional of the density.

DFT functionals vary from very simple to very complex. On Jacob's ladder of approximations, [15, 16] each rung represents a different level of approximation that should recover the results of lower rungs in the appropriate limits, but add more capabilities.

1. The lowest rung is the local density approximation (LDA), in which the XC energy density depends only on the density at a point and is that of the uniform electron gas (UEG). This is the simplest density functional, [13] and is used in materials science, but is insufficiently accurate for most chemical purposes. LDA typically overbinds molecules.

$$E_{XC}^{LDA} = \int \epsilon_{XC}^{UEG}(n(\mathbf{r}))\, n(\mathbf{r}) d\mathbf{r}. \tag{2.26}$$

2. On the next rung are generalized gradient approximations (GGAs), which are formulas that use both the density and its gradient at each point. These are typically more accurate than LDA. Most importantly, they greatly reduce the bond dissociation energy error, and generally improve transition-state barriers. But, unlike LDA, there is no single universal form. Popular GGAs include the J. P. Perdew, K. Burke, and M. Ernzerhof (PBE) [17], and A. D. Becke, C. Lee, W. Yang, and R. G. Parr (BLYP) [18, 19].

$$E_{XC}^{GGA} = \int \epsilon_{XC}^{GGA}(n(\mathbf{r}), \nabla n(\mathbf{r}))\, n(\mathbf{r}) d\mathbf{r}. \tag{2.27}$$

3. At the next level, we have meta-GGAs, which additionally depend on the Kohn-Sham kinetic energy density. Examples include J. Tao, J. P. Perdew, V. N. Staroverov, and G. E. Scuseria (TPSS) [20].

$$E_{XC}^{mGGA} = \int \epsilon_{XC}^{mGGA}\left(n(\mathbf{r}), \nabla n(\mathbf{r}), \nabla^2 n(\mathbf{r}), \tau(\mathbf{r})\right) n(\mathbf{r}) d\mathbf{r}, \tag{2.28}$$

with

$$\tau(\mathbf{r}) = \sum_{i}^{occ} |\nabla \phi_i(\mathbf{r})|^2. \tag{2.29}$$

4. We next encounter hybrid functionals, which mix some of the exchange terms of HF with a GGA. One of the most popular functional of this kind is B3LYP. By mixing in only a fraction of exact exchange (EXX), it is possible to mimic effects of static correlation, and produce a highly accurate functional. This is more costly to compute because exact exchange is non-local, depending not only on the electron density but also on the density matrix. The functional used can be written as

$$E_{XC}^{Hyb} = \alpha_X E_X^{EXX} + (1-\alpha_X) E_{XC}^{mGGA}\left[n(\mathbf{r}), \nabla n(\mathbf{r}), \nabla^2 n(\mathbf{r}), \tau(\mathbf{r})\right]. \tag{2.30}$$

The local part of this functional can be a meta-GGA, a GGA, or even an LDA. We have written E_{XC}^{mGGA} just as an example.

2.4. GREEN'S FUNCTIONS

We now discuss the main ideas behind the non-equilibrium Green's function (NEGF) formalism, and its application to transport calculations. NEGF methods are regularly used to calculate current and charge densities in nanoscale conductors under bias [21–24]. With it most of the properties of the system can be calculated.

The Green's function is defined as the impulse response of the system to a constant perturbation. Lets consider the time dependent Schrödinger equation of a system in presence of a potential $\hat{V}$:

$$\left(\hat{H}_0 + \hat{V}\right)\Phi = i\hbar\frac{\partial}{\partial t}\Phi, \tag{2.31}$$

with $\hat{H}_0$ the hamiltonian of the unperturbed system.

For the unperturbed system,

$$\left[i\hbar\frac{\partial}{\partial t} - \hat{H}_0\right]\Phi_0 = 0,$$

such that its Green's function is defined as:

$$\left[i\hbar\frac{\partial}{\partial t} - \hat{H}_0\right]\hat{G}_0(t,t') = \hat{I}\delta(t-t'). \tag{2.32}$$

Taking into account that $\Phi(t) = \Phi_0(t) + \Delta\Phi(t)$ and replacing it in the equation 2.31, we get

$$\begin{aligned}\Delta\Phi(t) &= \int dt'\hat{G}_0(t,t')\hat{V}\Phi(t'),\\ \Phi(t) &= \Phi_0(t) + \int dt'\hat{G}_0(t,t')\hat{V}\Phi(t').\end{aligned} \tag{2.33}$$

Equation 2.33 is an implicit equation. It can be transformed into an expansion in powers of the potential:

$$\Phi(t) = \Phi_0(t) + \int dt'\hat{G}_0(t,t')\hat{V}\left[\Phi_0(t') + \int dt''\hat{G}_0(t',t'')\hat{V}\left[\Phi_0(t'') + \cdots\right]\right]. \tag{2.34}$$

We can also define a full Green's function $G(t,t')$ by

$$\left[i\hbar\frac{\partial}{\partial t} - \hat{H}_0 - \hat{V}\right]\hat{G}(t,t') = \hat{I}\delta(t-t'), \tag{2.35}$$

such that

$$\Phi(t) = \Phi_0(t) + \int dt'\hat{G}(t,t')\hat{V}\Phi_0(t'), \tag{2.36}$$

where the perturbing potential $\hat{V}$ acts on the unperturbed wave-function. By comparing equation 2.36 with equation 2.34 we get the Dyson equation

$$\hat{G}(t,t') = \hat{G}_0(t,t') + \int dt''\hat{G}_0(t',t'')\hat{V}\hat{G}(t',t'') \tag{2.37}$$

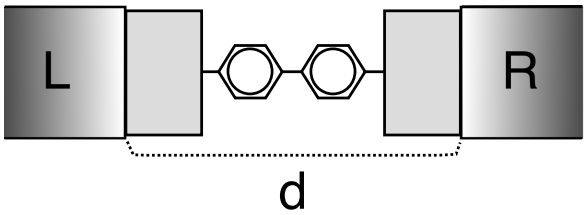

Figure 2.1: Setup for a two-terminal junction. L, R are the left and right electrodes respectively, and d is the device.

$G(t,tl)$ is connected to the time evolution operator for a time independent Hamiltonian $\left(U(t,t') = e^{-\frac{i}{\hbar}(t-t')\hat{H}}\right)$. Time can be split into a forward time and backward time by introducing the Heaviside $\Theta(t)$ function:

$$G^+(t,t') = -\Theta(t-t')e^{-\frac{i}{\hbar}(t-t')\hat{H}}, \tag{2.38}$$

$$G^-(t,t') = \Theta(t'-t)e^{-\frac{i}{\hbar}(t-t')\hat{H}}. \tag{2.39}$$

These are the retarded and the advanced Green's functions respectively, G^+, propagates a state $\Phi(t)$ forward in time, and the advanced Green's functions, G^-, propagates the state backward in time.

Since the Hamiltonian is Hermitian, we have

$$\left(\hat{G}^+(t,t')\right)^\dagger = \left(\hat{G}^-(t'-t)\right)^\dagger \tag{2.40}$$

If we Fourier-transform the retarded/advanced Green's function, we find the complementary expressions in the energy domain

$$\begin{aligned}\hat{G}^\pm(E) &= \lim_{\eta\to 0}\int_{-\infty}^{\infty} d(t-t' e^{i\frac{E(t-t')}{\hbar}}\hat{G}^\pm(t,t')e^{\mp\frac{\eta(t-t')}{\hbar}},\\ \hat{G}^\pm(E) &= \lim_{\eta\to 0}\frac{\hat{I}}{(E+i\eta)\hat{I}-\hat{H}}.,\end{aligned} \tag{2.41}$$

where $\eta > 0$ is added to ensure convergence.

The Dyson equation is Fourier transformed to

$$\hat{G}^\pm(E) = \hat{G}_0^\pm(E) + \hat{G}_0^\pm(E)\hat{V}\hat{G}^\pm(E) \tag{2.42}$$

2.4.1. GREEN'S OPERATOR FOR THE SCATTERING REGION

We are interested in a setup like the one shown in Fig. 2 where a left electrode (L) is connected to a right electrode (R) through a scattering region (d), L and R are semi-infinite regions.

We are looking for expressions that describe the transport in terms of operators of region d only.

Let us divide the Hamiltonian and the wave function of the system into contacts ($\hat{H}_{L,R}$ and $|\Phi_{L,R}\rangle$) and device ($\hat{H}_d$ and $|\Phi_d\rangle$).

$$\begin{pmatrix} \hat{H}_L & \hat{\tau}_L^\dagger & 0 \\ \hat{\tau}_L & \hat{H}_d & \tau_R^\dagger \\ 0 & \hat{\tau}_R & \hat{H}_R \end{pmatrix} \begin{pmatrix} |\Phi_L\rangle \\ |\Phi_d\rangle \\ |\Phi_R\rangle \end{pmatrix} = E \begin{pmatrix} |\Phi_L\rangle \\ |\Phi_d\rangle \\ |\Phi_R\rangle \end{pmatrix} \tag{2.43}$$

where $\hat{\tau}_L$ and $\hat{\tau}_R$ describe the interaction between device and electrodes and we assume that the last ones are independent.

The Green's function of the entire system is determined by equation 2.41.

$$\begin{pmatrix} E\hat{I} - \hat{H}_L & \hat{\tau}_L^\dagger & 0 \\ \hat{\tau}_L & E\hat{I} - \hat{H}_d & \hat{\tau}_R^\dagger \\ 0 & \hat{\tau}_R & E\hat{I} - \hat{H}_R \end{pmatrix} \begin{pmatrix} \hat{G}_L^\pm & \hat{G}_{Ld}^\pm & \hat{G}_{LR}^\pm \\ \hat{G}_{dL}^\pm & \hat{G}_d^\pm & \hat{G}_{Rd}^\pm \\ \hat{G}_{RL}^\pm & \hat{G}_{dR}^\pm & \hat{G}_R^\pm \end{pmatrix} = \begin{pmatrix} \hat{I} & 0 & 0 \\ 0 & \hat{I} & 0 \\ 0 & 0 & \hat{I} \end{pmatrix} \tag{2.44}$$

From this, we get an expression for the propagator $\hat{G}_d^\pm$ in the presence of the leads

$$\hat{G}_d^\pm = \left(E\hat{I} - \hat{H}_d - \hat{\Sigma}_L^\pm - \hat{\Sigma}_R^\pm\right)^{-1}, \tag{2.45}$$

where $\hat{\Sigma}_L^\pm = \hat{\tau}_L^\dagger \hat{g}_L^\pm \hat{\tau}_L$ and $\hat{\Sigma}_R^\pm = \hat{\tau}_R^\dagger \hat{g}_R^\pm \hat{\tau}_R$ are the *self-energies* of the electrodes and in general are complex,

$$\mathrm{Im}\left(\hat{\Sigma}_i^+\right) = -\frac{i}{2}\left(\hat{\Sigma}_i^+ - \hat{\Sigma}_i^-\right) = -\frac{\hat{\Gamma}_i(E)}{2}. \tag{2.46}$$

Γ_i is the non-Hermitian part of the self-energies; it is a consequence of the open nature of the system and allows particles to move in and out of the device region.

Te operators

$$\hat{g}_L = \left(E\hat{I} - \hat{H}_L\right)^{-1} \quad \text{and} \quad \hat{g}_R = \left(E\hat{I} - \hat{H}_L\right)^{-1},$$

are the Green's functions of the uncoupled electrodes. This reduces the problem to compute the electrodes self-energies from $\hat{g}_L$ and$\hat{g}_R$.

A very important concept is that of the spectral function defined by

$$\hat{A} = i\left[\hat{G}^+ - \hat{G}^-\right] = \hat{G}^+\hat{\Gamma}\hat{G}^- \tag{2.47}$$

This quantity plays the role of a generalized density of states inside the device taking the leads into account.

Evaluating in a position basis, we obtain the density correlation

$$\begin{aligned} \rho(\mathbf{r},\mathbf{r}',E) &= \frac{1}{2\pi}\langle \mathbf{r}|\hat{A}|\mathbf{r}'\rangle, \\ &= i\frac{G^+(\mathbf{r},\mathbf{r}',E) - G^-(\mathbf{r},\mathbf{r}',E)}{2\pi}, \\ &= -\frac{1}{\pi}\mathrm{Im}\left(G^+(\mathbf{r},\mathbf{r}',E)\right). \end{aligned} \tag{2.48}$$

Setting $\mathbf{r} = \mathbf{r}'$ we get the local density of states (LDOS), which can be integrated over the space to obtain the density of states ($D(E)$) or over the energy to obtain the spatial

density ($n(\mathbf{r})$):

$$
\begin{aligned}
D(\mathbf{r},E) &= -\frac{1}{\pi}\,\mathrm{Im}\left(G^{+}(\mathbf{r},\mathbf{r},E)\right),\\
D(E) &= -\frac{1}{\pi}\int d\mathbf{r}\,\mathrm{Im}\left(G^{+}(\mathbf{r},\mathbf{r},E)\right),\\
n(\mathbf{r}) &= -\frac{1}{\pi}\int dE\,\mathrm{Im}\left(G^{+}(\mathbf{r},\mathbf{r},E)\right) f(E,\mu),
\end{aligned}
\tag{2.49}
$$

with μ the chemical potential of the electrodes at zero bias. The spatial density is a crucial quantity in DFT as the Hamiltonian depends on this density.

NON-EQUILIBRIUM CALCULATIONS

Out of equilibrium, the density is obtained from the total spectral functions. By specifying $\hat{\Gamma}$ for each reservoir i, the total spectral function is

$$
\begin{aligned}
\hat{A} &= \hat{A}_L + \hat{A}_R,\\
&= \hat{G}^{+}\hat{\Gamma}_L\hat{G}^{-} + \hat{G}^{+}\hat{\Gamma}_R\hat{G}^{-}
\end{aligned}
\tag{2.50}
$$

these L and R contact spectral functions describe the incoming and outgoing particles from each reservoir when there is no direct coupling between them. This is an essential approximation in NEGF-DFT [24].

$$
\begin{aligned}
n(\mathbf{r}) = \frac{1}{2\pi}\int dE\,\big[&G_d^{+}(\mathbf{r},E)\Gamma_L(\mathbf{r},E)G_d^{-}(\mathbf{r},E)f(E,\mu_L)\\
&+ G_d^{+}(\mathbf{r},E)\Gamma_R(\mathbf{r},E)G_d^{-}(\mathbf{r},E)f(E,\mu_R)\big].
\end{aligned}
\tag{2.51}
$$

We can split this expression into an equilibrium term and a non-equilibrium correction:

$$
\begin{aligned}
n(\mathbf{r}) = &-\frac{1}{\pi}\int dE f(E,\mu_L)\,\mathrm{Im}\left(G_d^{+}(\mathbf{r},E)\right)\\
&+\frac{1}{2\pi}\int dE\left[f(E,\mu_L)-f(E,\mu_R)\right]G_d^{+}(\mathbf{r},E)\Gamma_R(\mathbf{r},E)G_d^{-}(\mathbf{r},E),
\end{aligned}
\tag{2.52}
$$

or equivalently

$$
\begin{aligned}
n(\mathbf{r}) = &-\frac{1}{\pi}\int dE f(E,\mu_R)\,\mathrm{Im}\left(G_d^{+}(\mathbf{r},E)\right)\\
&+\frac{1}{2\pi}\int dE\left[f(E,\mu_R)-f(E,\mu_L)\right]G_d^{+}(\mathbf{r},E)\Gamma_L(\mathbf{r},E)G_d^{-}(\mathbf{r},E).
\end{aligned}
\tag{2.53}
$$

It can be seen that for $\mu_L = \mu_R$ the second term in equations 2.52 and 2.53 vanishes, getting the equilibrium term.

It can be proved that from the Green's function, it is possible to obtain the elements of the scattering matrix, from which the transmission function can be calculated. Using this procedure the transmission function has a compact form:

$$
T(E) = \mathrm{Tr}\left[\hat{\Gamma}_L(E)\hat{G}^{+}(E)\Gamma_R(E)\hat{G}^{-}(E)\right]
\tag{2.54}
$$

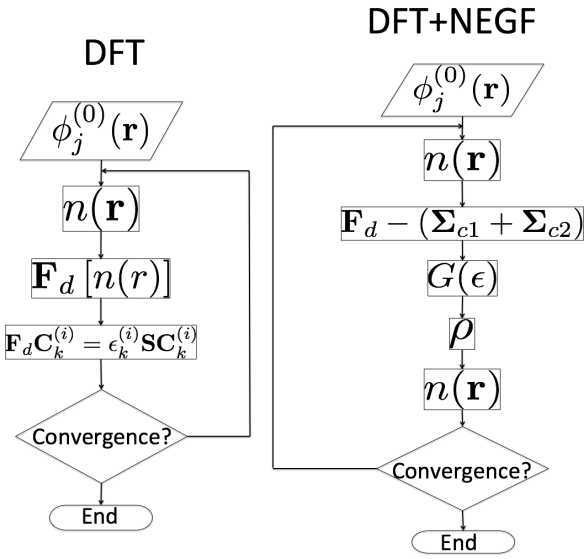

Figure 2.2: Comparison between the DFT and DFT+NEGF self consistency.

The electric current of the system can be calculated by a Landauer-like expression

$$I = \frac{2e}{h}\int dE\left[f(E,\mu_L) - f(E,\mu_R)\right]\mathrm{Tr}\left[\hat{\Gamma}_L(E)\hat{G}^{+}(E)\Gamma_R(E)\hat{G}^{-}(E)\right] \tag{2.55}$$

2.5. DFT+NEGF

Usually in quantum chemistry packages the Hamiltonian is represented using non- orthogonal basis sets, and from them the Fock matrix $\mathbf{F}^{KS} = [\langle\phi_i|\hat{H}^{KS}|\phi_j\rangle]$ and the overlap matrix $\mathbf{S}^{KS} = [\langle\phi_i|\phi_j\rangle]$ are calculated. From the Fock and overlap matrices for the bulk leads the surface Green's functions $\mathbf{G}_{L,R}(E)$ and the self-energies $\Sigma_{L,R}(E) \sim \tau G_{L,R}(E)\tau^{\dagger}$ matrices are calculated, with τ the coupling between the layers in the leads. These are combined with the Fock and overlap matrices of the device to find the full retarded Green's function:

$$\mathbf{G}_d(E) = [E\mathbf{S}_d - \mathbf{F}_d - (\Sigma_L(E) + \Sigma_R(E))]^{-1} \tag{2.56}$$

A modified self consistent field approach based on DFT makes use of the Green's functions to calculate the properties of the system, as can be seen in figure 2.2.

2.6. SIMPLE MODELS

In this section we develop a few simple models that are relevant for studying a molecule in a junction. These simple models will help us to describe the systems studied in chapters 3, 4 and 6.

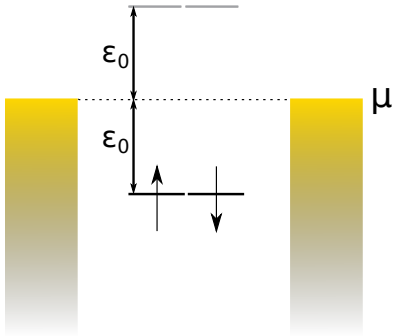

Figure 2.3: Scheme of the system used. The energy levels of the site are coupled to wide band limit electrodes. At zero gate, the occupied and unoccupied energy levels lie at energies ϵ_0 below and over the chemical potential of the electrodes respectively.

2.6.1. EXTENDED ANDERSON JUNCTION

Let us consider a system formed by one impurity with two energy levels in between two electrodes with identical chemical potential μ. While one of the energy levels is fully occupied with a chemical potential ϵ_0 below that of the electrodes, the other energy level is unoccupied and lies at ϵ_0 above the chemical potential, as can be seen in Fig. 2.3. Additionally, we apply a gate V_g over the central region in order to shift the energy levels and change their occupation.

For some gate values, due to the discrete behavior of the charges, we expect to see spin polarization and plateaus with constant charge, close to an integer value. This indicates that only one type of spin is added to or removed from the system when changing the gate. These plateaus occur in the levels corresponding to fixed occupation.

The polarization in this system can be explained by means of an Anderson junction [25] that consist of an interacting impurity site coupled to identical featureless left and right leads:

$$\hat{H} = \sum_j \left(\epsilon_j \hat{n}_j + U \hat{n}_{j\sigma} \hat{n}_{j\sigma*}\right) + \frac{1}{2} \sum_{i \neq j,\sigma,\sigma'} \left(V \hat{n}_{j\sigma} \hat{n}_{i\sigma'}\right) + \hat{H}_{leads} + \hat{H}_T, \tag{2.57}$$

with ϵ_j the on-site energy, U the Coulomb repulsion between two electrons in the same level, V the coulomb repulsion between two electrons in different energy levels, $\hat{n} = \hat{n}_\sigma + \hat{n}_{\sigma*}$. $\hat{H}_{leads}$ and H_T are the Hamiltonian of the two leads and the their coupling to the site respectively. j, i and σ, σ' run over the energy levels and spin respectively. We have used $\sigma* = -\sigma$.

In the wide band limit, the effect of the tunneling is represented by an energy-independent constant Γ.

Neglecting the Kondo effect, and the correlations with the leads, the Green's function on the central impurity site can be calculated as [25, 26]:

$$\hat{G}(E)_{j,\sigma} = \frac{E - \epsilon_j - V_g - U\hat{n}_{j,\sigma^*} - \sum_{i \neq j,\sigma'} V \hat{n}_{i,\sigma'} - i\Gamma}{(E - \epsilon_j - V_g - U\hat{n}_{j,\sigma^*} - \sum_{i \neq j,\sigma'} V \hat{n}_{i,\sigma'})^2 - \Gamma^2}, \tag{2.58}$$

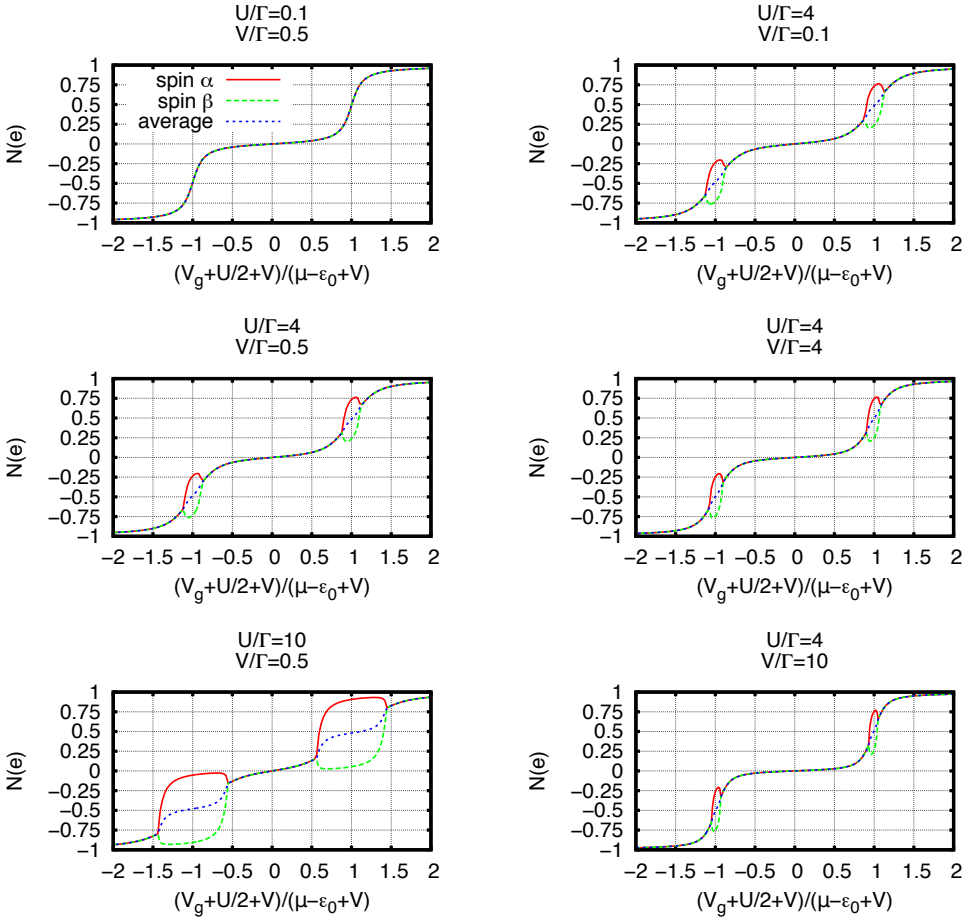

Figure 2.4: Number of electrons added to the system per spin as a function of gate for the two level system including the coulomb repulsion. The left column keeps the V/Γ ratio constant while the right column keeps the U/Γ ratio constant.

The spectral function $A(E) = -2\mathrm{Im}(G(E))$ depends on the occupation n_σ on the site. Therefore $n_{j\sigma}$ should be determined self-consistently with the possibility of having more than one stationary state.

$$\begin{aligned}\langle n_{j,\sigma}\rangle &= \frac{1}{\pi}\int_{-\infty}^{\mu} dE A_{j,\sigma}(E) \\ &= \frac{1}{\pi}\left(\mathrm{atan}\frac{\left(\mu-\epsilon_j-V_g-U\langle n_{j,\sigma^*}\rangle-\sum_{i\neq j,\sigma'}V\langle n_{i,\sigma'}\rangle\right)}{\Gamma}+\frac{\pi}{2}\right)\end{aligned} \tag{2.59}$$

Polarization and plateaus on the occupation $\langle n_\sigma\rangle$ are related to the U/Γ ratio. On average, the central region is not spin-polarized, hence, the chemical potentials for both spin directions are identical.

From the occupation $n_{j,\sigma}$, it is easy to calculate the number electrons added to the system per spin as a function of the applied gate (see Fig. 2.4). The V/Γ ratio does not affect the splitting occurrence, but it determines its width. It is clear that in the weak coupling condition ($\Gamma < U$) and depending on the gate value, the system present plateaus and spin polarization. This splitting depends on the initial guess for the electron densities. If they are taken equal, the converged configuration does not always show spin splitting.

2.6.2. PINNING + TWO SITES MODEL

Several mechanisms for explaining rectification in molecular systems have been proposed in the past. Part of these rely on inelastic processes – the famous Aviram-Ratner rectifier [27] falls into this class. Here we review two important mechanisms based on a coherent transport model.

The first mechanism relies on strongly antisymmetric capacitive coupling, which leads to 'pinning': an orbital is then more or less rigidly fixed in energy with respect to the Fermi energy of one of the two electrodes. If this level lies just above the fermi energy, changing the bias one way brings it into the bias window, whereas a bias change in the other direction, leaves the level outside [28] – see figure 2.5.

The other mechanism relies on a two-site structure and on resonance between orbitals located on the two sites. In such a system, the charge transport increases when the energy of the two sites is equal and is very small in other cases.

We consider a mixture of these two models, that is, we take into account the pinning produced by asymmetric couplings within the two-site structure.

We consider a molecular system in which the HOMO and HOMO-1 orbitals can be expressed as symmetric and antisymmetric combinations of orbitals located on two conjugated moieties, connected by a non-conjugated linker. Due to the symmetry of the molecule in gas phase, the two halves have the same energy, the system can accommodate bonding and anti-bonding orbitals. Resonant transport occurs when the energy of the two sites is equal [29].

When asymmetries are introduced in the junction, for instance accumulation of more solvent molecules at one side than the other, site energies become different and the resonance condition between the two parts of the complex can be achieved by means of a bias voltage [30].

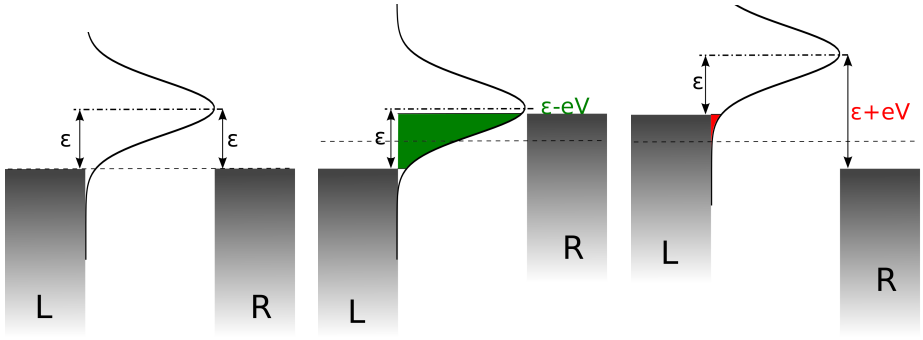

(a) Zero bias **(b)**Positive bias **(c)**Negative bias

Figure 2.5: Illustration of the first rectification mechanism for a LUMO like molecular junction, with the molecular resonance fixed at ε relative to the left electrode chemical potential. **(a)**, Zero-bias case depicting a molecular resonance with peak energy at ε relative to the left (L) and right (R) electrodes μ. **(b)**, With a positive forward bias. For this system, the area of the resonance falls within the bias window and the current is high. **(c)**, With a negative forward bias. A smaller area of the resonance falls within the bias window and the current is low.

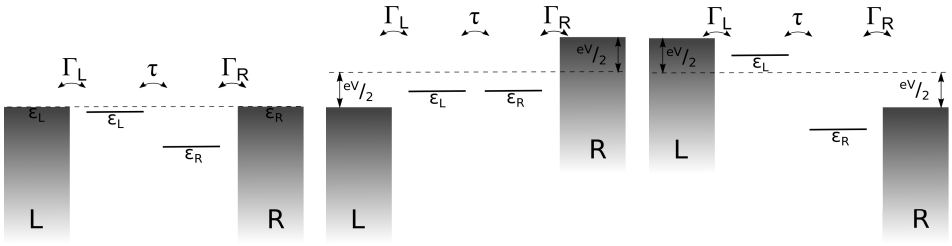

(a) Zero bias **(b)**Positive bias **(c)**Negative bias

Figure 2.6: Illustration of the charge transport for an asymmetric two-site system. **(a)**, Zero-bias case depicting two molecular levels. **(b)**, With a positive forward bias. The two molecular levels are in resonance and the current is high. **(c)**, With a negative forward bias. The levels are apart from each other, the transport is blocked and the current is low.

At zero bias, the left and right sites are at energies ϵ_L and ϵ_R respectively, with $\epsilon_L > \epsilon_R$. When a positive bias is applied, the two sites are pulled towards each other, leading to an increase of the electric current until they reach the resonance. For negative bias, the sites energies are pulled away from each other giving as a result low current for all voltages – See Fig. 2.6.

The two sites of the molecule can be described using the next hamiltonian

$$\mathbf{H} = \begin{pmatrix} \varepsilon_L + \frac{1}{2}\alpha_L eV & -\tau \\ -\tau & \varepsilon_R - \frac{1}{2}\alpha_R eV \end{pmatrix}, \tag{2.60}$$

where $\alpha_{L,R}$ describes the fraction of the voltage that drops at every side of the junction, and τ the coupling between the left and the right sites.

The eigenstates of this hamiltonian correspond to the bonding and anti bonding or-

bitals where their energy splitting Δ in presence of an applied bias is

$$\Delta = \frac{1}{2}\sqrt{\left((\alpha_L + \alpha_R)\, eV + 2\,(\varepsilon_L - \varepsilon_R)\right)^2 + (4\tau)^2} \tag{2.61}$$

In order to calculate the transport properties, the left and right sites are coupled to the leads in the wide band limit approximation [22, 23]

$$\Gamma_{\mathbf{L}} = \begin{pmatrix} \Gamma_L & 0 \\ 0 & 0 \end{pmatrix}, \Gamma_{\mathbf{R}} = \begin{pmatrix} 0 & 0 \\ 0 & \Gamma_R \end{pmatrix}. \tag{2.62}$$

$\Gamma_{L,R}$ are the electronic coupling of left and right sites to the respective electrode.
The transmission then is given by

$$\mathscr{T}(\epsilon) = \mathrm{Tr}\left[\Gamma_L \mathbf{G}^r(\epsilon)\Gamma_R \mathbf{G}^a(\epsilon)\right]. \tag{2.63}$$

$\mathbf{G}^r(\epsilon)$ and $\mathbf{G}^a(\epsilon)$ are the retarded and advanced Green's functions, respectively.

$$\mathbf{G}^r(\epsilon) = \left(\epsilon\mathbf{I} - \mathbf{H} + \frac{i}{2}(\Gamma_L + \Gamma_R)\right)^{-1}. \tag{2.64}$$

The current then is calculated using [31]

$$I = \frac{2e}{\hbar}\int \frac{d\epsilon}{2\pi}\left(f_L(\epsilon) - f_R(\epsilon)\right)\mathscr{T}(\epsilon), \tag{2.65}$$

with $f_{L,(R)}(\epsilon)$ the Fermi function of the left (right) electrode.

We know that the voltage drop in the molecule is equal or smaller than the voltage drop imposed to the electrodes. So we can say that the left energy level (ϵ_L) and the right energy level (ϵ_R) of the molecule are going to be shifted by $\frac{1}{2}\alpha_L eV$ and $-\frac{1}{2}\alpha_R eV$ respectively. Such that the voltage in the molecule is

$$\Delta V_M = \frac{1}{2}\alpha_L eV - \left(\frac{1}{2}\alpha_R eV\right) \tag{2.66}$$

If α_L and α_R depend on the voltage, we would have $\alpha_L(eV)$ and $\alpha_R(eV)$ what leads us to

$$\Delta V_M = \frac{1}{2}\alpha_L(eV) * eV - \left(\frac{1}{2}\alpha_R(eV) * eV\right) \tag{2.67}$$

REFERENCES

[1] A. Rauk, *Appendix a: Derivation of hartreefock theory,* in *Orbital Interaction Theory of Organic Chemistry* (John Wiley and Sons, Inc., 2002) pp. 218–246.

[2] M. Born and R. Oppenheimer, *Zur quantentheorie der molekeln,* Annalen der Physik **389**, 457 (1927).

[3] J. Thijssen, *Computational Physics*, 2nd ed. (Cambridge, 2007).

[4] T. Tsuneda, *Density Functional Theory in Quantum Chemistry*, 1st ed. (Springer Japan, 2014).

[5] D. R. Hartree, *The wave mechanics of an atom with a non-coulomb central field. part i. theory and methods,* Mathematical Proceedings of the Cambridge Philosophical Society **24**, 89110 (1928).

[6] E. Baerends, D. Ellis, and P. Ros, *Self-consistent molecular hartreefockslater calculations i. the computational procedure,* Chemical Physics **2**, 41 (1973).

[7] F. Hund, *Zur deutung einiger erscheinungen in den molekelspektren,* Zeitschrift für Physik **36**, 657 (1926).

[8] R. S. Mulliken, *Electronic states and band spectrum structure in diatomic molecules. iv. hund's theory; second positive nitrogen and swan bands; alternating intensities,* Phys. Rev. **29**, 637 (1927).

[9] J. E. Lennard-Jones, *The electronic structure of some diatomic molecules,* Trans. Faraday Soc. **25**, 668 (1929).

[10] Y.-C. Yim and H. Eyring, *Derivation of a formula for the resonance integral for a nonorthogonal basis set,* Proceedings of the National Academy of Sciences of the United States of America **78**, 2649 (1981).

[11] C. Pisani, R. Dovesi, and C. Roetti, *Hartree-Fock Ab Initio Treatment of Crystalline Systems*, Lecture Notes in Chemistry (Springer Berlin Heidelberg, 2012).

[12] P. Hohenberg and W. Kohn, *Inhomogeneous electron gas,* Phys. Rev. **136**, B864 (1964).

[13] W. Kohn and L. J. Sham, *Self-consistent equations including exchange and correlation effects,* Phys. Rev. **140**, A1133 (1965).

[14] M. Levy, *Universal variational functionals of electron densities, first-order density matrices, and natural spin-orbitals and solution of the v-representability problem,* Proceedings of the National Academy of Sciences **76**, 6062 (1979), http://www.pnas.org/content/76/12/6062.full.pdf .

[15] J. P. Perdew and K. Schmidt, *Jacobs ladder of density functional approximations for the exchange-correlation energy,* AIP Conference Proceedings **577**, 1 (2001), http://aip.scitation.org/doi/pdf/10.1063/1.1390175 .

[16] J. P. Perdew, A. Ruzsinszky, J. Tao, V. N. Staroverov, G. E. Scuseria, and G. I. Csonka, *Prescription for the design and selection of density functional approximations: More constraint satisfaction with fewer fits,* The Journal of Chemical Physics **123**, 062201 (2005), http://dx.doi.org/10.1063/1.1904565 .

[17] J. P. Perdew, K. Burke, and M. Ernzerhof, *Generalized gradient approximation made simple,* Phys. Rev. Lett. **77**, 3865 (1996), pBE.

[18] A. D. Becke, *Density-functional exchange-energy approximation with correct asymptotic behavior,* Phys. Rev. A **38**, 3098 (1988).

[19] C. Lee, W. Yang, and R. G. Parr, *Development of the colle-salvetti correlation-energy formula into a functional of the electron density,* Phys. Rev. B **37**, 785 (1988).

[20] J. Tao, J. P. Perdew, V. N. Staroverov, and G. E. Scuseria, *Climbing the density functional ladder: Nonempirical meta–generalized gradient approximation designed for molecules and solids,* Phys. Rev. Lett. **91**, 146401 (2003).

[21] R. Mattuck, *A Guide to Feynman Diagrams in the Many-Body Problem* (Dover, 1976).

[22] A.-P. Jauho, N. S. Wingreen, and Y. Meir, *Time-dependent transport in interacting and noninteracting resonant-tunneling systems,* Phys. Rev. B **50**, 5528 (1994).

[23] H. Haug and A.-P. Jauho, *Quantum Kinetics in Transport and Optics of Semiconductors,* 1st ed. (Springer-Verlag, 1997).

[24] S. Datta, *Electronic Transport in Mesoscopic Systems,* 1st ed. (Cambridge University Press, 1997).

[25] P. W. Anderson, *Localized magnetic states in metals,* Phys. Rev. **124**, 41 (1961).

[26] Z.-F. Liu and K. Burke, *Density functional description of coulomb blockade: Adiabatic versus dynamic exchange correlation,* Phys. Rev. B **91**, 245158 (2015).

[27] A. Aviram and M. A. Ratner, *Molecular rectifiers,* Chem. Phys. Lett. **29**, 277 (1974).

[28] B. Capozzi, J. Xia, O. Adak, E. J. Dell, Z.-F. Liu, J. C. Taylor, J. B. Neaton, L. M. Campos, and L. Venkataraman, *Single-molecule diodes with high rectification ratios through environmental control,* Nat Nano **10**, 522 (2015).

[29] M. L. Perrin, R. Frisenda, M. Koole, J. S. Seldenthuis, J. A. Celis Gil, H. Valkenier, J. C. Hummelen, N. Renaud, F. C. Grozema, J. M. Thijssen, D. Dulić, and van der ZantHerre S. J., *Large negative differential conductance in single-molecule break junctions,* Nat Nano **9**, 830 (2014).

[30] M. L. Perrin, E. Galan, R. Eelkema, F. Grozema, J. M. Thijssen, and H. S. J. van der Zant, *Single-molecule resonant tunneling diode,* The Journal of Physical Chemistry C **119**, 5697 (2015), http://dx.doi.org/10.1021/jp512803s .

[31] Y. Meir and N. S. Wingreen, *Landauer formula for the current through an interacting electron region,* Phys. Rev. Lett. **68**, 2512 (1992).

3

IMAGE EFFECTS IN TRANSPORT AT METAL-MOLECULE INTERFACES

Whatever doesn't kill you, simply makes you... "stranger"

The Joker
The dark knight. Dir. C. Nolan, CA: Warner Home Video, 2008

We present a method for incorporating image-charge effects into the description of charge transport through molecular devices. A simple model allows us to calculate the adjustment of the transport levels, due to the polarization of the electrodes as charge is added to and removed from the molecule. For this, we use the charge distributions of the molecule between two metal electrodes in several charge states, rather than in gas phase, as obtained from a DFT-based transport code. This enables us to efficiently model level shifts and gap renormalization caused by image-charge effects, which are essential for understanding molecular transport experiments. We apply the method to benzene di-amine molecules and compare our results with the standard approach based on gas phase charges. Finally, we give a detailed account of the application of our approach to porphyrin-derivative devices recently studied experimentally by Perrin et. al., which demonstrates the importance of accounting for image-charge effects when modeling transport through molecular junctions.

This chapter has been published in The Journal of Chemical Physics **143**, 174106 (2015) [1].

3.1. INTRODUCTION

Understanding the physics determining charge transport at interfaces between metal electrodes and molecules is key to the advancement of the field of molecular electronics. In a molecular device, the alignment of frontier molecular orbital levels relative to the metals' Fermi energies determines the contribution of the different channels available for transport. Due to their proximity to the electrodes, the levels themselves are shifted relative to those of the molecule in gas phase, and may hybridize with electrode levels as well. Together, level alignment and hybridization determine electron transport in the molecular junction.

In this chapter we describe an approach to investigating these effects based on density-functional theory (DFT) [2] and the non-equilibrium Green's functions (NEGF) formalism.[3–11] DFT is frequently used in calculations of charge transport because of its efficiency, and because computationally it scales well to realistic nanoscale junction sizes. It does suffer from a few drawbacks, however, the most important of which are poor predictions of one- and two-particle excitations.[2, 12] The reason for the failure of DFT to predict excitation energies from a single neutral-state calculation is mainly due to the inclusion of spurious self-interactions,[13, 14] and the omission of dynamic polarization effects.[15, 16] Both effects are captured in GW calculations,[16–18] usually within the COHSEX approach,[15] and time-dependent density-functional theory (TDDFT).[19–21] However, these are computationally expensive and not (yet) feasible except for very small molecules, in contrast to DFT-based approaches.

Approximate methods have been proposed and used with some success to address the shortcomings of DFT in predicting excitations. These include the use of a scissors-operator[22, 23] and simple image-charge models based on atomic charges,[16, 23–25] used to address the location of resonant levels in the transport region of the molecular device.

In this chapter, we focus on the latter and argue that image charges used in an electrostatic-energy calculation should be taken from the molecule in the presence of contacts rather than from the gas phase. In section 3.2 we provide a brief introduction to interface effects, and outline our method for the calculation of the image-charge effects. In section 5.3, we apply our method to the 1,4-benzenediamine molecule between two gold electrodes and compare it to other approaches which have appeared in the literature[22, 23, 25]. Then, in section 3.4, we cover the application of our method to Zn-porphyrin devices studied in recent experiments by Perrin et. al. [26], in which image-charge effects play an important role.

3.2. THEORETICAL MODEL

We illustrate the most important physical effects as a molecule approaches a clean metal surface in Fig. 3.1, following Ishii et. al. [27] The shift of the levels occurring when a molecule is moved towards a metal surface can be divided into two classes. The first type of shift is due to a change in the background potential induced by the proximity of the metal and, although different molecular orbitals may shift differently from their gas phase values, generally the *direction* of these shifts is the same for all, and the differences between them are rather small. Therefore, we denote these shifts as "rigid". Usually,

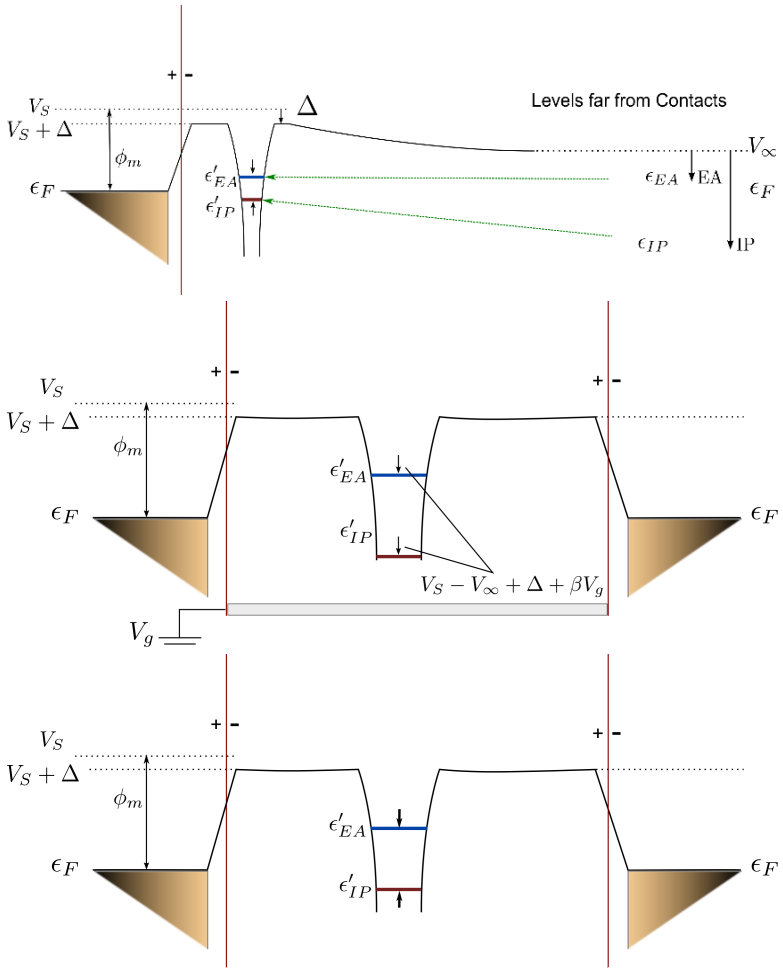

Figure 3.1: **Energy landscape during the formation of a metal-molecule interface.** (a) Combined rigid and dynamical image-charge effects on molecular levels at a single interface, relative to the molecule in isolation far away. These are a superposition of (b) and (c), where in (b) the surface dipole (shaded red/green) raises the background potential by $V_s - V_\infty$. The static image-charge effect, intrinsic molecular and interface dipoles shift the molecular levels back by Δ, while electrostatic gating shifts by βV_g. (c) Levels are also subject to renormalization of the gap between the electron affinity ϵ_{EA} and the ionization potential ϵ_{IP} levels, where the prime indicates the position after the shift.

these shifts are upward with respect to the gas phase.

These background effects have their origin in the so-called "push back", or "pillow" effect, which refers to the reduction of the spill-out of electronic charge from the surface occurring for a clean metal surface. This spill-out results in a surface dipole which increases the work function. As the push back effect reduces this spill-out (the molecule pushes the electronic charge back into the metal) it *lowers* the work function.[27–31] A second mechanism resulting in a uniform shift of the orbital levels is charge transfer as a result of chemisorption, which also changes the surface dipole. Finally, the charge distribution on the (possibly neutral) molecule generates an image charge distribution in the metal. The potential between the charges on the molecule and their images then results in a shift. The uniform shift resulting from all three mechanisms is denoted as Δ – see Fig. 3.1. Oszwaldowski et. al. have introduced a many-body method based on DFT[32] for capturing some of this dependence, deriving from dipole and pillow effects.

The length scale over which the changes to the energy landscape due to a surface dipole layer take place is related to the lateral extent of the surface dipole layer formed at the metal surface. This is typically the scale of the electrode in a mechanically controlled break-junction (MCBJ) experiment, which is of the order of 5 nm.[1] The magnitude of Δ is suggested by the measurements summarized by Ishii et. al.: roughly $0.5-1$ eV, typically a negative correction on an Au substrate. Measurements by Koch et. al. [33–35] on thin-films with different molecules support these considerations: they find a constant-shift region very near the interface, followed by a linear shift of ~ 1 eV over a range of roughly 8 Å beyond which a regime with constant Δ sets in.

In addition to this rigid shift, there is a shift which is very different between occupied and unoccupied levels, causing the transport gap between them to close ("renormalize") as the molecule approaches the surface. The upward shift of occupied levels is caused by the fact that an electron moving away from the molecule leaves a positive hole behind. The electrostatic force needed to overcome when moving an electron from the molecule to infinity is for a substantial part responsible for the ionization potential of the molecule. If the molecule is close to a metal, removing electron from it will not only leave a positive hole behind, but also a negative image charge in the metal bulk. This *reduces* the binding energy and therefore the ionization potential (IP).

Adding an electron to the molecule usually costs energy – this is the *addition energy*, AE. Close to a metal surface, however, the additional electron feels an attraction from the positive image charge it creates in the metal. Therefore, also the addition energy is reduced. We see that the gap between the occupied and unoccupied levels therefore shrinks; this is denoted the gap renormalisation. In a transport junction, this gap is called the *transport gap*. It should be noted that the above discussion relies on weak coupling between the molecule and the metal, implying a preferentially integer electron occupation on the molecule. The rigid shift and the gap renormalization are effect is schematically represented in Fig. 3.1.

Gap renormalization has been studied extensively in the literature [15, 16, 18, 22, 36]. It was shown by Neaton et. al. [16] that for small molecules this effect can be well fitted by an image-potential of the form $-\frac{1}{4z}$ (with z the distance to the image plane). These

[1] Estimated from the fits of the junction area in Perrin et. al. experiments[26], which fit this as 28 nm^2 and considered the range of $10-50$ nm^2 as representative.

effects are important in many nanoscale molecular systems, as has been argued on both experimental[24, 37, 38] and theoretical grounds [16, 18, 22, 23, 25, 36] and are crucial for understanding and designing future molecular devices.

Electrostatic relaxation upon changing the charge on a molecule is not appropriately accounted for in DFT calculations, and in particular, it is missed in DFT-based NEGF calculations commonly used in studying single-molecule charge transport. [5, 6, 8, 11, 39] We note that there are two types of relaxation: the first is the relaxation of the resident electrons on the molecule upon removing or adding an electron. These effects are responsible for the difference that is observed between the HOMO (highest occupied level found in a DFT calculation) and the ionization potential, and similar for the AE and the LUMO. This notion has led to applying the molecular shifts to the transport junction, one of the ingredients in the 'scissors operator' approach. [16, 18, 22] We have however seen that the image charges in the metal also shift the IP and AE, and these effects vary with the distance from the molecule to the metal contacts. This distance dependence is accessible in experiments (see section 3.4.1) and the focus of this chapter. Kaasbjerg and Flensberg[25] have addressed this effect and reported substantial gap reductions, and even dramatic ones in the presence of a gate. GW calculations in principle address such polarization effects, but these require very heavy computer resources even for small systems. Here, we use classical electrostatic calculations to address polarization effects due to the contacts, based on charge distributions obtained from DFT calculations in different charge states. We note that DFT is designed for and has proven to be reliable for calculating ground state properties, and these are the only ones used in our calculations.

3.3. IMAGE CHARGE EFFECTS FOR BENZENEDIAMINE (BDA)

To analyze the transport through the molecule, we perform DFT-NEGF calculations for the Au-BDA-Au fragment attached to a FCC (111) surface (Fig. 3.2). We consider a junction of type (I,I) according to the Quek et. al. classification [22]. For our calculations we use a TZP-basis of numerical atomic orbitals on the molecule, a DZ-basis of numerical atomic orbitals on the metal atoms and the GGA PBE functional in our implementation of NEGF-based transport in the ADF/Band quantum chemistry package [11, 40, 41].

For the molecule in the junction, we relax the geometry and we find the minimum energy configuration. Then, we stretch the junction separating the contacts with the molecule's conformation unchanged.

The spin-resolved occupation (see Fig. 3.5) indicates how the filling of the individual levels changes upon varying the gate. We have calculated the spin-resolved occupation for two cases: one where the molecule is close to the contacts (we consider the energy minimum for this, see Fig. 3.2 (c)) and one where the molecule is far away. Sometimes, we see spin-polarization, unless the occupation happens to be an even integer. We also observe absence of this polarization in the strong coupling limit for the charge between 0 and 1.

We expect the presence of polarization to be related to the weak coupling condition $\Gamma < U$, where U is the Coulomb repulsion for electrons at the relevant level. Polarization is not expected when $\Gamma > U$. This appears to be the case in the short distance configuration (strong coupling limit) when the charge is between 0 and 1.

We emphasize that this polarization is not physically correct as the system has un-

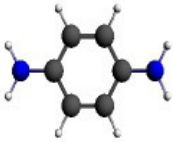

a) BDA Gas-Phase Geometry

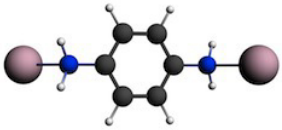

b) Au-BDA Fragment Geometry

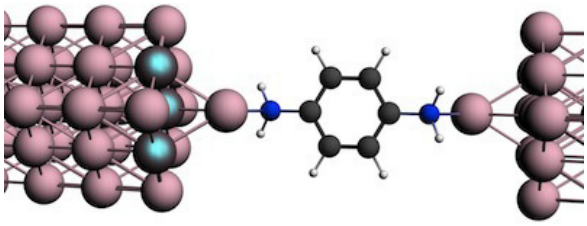

c) Au-BDA Junction Geometry

Figure 3.2: Geometries of BDA in (a) gas phase and (b) as a fragment. (c) (I,I) junction geometry. Metal ions are pink-grey, the blue-gray atoms are the substrate atoms coupled to the protruding gold atom. Left and right Au atoms show placement relative to a (111) surface.

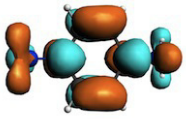

a) LUMO+1

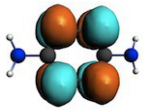

b) LUMO

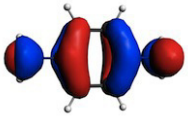

c) HOMO

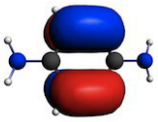

d) HOMO-1

Figure 3.3: Orbitals of BDA molecule in gas-phase ordered by decreasing energy.

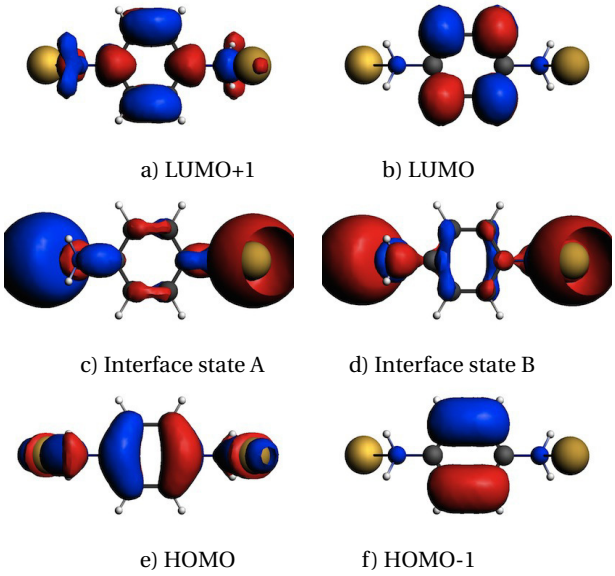

a) LUMO+1 b) LUMO

c) Interface state A d) Interface state B

e) HOMO f) HOMO-1

Figure 3.4: Au-BDA-Au Fragment orbitals labeled by their correspondence with the BDA gas phase orbitals (see Fig. 3.3) and ordered by decreasing energy.

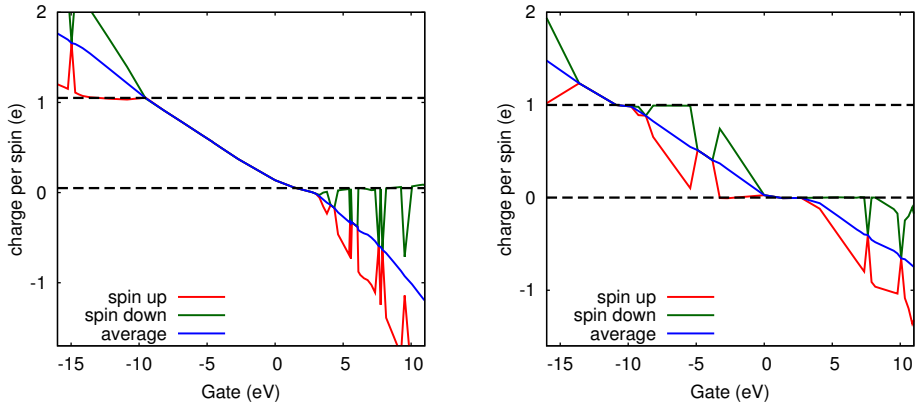

a) Molecule close to the contacts (strong coupling). b) Molecule far from the contacts (weak coupling).

Figure 3.5: Spin-resolved occupation as a function of the applied gate when (a) the molecule is close to the contacts and (b) the molecule is far from the contacts.

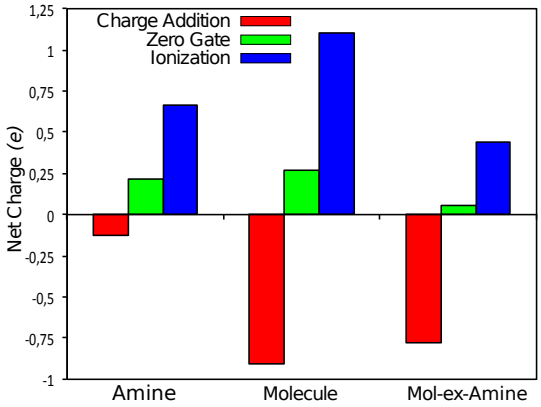

Figure 3.6: Hirshfeld projected charges for the three gated transport levels (the reference state and $\approx \pm e$ charged states), showing the difference in charging the molecule, amine groups and molecule-without-amine as the gate field is varied.

polarized leads – hence the chemical potentials for both spin directions are identical. However, it has been pointed out by several researchers that the spin-polarized states found in DFT calculations can give us valuable information about the levels and their occupation [12, 42, 43].

For the weak-coupling case, we see 'plateaus' occurring in the levels corresponding to fixed occupation demonstrating that only one type of spin is added to or removed from the system when changing the gate. These plateaus are sometimes interrupted by unpolarized points; we assign these to anomalies inthe self-consistency cycle.

In the stronger-coupling case, we also see plateaus, although they are less flat, and, importantly, they do not correspond to integer occupation, but slightly above. Apparently there is some 'extra' charge on the molecule in these cases – however, the deviations may also be related to the (Hirschfeld) calculation of the atomic charges. We conclude from figure 3.5 (a), that there is a constant background charge on the molecule, corresponding to $+0.05e$ per spin (see dashed line). The fact that the two easily identifiable plateaus (red curve around -10 eV and green curve around $+5$ eV) are separated by (very nearly) 1e per spin, indicates how charges should be added or removed from the reference state.

The reference charge of the molecule in the junction, for the relaxed geometry, is $+0.274e$. This is due to *both* spin directions – therefore we have a charge of $+0.137e$ per spin. In this state, the molecule has already some extra charge due to partial charge transfer across the interface [18]. This is a charge excess of $+0.087e$ with respect to the background charge $+0.05e$. In order to remove one electron from the molecule, we therefore need to add $+0.913e$ and to put an extra electron corresponds to $-1.087e$ (see Fig. 3.6).

Fig. 3.10 shows the compositions of the peaks in the transmission through the Au-BDA-Au junction near ϵ_f. For these, we project the eigenstates of the transport calculation onto the orbitals of the Au-BDA-Au fragment [11].

The HOMO projection is composed of many such orbitals as a result of the hybridiza-

tion with Au, in contrast to the LUMO, the LUMO+1 and the HOMO−1 states. The HOMO and LUMO+1 are more dominant in charge transport than the LUMO and HOMO−1 states which contribute weakly due to their strong localization at the center of the molecule. The interface states *A* and *B* do not show up as peaks in the transmission due their very low density at the center of the molecule – see Fig. 3.4.

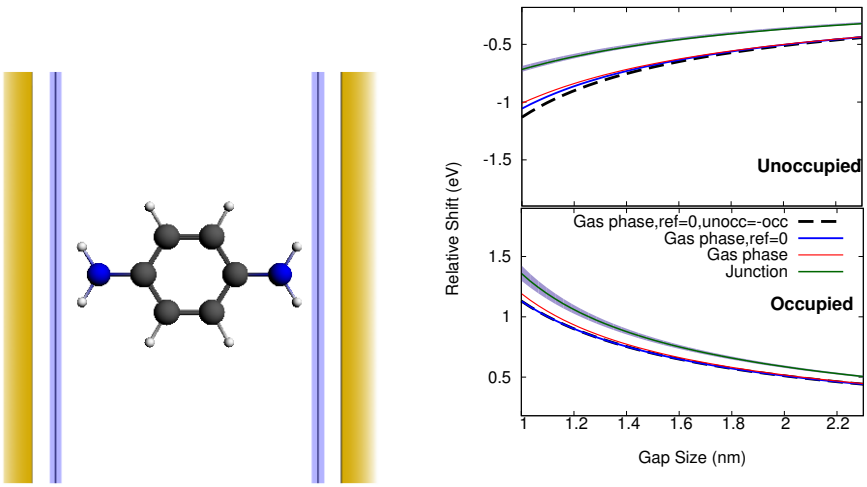

a) Geometry for Image-Charge Shifts b) Transport Gap Renormalization

Figure 3.7: (a) Geometry used in the image-charge model (with uncertainties) (b) Comparison of results for total image-charge corrections using charges from gas phase calculations of BDA and from the molecular junction as a function of the distance between the contacts.

We now consider the results for the calculation of the image charge effect. In Fig. 3.7 a), we show the geometry used for our image-charge calculation and in Fig. 3.7 b) we show the resulting shifts of the occupied and unoccupied levels as function of the distance between the two contacts. The uncertainty bands are calculated based on a ±0.25 Å uncertainty in the position of the image planes. In Fig. 3.7 (b), we also compare the results obtained by our method using different assumptions during the calculations. The dashed line is calculated using the gas phase charge distribution, zero charge on each atom for the reference state and omit the atomic charges associated with the EA, following the Mowbray et. al. assumptions. Using *different* charges for the calculation of the image charge effect of the occupied level (blue line), the symmetry for the shifts of the occupied and unoccupied levels is not maintained, although the curves remain close. Using the charge distribution of the neutral molecule as reference state (red line), these differences increase slightly. Finally, using the junction charge distribution (green line), results in a substantial difference. This shows that by using charges obtained with the junction geometry (from a NEGF+DFT calculation) for the image-charge calculation, we are including features that are absent when the gas phase charges are used.

3.4. AU-ZNTPPDT MOLECULAR DEVICES

We now proceed to a more complicated application of the method, which allows for comparison with a recent experiment that revealed the image-charge effects on both occupied and unoccupied molecular levels.

3.4.1. EXPERIMENTAL RESULTS

We consider the experimental findings of Perrin et. al. [26, 44, 45] who studied thiol-terminated zinc-porphyrin molecules [Zn(5,15-di(p-thiolphenyl)-10,20-di(p-tolyl)porphyrin)], abbreviated as ZnTPPdT. In the experiments, the current was recorded as a function of gate and bias voltage, and of the electrode separation. Peaks in the differential conductance were identified as transport resonances. These resonances show a marked "mechanical gating" effect, where a level shift is induced by a change in the metal-molecule distance (for both the occupied and unoccupied levels of the molecule). The efficiency of the effect can be expressed by a mechanical gate coupling (MGC) defined as

$$\epsilon_F = \frac{dV_b}{dx}, \tag{3.1}$$

where V_b is the bias voltage and x the electrode separation .

We show experimental data for these shifts in Fig. 3.8, where the measurements show a distance-dependent energy for the lowest resonance. A linear fit of the resonance positions was used to find the MGC. The broadness of the distribution is presumably due to the fact that ZnTPPdT is not a rod-like molecule; it can form molecular junctions with various geometries, as has been reported previously for similar molecules.[45]

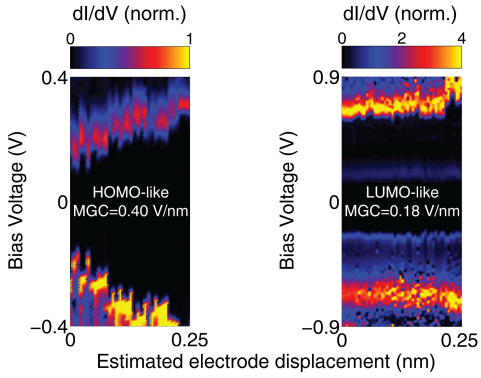

Figure 3.8: Representative measurement,[26] showing HOMO-like and LUMO-like observed MGC's. Note the dilation of the y-axis in the case of LUMO-like resonances.

The MGC's values are in the range of $0.2-1$ V_b/nm Combined with a typical range of 0.5 nm over which the junctions formed are stable, implying levels shift of roughly $50-250$ meV in energy, if we assume the bias voltage drops symmetrically. An average MGC values of 0.40 V/nm was found for occupied, and 0.18 V/nm for unoccupied levels.

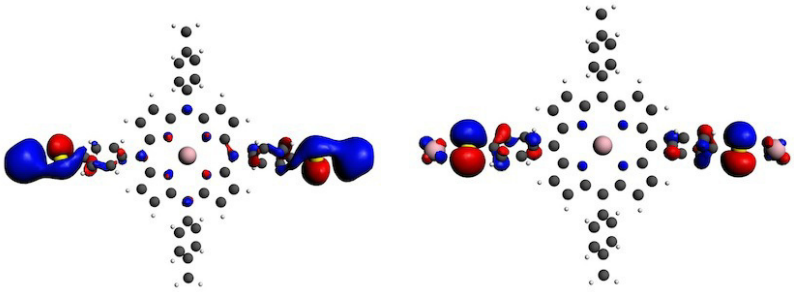

a) Interface State A b) Interface State B

Figure 3.9: Typical interface levels which form on hybridizing with Au: 6 total between the analogue of the gas phase HOMO and LUMO.

3.4.2. CALCULATIONS

We will now show that our approach yields trends matching the experiment, and explains the asymmetry in the shifts found between occupied and unoccupied levels.

We focus on the frontier orbitals (HOMO and LUMO) which are generally considered to be the most useful for transport. We find a the HOMO-LUMO gap to be 1.8 eV in our LDA and GGA calculations and 2.7 eV using the B3LYP functional, consistent with the reports of Park et. al.[46], and in general agreement with their redox measurements of roughly 2.2 eV.

Our Au-ZnTPPdT binding geometry is based on a phenyl ring bonded to an FCC (111) gold surface via a thiolate bond, in a hollow-site configuration.[47–50]

In the calculations, the binding is characterized by chemisorption, with significant charge transfer to the thiols, which act as acceptors. This is in agreement with the literature on such bindings. [51–55]

All calculations were performed using a TZP-basis of numerical atomic orbitals on the molecule, using the LDA functional with thiols located at a 2.59 Å from the electrodes.

In figure 3.9, we show two interface orbitals of the ZnTPP-fragment, which contains two extra gold atoms. There are six such states, in addition to the direct counterparts of the LUMO, HOMO and HOMO-1 of the gas phase. Of these six, two pairs relate to the HOMO, and one to the LUMO. The orbital levels in these fragment pairs appear to be of a bonding/anti-bonding character, with splittings on the order of 0.1 eV.

Fig. 3.10 shows the transmission of a typical transport calculation for the MCBJ geometry.

We observe a cluster of HOMO-like peaks near ϵ_f (defined as 0 eV), some small peaks inside the gap near 0.4 eV, and the nearly-degenerate LUMO and LUMO+1 around 1.7 eV. Fig. 3.10 (b), shows the decomposition of the transmission into fragment orbitals directly corresponding to molecular orbitals, and in Fig. 3.10 (c) for the interface orbitals.

The peaks right below the Fermi level derive mostly from the HOMO,[2] with significant amounts of interface levels mixed in. Fig. 3.10 (c) shows the role of the 6 interface levels labeled $L_{A,B}$, $H^1_{A,B}$ and $H^2_{A,B}$, derived from hybridization of HOMO and LUMO with

[2] Identified by analyzing the orbital symmetries of the wave functions of these levels.

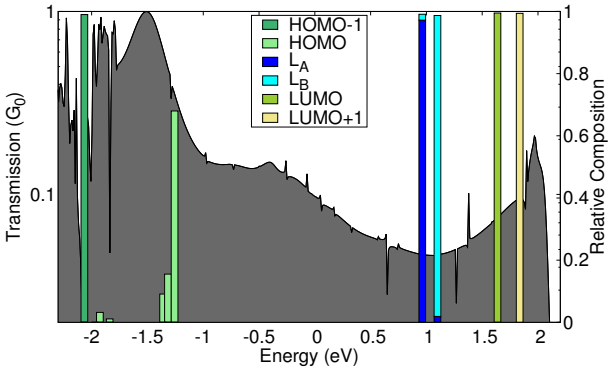

a) BDA peaks Decomposition with Molecular Orbital Levels (grey shaded curve is transmission)

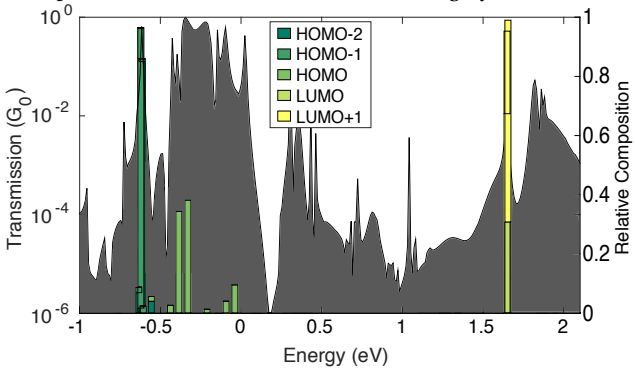

b) ZNTPPDT Peaks Decomposition with Molecular Orbital Levels (grey shaded curve is transmission)

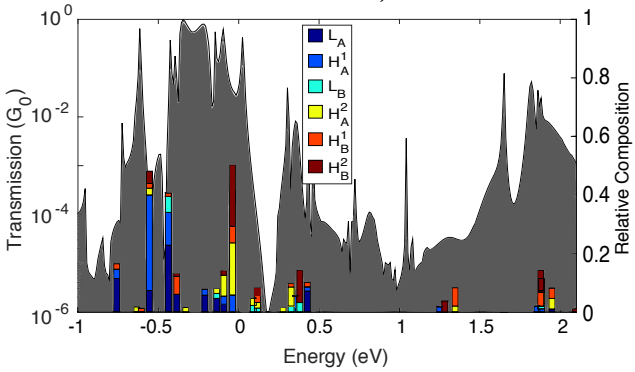

c) ZNTPPDT Peaks Decomposition with Interface Levels

Figure 3.10: Peaks Decomposition with fragment Orbital Levels (grey shaded curve is transmission). Composition of peaks in transport, constructed by projection onto fragment molecular orbitals. a) BDA molecule a state with value 1 is a decoupled state, and completely un-hybridized (HOMO-1), while HOMO, is strongly hybridized, with the rest originating from Au. b) ZNTPPDT molecule a state with value 1 is a decoupled state, and completely un-hybridized (HOMO-4 through –7), while HOMO-1, –2 and HOMO are strongly hybridized with each other *and* the Au electrodes (reflected in their 30-50% representation in the junction levels, with the rest originating from Au). The LUMO and LUMO+1 peaks are likewise strongly mixed with each other, coupling much less to the Au, reflected in the much narrower transport peaks near 1.7 eV. (a) As in (a) for the interface levels rather than for the molecular orbitals shown in (a).

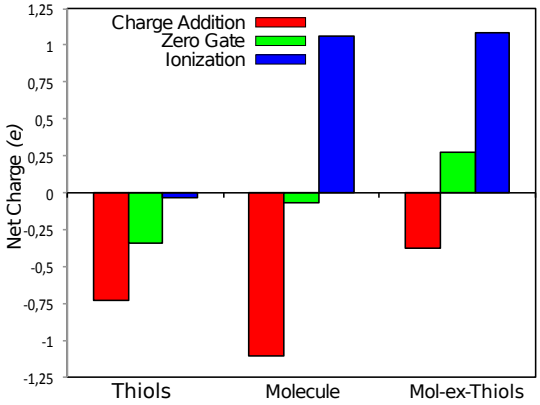

Figure 3.11: Partial charges for the three gated transport levels (the reference state and gated such that the net charge is $\approx \pm e$), showing the difference in charging the molecule, thiols and molecule-without-thiols as the gating is varied. At zero-field, the molecule is roughly neutral, with negative thiols and a positive core.

the gold.

For ZnPPTdT, the level splitting between the interface states is extremely small. This means that there is not a unique state going to be filled, and this precludes spin polarization and plateaus like those in Fig. 3.5 are absent. On the other hand, the total charge in the reference state is only $0.05e$, distributed over the two spin directions, and this will therefore contribute only very slightly to the difference between the curves for occupied and unoccupied levels. We therefore just add or subtract one unit charge in order to find the reduced and oxidized states.

We have applied our method for calculating image-charge effects to this junction. In the reference state the net charge is $-0.05e$ with a strongly negative charge ($-0.34e$) on the thiols, and $+0.29e$ on the rest of the molecule, mainly on the Zn ion. Figure 3.12 shows the difference in charge for the ionized $(N-1)$ states with respect to the reference state. This difference resides mostly on the arms, increasing the image charge effect a lot due to the proximity of the extra charge to the contacts.

The fact that in the reference state, the charge on the thiols is approximately the opposite of the charge on the rest of the molecule, is responsible for a significant difference in slope for the occupied and unoccupied levels.

The calculated level shifts as a function of distance are plotted in Fig. 3.13 (a). Our calculations predict MGC's in the range of $1.1-2.8$ eV/nm for an occupied level and $0.4-2.1$ eV/nm for an unoccupied level (in opposite directions), depending on the electrode separation. The different slopes differ significantly indeed, confirming the experimental findings.

To obtain this difference, a detailed calculation of the molecule inside the junction is essential. Using gas-phase orbitals, the wrong orbital (LUMO) would have been chosen as the unoccupied transport level, and the substantial contribution of the charge located at the arms of the hybridized HOMO would have been missed.

Our calculations reveal that the background image-charge effect contributes significantly to the MGC and explains the distance-dependent renormalization of the position

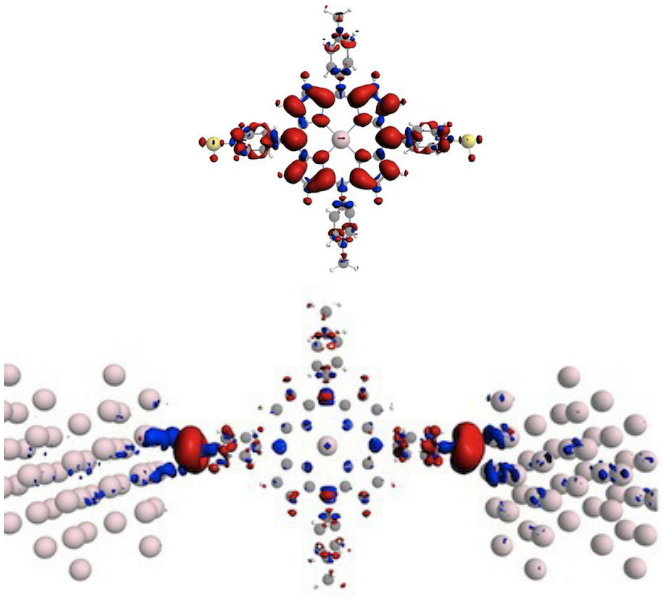

Figure 3.12: Difference in charge distribution in the $N+1$ relative to the N electron charge states. Red indicates the increase of negative charge when adding an electron; blue the decrease. Differences for (a) gas phase DFT calculations (LUMO like difference) and (b) for gated DFT+NEGF transport calculations (recalling the interface levels of Fig. 3.9).

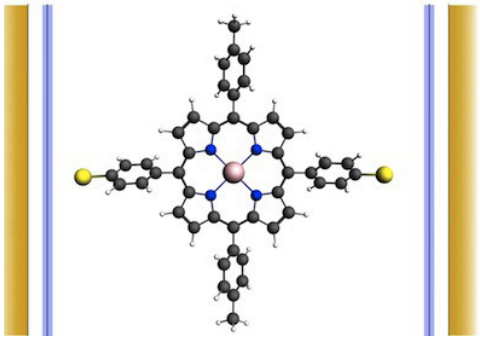

a) Geometry for Image-Charge Shifts

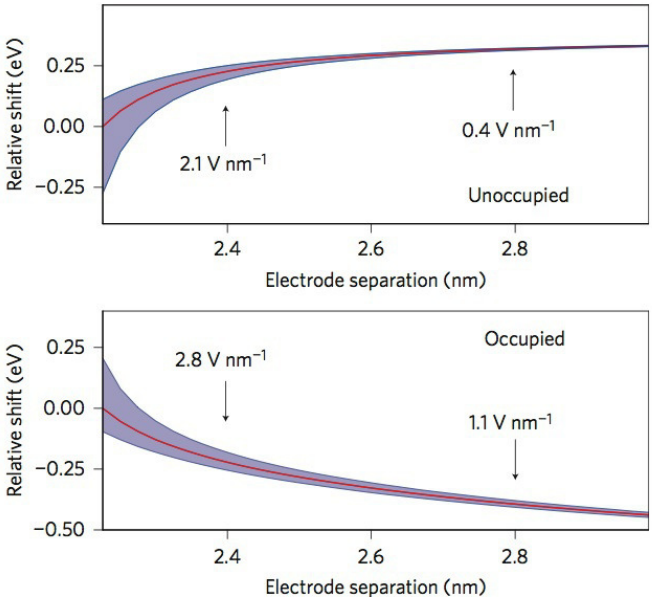

b) Transport Gap Renormalization

Figure 3.13: (a) Geometry used in the image-charge model, and (b) shifts predicted by the model (with uncertainties) showing the occupied- and unoccupied-levels both shifting towards ϵ_F with MGC's (the derivative with distance) in the range of 0.2 – 1.4 eV/nm, expressed in the symmetrically applied bias.

of the molecular orbital levels with respect to the Fermi level of the electrodes. Taking the reference state to be the gas phase neutral state suppresses the asymmetry between the shifts for occupied and unoccupied levels. This supports our conclusion that for the measurements of Fig. 3.8 an interface-stabilized level of the fragment has lost some charge, as is suggested by the peak above the Fermi level in our transport calculations, and that this level is being addressed in electron transport through the unoccupied state.

3.5. CONCLUSIONS

In summary, we have presented a method for calculating the image-charge effects which change the alignment of the occupied and unoccupied levels in molecular devices with the Fermi levels of the electrodes. Our approach is based on the charge distribution of the molecule in the junction in different charge states. It is essential to use these rather than their gas phase equivalents for two reasons. First, the relevant charge states may have a different character in gas phase molecules and molecules in a junction, due to the formation of "interface levels" in the latter. These are stabilized by the metal-molecule interface, and have no counterpart in the gas phase. Second, unlike in the gas phase, the reference state in the junction (at zero bias and gate) can carry a net charge, which implies a significant contribution to the reduction of the metal work function upon chemisorption of a molecule.

We have applied our method to a standard benzenediamine molecule and found results in good agreement with those obtained using Mowbray's et. al. model. The results differ however in our approach, mainly due to the nonzero charge in the reference state, and because we also address interface states that differ essentially from gas level orbitals.

Perrin et. al. [26] experiments on Au-ZnTPPdT reveal distance-dependent level shifts which are in agreement with our calculations. In this experiment, the fact that the reference state is non-neutral causes the MGC for occupied and unoccupied levels to be quite different. Our model agrees with the experimentally determined shifts within a factor of two.

Our approach demonstrates that for addressing image-charge effects within DFT, considering molecules in the junction is essential.

REFERENCES

[1] C. J. O. Verzijl, J. A. Celis Gil, M. L. Perrin, D. Dulić, H. S. J. van der Zant, and J. M. Thijssen, *Image effects in transport at metal-molecule interfaces,* The Journal of Chemical Physics **143**, 174106 (2015), http://dx.doi.org/10.1063/1.4934882.

[2] R. O. Jones and O. Gunnarsson, *The density functional formalism, its applications and prospects,* Rev. Mod. Phys. **61**, 689 (1989).

[3] Y. Meir and N. S. Wingreen, *Landauer formula for the current through an interacting electron region,* Phys. Rev. Lett. **68**, 2512 (1992).

[4] S. Datta, *Nanoscale device modeling: the green's function method,* Superlatt. Microstruct. **28**, 253 (2000).

[5] M. Brandbyge, J.-L. Mozos, P. Ordejón, J. Taylor, and K. Stokbro, *Density-functional method for nonequilibrium electron transport,* Phys. Rev. B **65**, 165401 (2002).

[6] K. Stokbro, J. Taylor, M. Brandbyge, and P. Ordejón, *TranSIESTA – a spice for molecular electronics,* Ann. N.Y. Acad. Sci. **1006**, 212 (2003).

[7] F. Evers, F. Weigend, and M. Koentopp, *Coherent transport through a molecular wire: Dft calculation,* Physica E: Low-dimensional Systems and Nanostructures **18**, 255 (2003), 23rd International Conference on Low Temperature Physics (LT23).

[8] A. R. Rocha, V. M. García-Suárez, S. Bailey, C. Lambert, J. Ferrer, and S. Sanvito, *Spin and molecular electronics in atomically generated orbital landscapes,* Phys. Rev. B **73**, 085414 (2006).

[9] F. Evers and A. Arnold, *CFN Lectures on Functional Nanostructures*, 1st ed., edited by C. Röthig, G. Schön, and M. Vojta, Springer Lecture Notes in Physics, Vol. 2 (Springer, 2006) pp. 27–54.

[10] A. Arnold, F. Weigend, and F. Evers, *Quantum chemistry calculations for molecules coupled to reservoirs: Formalism, implementation, and application to benzenedithiol,* J. Chem. Phys. **126**, 174101 (2007).

[11] C. J. O. Verzijl and J. M. Thijssen, *A DFT-based molecular transport implementation in ADF/BAND,* J. Phys. Chem. C **116**, 24393 (2012).

[12] K. Burke, *Perspective on density functional theory,* J. Chem. Phys. **136**, 150901 (2012).

[13] J. P. Perdew and A. Zunger, *Self-interaction correction to density-functional approximations for many-electron systems,* Phys. Rev. B **23**, 5048 (1981).

[14] C. Toher, A. Filippetti, S. Sanvito, and K. Burke, *Self-interaction errors in density-functional calculations of electronic transport,* Phys. Rev. Lett. **95**, 146402 (2005).

[15] M. S. Hybertsen and S. G. Louie, *Electron correlation in semiconductors and insulators: Band gaps and quasiparticle energies,* Phys. Rev. B **34**, 5390 (1986).

[16] J. B. Neaton, M. S. Hybertsen, and S. G. Louie, *Renormalization of molecular electronic levels at metal-molecule interfaces,* Phys. Rev. Lett. **97**, 216405 (2006).

[17] F. Aryasetiawan and O. Gunnarsson, *The GW method,* Rep. Prog. Phys. **61**, 237 (1998).

[18] K. S. Thygesen and A. Rubio, *Renormalization of molecular quasiparticle levels at metal-molecule interfaces: Trends across binding regimes,* Phys. Rev. Lett. **102**, 046802 (2009).

[19] G. Stefanucci and C.-O. Almbladh, *Time-dependent partition-free approach in resonant tunneling systems,* Phys. Rev. B **69**, 195318 (2004).

[20] S. Kurth, G. Stefanucci, C.-O. Almbladh, A. Rubio, and E. K. U. Gross, *Time-dependent quantum transport: A practical scheme using density functional theory,* Phys. Rev. B **72**, 035308 (2005).

[21] E. Perfetto, G. Stefanucci, and M. Cini, *Correlation-induced memory effects in transport properties of low-dimensional systems,* Phys. Rev. Lett. **105**, 156802 (2010).

[22] S. Quek, L. Venkataraman, H. Choi, S. Louie, M. Hybertsen, and J. Neaton, *Amine–gold linked single-molecule circuits: Experiment and theory,* Nano Lett. **11**, 3477 (2007).

[23] D. J. Mowbray, G. Jones, and K. S. Thygesen, *Influence of functional groups on charge transport in molecular junctions,* J. Chem. Phys. **128**, 111103 (2008).

[24] P. Hedegård and T. Bjørnholm, *Charge transport through image charged stabilized states in a single molecule single electron transistor device,* Chem. Phys. **319**, 350 (2005).

[25] K. Kaasbjerg and K. Flensberg, *Strong polarization-induced reduction of addition energies in single-molecule nanojunctions,* Nano Lett. **8**, 3809 (2008).

[26] M. L. Perrin, C. J. O. Verzijl, C. A. Martin, A. J. Shaikh, R. Eelkema, van EschJan H., J. M. van Ruitenbeek, J. M. Thijssen, H. S. J. van der Zant, and D. Dulić, *Large tunable image-charge effects in single-molecule junctions,* Nat Nano **8**, 282 (2013).

[27] H. Ishii, H. Oji, E. Ito, N. Hayashi, D. Yoshimura, and K. Seki, *Energy level alignment and band bending at model interfaces of organic electroluminescent devices,* J. Lumin. **87-89**, 61 (2000).

[28] K. Seki, E. Ito, and H. Ishii, *Energy level alignment at organic-metal interfaces studied by uv photoemission,* Synth. Met. **91**, 137 (1997), International Conference on Electroluminescence of Molecular Materials and Related Phenomena.

[29] H. Ishii, K. Sugiyama, E. Ito, and K. Seki, *Energy level alignment and interfacial electronic structures at organic-metal and organic-organic interfaces,* Adv. Mat. **11**, 605 (1999).

[30] H. Vázquez, F. Flores, R. Oszwaldowski, J. Ortega, R. Pérez, and A. Kahn, *Barrier formation at metal-organic interfaces: dipole formation and the charge neutrality level,* Appl. Surf. Sci. **234**, 107 (2004), the Ninth International Conference on the Formation of Semiconductor Interfaces.

[31] H. Vázquez, R. Oszwaldowski, P. Pou, J. Ortega, R. Pérez, F. Flores, and A. Kahn, *Dipole formation at metal/ptcda interfaces: Role of the charge neutrality level,* Europhys. Lett. **65**, 802 (2004).

[32] R. Oszwaldowski, H. Vázquez, P. Pou, J. Ortega, R. Pérez, and F. Flores, *Exchange-correlation energy in the orbital occupancy method: electronic structure of organic molecules,* J. Phys.: Condens. Matter **15**, S2665 (2003).

[33] S. Duhm, G. Heimel, I. Salzmann, H. Glowatzki, R. L. Johnson, A. Vollmer, J. P. Rabe, and N. Koch, *Orientation-dependent ionization energies and interface dipoles in ordered molecular assemblies,* Nat. Mater. **7**, 326 (2008).

[34] B. Bröker, O. T. Hofmann, G. M. Rangger, P. Frank, R.-P. Blum, R. Rieger, L. Venema, A. Vollmer, K. Müllen, J. P. Rabe, A. Winkler, P. Rudolf, E. Zojer, and N. Koch, *Density-dependent reorientation and rehybridization of chemisorbed conjugated molecules for controlling interface electronic structure,* Phys. Rev. Lett. **104**, 246805 (2010).

[35] J. Niederhausen, P. Amsalem, J. Frisch, A. Wilke, A. Vollmer, R. Rieger, K. Müllen, J. P. Rabe, and N. Koch, *Tuning hole-injection barriers at organic/metal interfaces exploiting the orientation of a molecular acceptor interlayer,* Phys. Rev. B **84**, 165302 (2011).

[36] M. Hybertsen, L. Venkataraman, J. Klare, A. Whalley, M. Steigerwald, and C. Nuckolls, *Amine-linked single molecule circuits: Systematic trends across molecular families,* J. Phys.: Condens. Matter **20**, 374115 (2008).

[37] S. Kubatkin, A. Danilov, M. Hjort, J. Cornil, J.-L. Bredas, N. Stuhr-Hansen, P. Hedegård, and T. Bjornholm, *Single-electron transistor of a single organic molecule with access to several redox states,* Nature **425**, 698 (2003).

[38] C. Bruot, J. Hihath, and N. Tao, *Mechanically controlled molecular orbital alignment in single molecule junctions,* Nat. Nano **7**, 35 (2012).

[39] F. Evers and A. Arnold, *Molecular conductance from ab initio calculations: Self energies and absorbing boundary conditions,* in *CFN Lectures on Functional Nanostructures - Volume 2*, Lecture Notes in Physics, Vol. 820, edited by M. Vojta, C. Rthig, and G. Schn (Springer Berlin Heidelberg, 2011) pp. 27–53.

[40] G. te Velde and E. J. Baerends, *Precise density-functional method for periodic structures,* Phys. Rev. B **44**, 7888 (1991).

[41] G. Wiesenekker and E. J. Baerends, *Quadratic integration over the three-dimensional brillouin zone,* J. Phys.: Condens. Matter **3**, 6721 (1991).

[42] Z.-F. Liu, J. P. Bergfield, K. Burke, and C. A. Stafford, *Accuracy of density functionals for molecular electronics: the anderson junction,* Phys. Rev. B **85**, 155117 (2012).

[43] J. P. Bergfield, Z.-F. Liu, K. Burke, and C. A. Stafford, *Bethe ansatz approach to the kondo effect within density-functional theory,* Phys. Rev. Lett. **108**, 066801 (2012).

[44] M. L. Perrin, C. A. Martin, F. Prins, A. J. Shaikh, R. Eelkema, J. H. van Esch, J. M. van Ruitenbeek, H. S. J. van der Zant, and D. Dulić, *Charge transport in a zinc-porphyrin single-molecule junction,* Beilstein J. Nanotechnol. **2**, 714 (2011).

[45] M. L. Perrin, F. Prins, C. A. Martin, A. J. Shaikh, R. Eelkema, J. H. van Esch, T. Briza, R. Kaplanek, V. Kral, J. M. van Ruitenbeek, H. S. J. van der Zant, and D. Dulić, *Influence of the chemical structure on the stability and conductance of porphyrin single-molecule junctions,* Angew. Chem. **123**, 11419 (2011).

[46] J. K. Park, H. R. Lee, J. Chen, H. Shinokubo, A. Osuka, and D. Kim, *Photoelectrochemical properties of doubly β-functionalized porphyrin sensitizers for dye-sensitized nanocrystalline-tio2 solar cells,* J. Phys. Chem. C **112**, 16691 (2008).

[47] J. Nara, W. T. Geng, H. Kino, N. Kobayashi, and T. Ohno, *Theoretical investigation on electron transport through an organic molecule: Effect of the contact structure,* J. Chem. Phys. **121**, 6485 (2004).

[48] D. Q. Andrews, R. Cohen, R. P. V. Duyne, and M. A. Ratner, *Single molecule electron transport junctions: Charging and geometric effects on conductance,* J. Chem. Phys. **125**, 174718 (2006).

[49] H. Kondo, H. Kino, J. Nara, T. Ozaki, and T. Ohno, *Contact-structure dependence of transport properties of a single organic molecule between au electrodes,* Phys. Rev. B **73**, 235323 (2006).

[50] R. B. Pontes, A. R. Rocha, S. Sanvito, A. Fazzio, and A. J. R. da Silva, *Ab initio calculations of structural evolution and conductance of benzene-1,4-dithiol on gold leads,* ACS Nano **5**, 795 (2011).

[51] Y. Xue and M. A. Ratner, *Microscopic study of electrical transport through individual molecules with metallic contacts. i. band lineup, voltage drop, and high-field transport,* Phys. Rev. B **68**, 115406 (2003).

[52] Y. Xue and M. A. Ratner, *Microscopic study of electrical transport through individual molecules with metallic contacts. ii. effect of the interface structure,* Phys. Rev. B **68**, 115407 (2003).

[53] J. C. Love, L. A. Estroff, J. K. Kriebel, R. G. Nuzzo, and G. M. Whitesides, *Self-assembled monolayers of thiolates on metals as a form of nanotechnology,* Chem. Rev. **105**, 1103 (2005).

[54] R. Hoft, M. Ford, and M. Cortie, *Prediction of increased tunneling current by bond length stretch in molecular break junctions,* Chem. Phys. Lett. **429**, 503 (2006).

[55] L. Romaner, G. Heimel, M. Gruber, J.-L. Brédas, and E. Zojer, *Stretching and breaking of a molecular junction,* Small **2**, 1468 (2006).

4

TRANSPORT GAP RENORMALIZATION AT A METAL-MOLECULE INTERFACE USING DFT-NEGF AND SPIN UNRESTRICTED CALCULATIONS

And why do we fall?
So we can learn to pick ourselves up.

Thomas Wayne
Batman begins. Dir. C. Nolan CA: Warner Home Video, 2005

A method is presented for predicting one-particle energies for a molecule in a junction with one metal electrode, using DFT methods. In contrast to previous work, in which restricted spin configurations were analyzed, we take spin polarization into account. Furthermore, in addition to junctions in which the molecule is weakly coupled, our method is also capable of describing junctions in which the molecule is chemisorbed to the metal contact. We implemented a fully self consistent scissor operator to correct the HOMO LUMO gap in transport calculations for single molecule junctions. We present results for various systems and compare our results with those obtained by other groups.

This chapter has been published in The Journal of Chemical Physics 147, 084102 (2017) [1]

4.1. INTRODUCTION

A major issue in calculations of molecular electronics devices is the alignment of molecular orbital levels relative to the Fermi energy of the metal electrodes.

In the gas phase, molecules have well defined energy levels, two of which relate to the orbitals that play a major role in charge transport: the highest occupied molecular orbital (HOMO) and the lowest unoccupied molecular orbital (LUMO).

According to Koopmans´ theorem, within the Hartree Fock approximation, the energy needed to remove one electron from an isolated molecule, known as Ionization Potential (IP), is equal to the energy difference between HOMO and vacuum level [2, 3]. Similarly, the Electron Affinity (EA), which is the energy needed to put an extra electron into the molecule, is the energy difference between the LUMO and the vacuum level. Koopmans theorem predicts the HOMO and LUMO levels in Hartree-Fock reasonably well. When the molecule is close to a metal surface, the molecular energy levels shift, due to various reasons, such as image charge formation and a modification of the interface dipole [4–7].

In DFT, Janack´s theorem predicts the HOMO in an analogous way, but there, orbital relaxation effects make this theorem unusuable in small systems, or large systems with weak polarization [8–11].

It has been demonstrated experimentally that the vicinity of a metal electrode leads to a reduction of the gap between the ionization potential and electron affinity of a molecule with respect to that of the gas phase [12–15]. The reduction of the IP and EA of the molecule is mainly due to the Coulomb interaction between the added charge on the molecule and the screening electrons in the leads. This feature, called the image-charge effect [5, 6, 16–18] becomes more relevant as the molecule gets closer to the metallic surface.

In standard DFT, approximations for the exchange and correlation potentials, which are widely used in transport calculations, do not account for the nonlocal correlation effects responsible of the adjustment of the frontier levels [19–22].

One way to include these non-local effects is to use the GW approximation constructed on top of DFT [23–25]. This approach has successfully predicted level alignment [16, 26–31]. However the GW scheme is very expensive computationally, which limits the size of the system that can be analyzed within this scheme, especially in a junction, which includes many lead atoms.

In the weak coupling regime, other methods like Constrained density functional theory (CDFT) and density functional theory together with non-equilibrium Green's function technique (DFT-NEGF) have been implemented to analyze the level alignment at the interfaces [18, 32–34].

In the work presented by Souza et al.[32], CDFT is used to determine the charge-transfer energy of a molecule physisorbed on a metallic surface. This method gives quantitatively accurate results at small molecule-metal separations, however in order to obtain quantitatively converged results, large metal cluster sizes are needed for large distances, and metal atoms with a few valence electrons must be use in order to keep the calculations manageable.

Using classical electrodynamics, it is possible to predict the level shifts close to a metallic surface [5, 6, 16–18]. In a previous chapter, we calculated the energy level ad-

justment of a molecule in the junction caused by image-charge effects using classical electrostatics [18]. Atomic charges for the molecule in the junction (from a NEGF-DFT calculation) rather than in the gas phase were used for the image-charge calculation. In this way, features that are absent in the gas phase are included. First, with the formation of interface levels, the relevant charge states of the molecule have a different character in gas phase than in a junction; and second, the reference state in the junction (at zero bias and gate) can carry a net charge, which implies a significant contribution to the reduction of the metal work function upon chemisorption of a molecule. However, with this approximation, only the level *shifts* are calculated but the values of the IP, EA and EA-IP gap can not be calculated explicitly.

Another method, introduced by Stadler et al. [33, 34], makes use of the NEGF formalism and calculates the addition energy for single molecule junctions in the Coulomb blockade regime. This method puts less severe restrictions on the kind of atoms that can be used for the leads than the Souza's approach. However, in this work, the input energy required for the transfer of one electron from the molecule to the electrodes or vice versa in terms of the external potential was calculated without taking into account anchoring groups, hence partial charge transfer cannot be accounted for. The results are therefore not directly applicable to experimental transport junctions with chemisorbed molecules. Stadler's method uses the electrostatic energy calculated in the transport code – no classical electrostatic calculation is needed.

In the present chapter, we adapt the method introduced by Stadler et al. to explicitly calculate the IP and the EA of a molecule close to a metallic electrode. We perform spin unrestricted calculations varying the gate voltage and we obtain the charge state of the molecule for every gate. To determine the energy needed to add/remove one electron, we take into account the partial charge transfer between molecule and lead. Initially, we consider a benzene ring, which is a standard molecule for this kind of calculations, and then we show that our method is valid even if we take into account anchoring groups and short molecule-metal separations. Additionally we implemented the CDFT method to speed up the process. In our implementation into the transport module of ADF-BAND, the determination of the potential shift in the CDFT method is automated for efficiency, in this way the location of the ionization and addition level are accurately determined. The DFT eigenvalues corresponding to the occupied and unoccupied levels can be shifted to those values by mean of a scissors operator such that the transmission through the junction is corrected, improving the conductance value when compared to experimental data.

In Section 4.3, we shall apply our method to a benzene ring, which is a standard molecule for this type of calculations in front of a metallic lead. We use two different materials for the lead and we compare our results with those obtained by others. In Section 4.4, we include anchoring groups and we apply our method to the 1,4 Benzenediamine molecule. We compare our results with those predicted by an electrostatic calculation of image charge effect. In Section 4.5, we extend our method to a single molecule junction formed by a 1,4 Benzenediamine molecule connected to two gold electrodes. Then we apply a fully self consistent field (SCF) scissors operator to correct the transmission through the molecular junction.

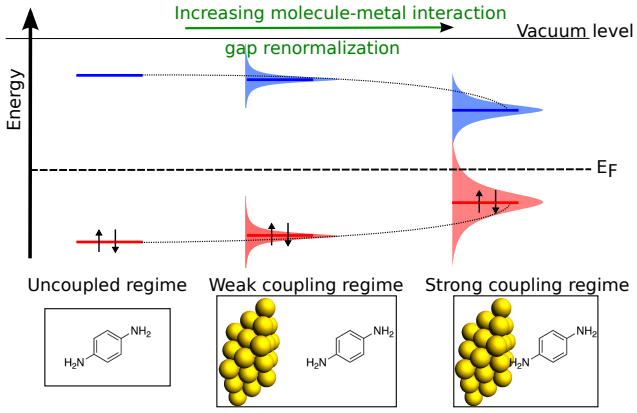

Figure 4.1: Schematic drawing of the molecular orbitals with respect to the Fermi energy (E_F). (left) Isolated molecule. (Middle) The molecule interacts with the metal lead only via long-range interactions. (Right) Chemical bonds between the molecule and the lead.

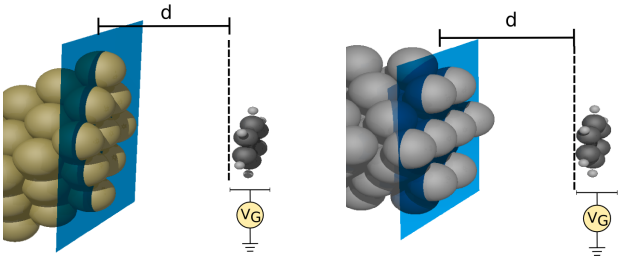

Figure 4.2: Cases studied with a benzene molecule parallel to a gold 111 (left) and a lithium 100 plane (right) lead surface. We show how we define the distance d and the gate applied over the molecule.

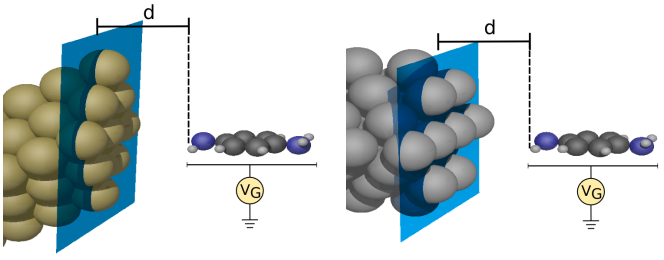

Figure 4.3: Scheme showing the 1,4 BDA and the lead. We show how we define the distance d and the Gate applied on the molecule for every lead. Gold lead (left), lithium lead (right).

4.2. MODEL

One of the most used experimental techniques for molecular devices is the mechanically controlled break junction (MCBJ). In this technique, a wire is suspended on top of a substrate that can bend. The bending results in a stretching of the top wire which may

break and form a nano-gap. We adapt the model implemented by Verzijl et. al. [35] to analyze the level alignment of a molecule in front of the nanowire and we perform spin unrestricted calculations[36] in the DFT-NEGF scheme.

We locate a planar molecule at a distance d in front of the lead surface. The distance d is the smallest distance measured from the centers of the atoms in the molecule to the lead surface (see Figures 4.2 and 4.3). We apply a gate potential, which is constant across the molecule, with the molecule defined as all the non-metallic atoms. The gate is applied to the orbitals of the electrons of the molecule (see supp. inf. ref. [18]) and we obtain the electronic configuration of the system after the self consistent procedure within the DFT-NEGF framework.

When the peak of the broadened levels aligns with the electrode's Fermi level, half of that level is occupied, so that the gate needed to remove half electron from the molecule corresponds to the IP_{mol} and the gate needed to add half corresponds to the EA_{mol} [33].

We analyze the spin resolved occupation of the molecule, which indicates how the filling of the individual levels changes upon varying the gate. Because of its nature as spatial decompositions, we prefer to use the spin-projected Hirshfeld charge decompositions rather than the basis-set decompositions like Mulliken.

Depending on the coupling strength between the molecule and the lead (Γ) with respect to the quantum splitting and the Coulomb repulsion for electrons at the relevant level (U), we distinguish three regimes (see Fig. 4.1). (i) Uncoupled ($\Gamma = 0$), (ii) the molecule and the lead are weakly coupled ($\Gamma < \Delta E$) and (iii) the molecule is strongly coupled to the lead ($\Gamma > \Delta E$). With ΔE the level splitting.

In the uncoupled regime, there is no partial charge transfer or broadening of the molecular energy levels which remain sharply defined. This regime appears when the molecule is very far from the electrode.

In the weak coupling regime, we have some broadening of the molecular energy levels. In the uncoupled and the weakly coupled regime, the molecule has approximately integer charge and spin $\frac{1}{2}$ or 0, hence the charge forms plateaus and present spin polarization when viewed as a function of the gate.

At large molecule-electrode separations, we would expect plateaus in the occupation of the different levels versus gate voltage. However, in DFT such plateaus do not occur, even for an isolated molecule. This due to the absence of the derivative discontinuity in the local functional used [37]. However, it has been pointed out by several researchers that the spin-polarized states found in DFT calculations can give valuable information about the many-body resonances of the spectral density [38–41].

Finally, in the strong coupling regime, the lead and the molecule are connected, leading to charge transfer across the interface, even at zero bias and gate[42], which contributes to the reduction of the EA-IP gap. The charge excess in the molecule is calculated with respect to the neutral state of the isolated molecule [18].

In the first two regimes, as the partial charge transfer at zero gate is very small, the molecule is expected to be neutral. This simplifies the process to determine the IP and EA. We determine the gate that we need in order to add or remove half integer charge to or from the molecule in the reference configuration (zero bias and gate) using our implementation of a CDFT method into the DFT-NEGF framework.

In CDFT, the minimum of the energy functional is searched under the constraint that

the charge, which is calculated as

$$N_{added} = \int_{molecule} n(\mathbf{r}) d^3 r, \tag{4.1}$$

has a predefined value.

The constraint is realized through a Lagrange parameter V, which translates into a gate potential applied to the molecule [43–45]. This extra potential is equivalent to a constant gate voltage and has been implemented in our transport code. We also implement an automated algorithm for finding the gate which gives a desired charge. This implementation reduces the cpu time substantially.

It is important to emphasize that there no classical image charge effect calculation is performed – the image charge effect is fully accounted for by the Hartree potential calculation done by DFT. The fact that the self-energy keeps the part of the contact not facing the molecule neutral is crucial for this.

4.3. BENZENE

We first consider a benzene molecule, with its plane parallel to the electrode surface. We use two different metal leads, Au and Li. Au is frequently used in experiments and Li allows us to compare our results with those obtained by Souza et al. [32] for the same system. Additionally, we compare the effects on the level alignment for both lead materials.

For the gold lead, we use a scattering region that contains 27 atoms arranged in a FCC lattice, whereas for the Li lead, the scattering region contains 32 atoms arranged in a BCC lattice. All the metal atoms are fixed at the crystal lattice positions. For Au, the lattice constant is 4.0782 Å and for Li 3.51 Å. In both cases, we do not consider periodic boundary conditions parallel to the surface of the electrode and there is no chemisorption between the surfaces and the molecule.

For our calculations, we use a DZP-basis of numerical atomic orbitals on the molecule, a SZ-basis of numerical atomic orbitals on the gold atoms, a DZ-basis of numerical atomic orbitals on the lithium atoms and the Perdew, Burke, and Ernzerhof (PBE) parametrization of the Generalized Gradient Approximation (GGA) functional in our implementation of NEGF-based transport in the Amsterdam Density Functional (ADF)/band quantum chemistry package [35, 46, 47].

Figure 4.4 shows the spin-resolved number of electrons on the molecule which is placed in front of a gold/lithium lead as a function of the applied gate for $d = 2$Å, $d = 6$Åand $d = 14$Å. We observe plateaus around zero gate corresponding to the (almost) neutral state, except for the chemisorbed molecules (2Å), as expected.

For short separation, for zero gate, we observe a charge, close, but not exactly equal to zero. This charge is due to interfacial charge transfer; there is no spin polarization. Changing the gate towards negative values, the spin polarization is still absent, whereas positive gate voltages quickly lead to splitting of the charge across the two spins. These configurations regularly switch to spin-polarized ones and back. Furthermore, the average curve shows an inflection close to zero gate voltage.

To determine the IP and EA, we identify the spin polarized plateau close to the neutral configuration. This plateau determines the background charge state of the molecule.

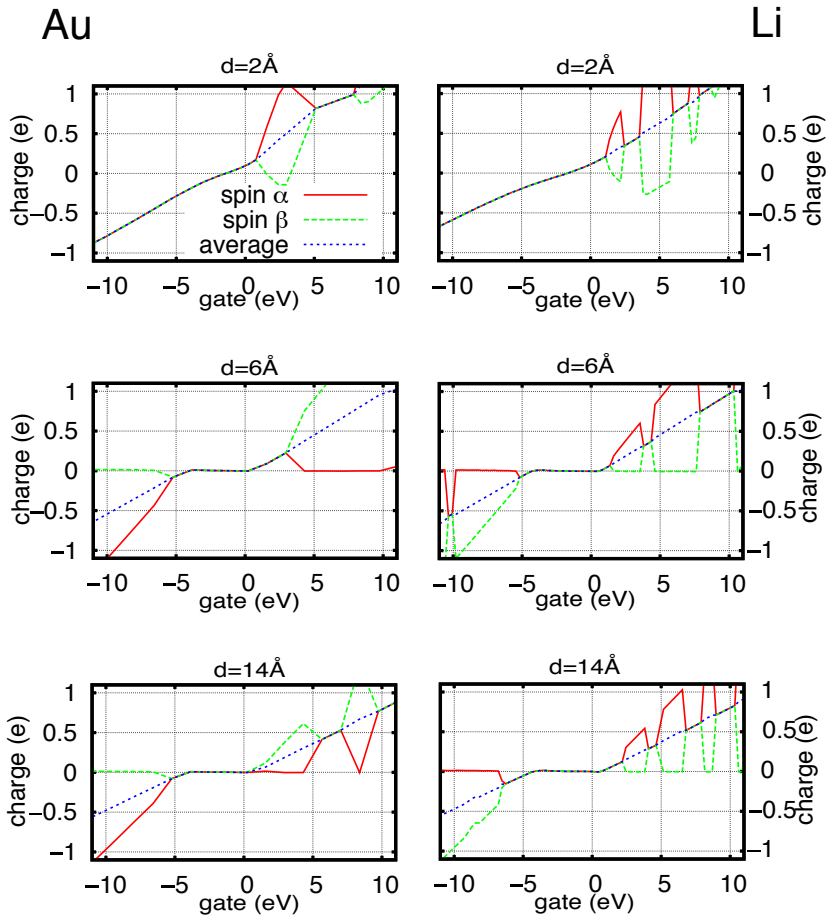

Figure 4.4: Hirshfeld spin-resolved charge excess in the benzene as a function of the applied gate for a distance equal to 2 Å, 6 Å and 14 Å between the lead and the molecule, using a Au lead (left) and a Li lead (right). Positive values in the charge mean that electrons have been removed from the molecule.

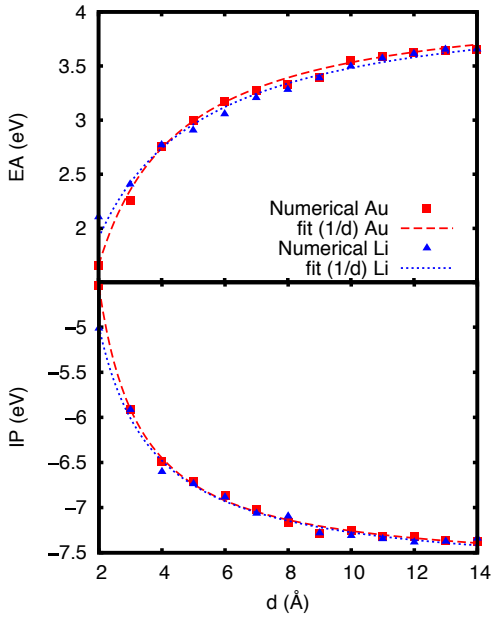

Figure 4.5: Ionization potential and electron affinity calculated in eV as a function of the distance between the Benzene and the lead in (Å) using **a)** gold lead and **b)** lithium lead.

Then, we look for the gate needed to remove/add half charge (IP/EA) with respect to the background.

In the case of larger separations, the background charge state coincides with zero charge excess as partial charge transfer at zero gate is absent.

In the uncoupled regime, the polarization is less constant than in the weak coupling regime, and the system switches between non-polarized charge and polarized charge.

Comparing the charge occupations for the different separations (Fig. 4.4), the presence of polarization is more common in the weak coupling condition $\Gamma < \Delta E$. Polarization should not occur or be less present when $\Gamma > \Delta E$. This appears to be the case when the molecule is close to the lead. Independently of the regime, the spin polarization is more common to switch on when the total charge excess in the molecule is a multiple integer of 0.5 e, it means just after an energy peak of the molecule is aligned with the electrode's Fermi energy. Whereas the charge excess for one of the spins stays constant, the other one changes, which indicates, as we established in section 4.2, that only one type of spin is added to or removed from the system. However, for this case of a benzene ring facing a lead in a parallel position, the behavior is rather switchy and it does always show clear plateaus, probably because of the absence of a derivative discontinuity in the XC potential.

In figure 4.5 we show the IP and EA as a function of the distance between the lead and the molecule for the two different metals used.

We fit our data using the electrostatic energy of a point charge q located in vacuum

at a distance d in front of a semi-infinite conductor, given by

$$V = \frac{qq'}{4d}. \tag{4.2}$$

We see that our method reproduces the image charge effect well. Furthermore, the differences between the two lead materials considered are small.

With a lithium lead, the image-charge plane that we obtained from our fits are 1.32 ± 0.06 Å and 1.41 ± 0.05 Å for the IP and the EA respectively. These values are in good agreement with the results obtained by Garcia-Lastra et al.[27] of 1.62 Å and Souza et al.[32] of 1.72 Å for EA and 1.80 Å for IP. The values obtained with a gold lead are 0.68 ± 0.07 Å for the IP and 0.58 ± 0.09 Å for the EA. In general the values obtained for the image-plane with gold are smaller; we attribute this effect to the higher electronic density of gold close to the surface.

Table 4.1: Comparison of benzene IP and EA. The first column shows the EA/IP obtained using our method with the molecule in front of two different metallic leads in the limit of large distances. The next two columns show the results obtained by Stadler et al.[34] and Souza et al.[32] respectively. Then the "Gas phase" column shows the results obtained Hartree-Fock, ΔSCF and GW[27] methods. In the last columns we show the experimental results reported in [48] and [49]

	Present work		Stadler	Souza	Gas phase			Exp.
	Au	Li	Al	Li	HF	ΔSCF	GW	
IP (eV)	7.70± .03	7.77± .06	–	7.38	9.64	9.74	7.9	9.4[48]
EA (eV)	4.14± .05	4.15± .07	–	4.89	3.18	1.50	2.7	1.1[49]
Gap (eV)	11.84± .08	11.92± .13	11.54	12.27	12.82	11.24	10.6	10.5

In our calculations and fits, we find that the values for the image-charge plane obtained are in general different for occupied and unoccupied energy levels. This is because the shape of the molecular orbitals also affect the size of the polarization giving as a result different behaviors in every case. We will return to this point with the BDA molecule in Sec. 4.4.

In table 4.1, we compare our results for the IP and EA with those obtained using other methods for gas phase ΔSCF, Hartree-Fock and GW[27], and methods that consider metallic surfaces like DFT-NEGF and CDFT. We can see that our results are in good agreement with those obtained by other authors.

4.4. 1,4 BENZENEDIAMINE (BDA)

We now proceed to a system in which covalent bonds may occur, due to anchoring groups at the ends of the molecule. In this case the molecule has a different orientation with respect to the lead.

We put a 1,4 BDA molecule in front of the lead with the carbon atoms plane perpendicular to the lead surface. One of the amine groups of the molecule is located at a distance d from the electrode (Fig. 4.3). For this molecule we use a DZP-basis of numerical atomic orbitals and the GGA functional.

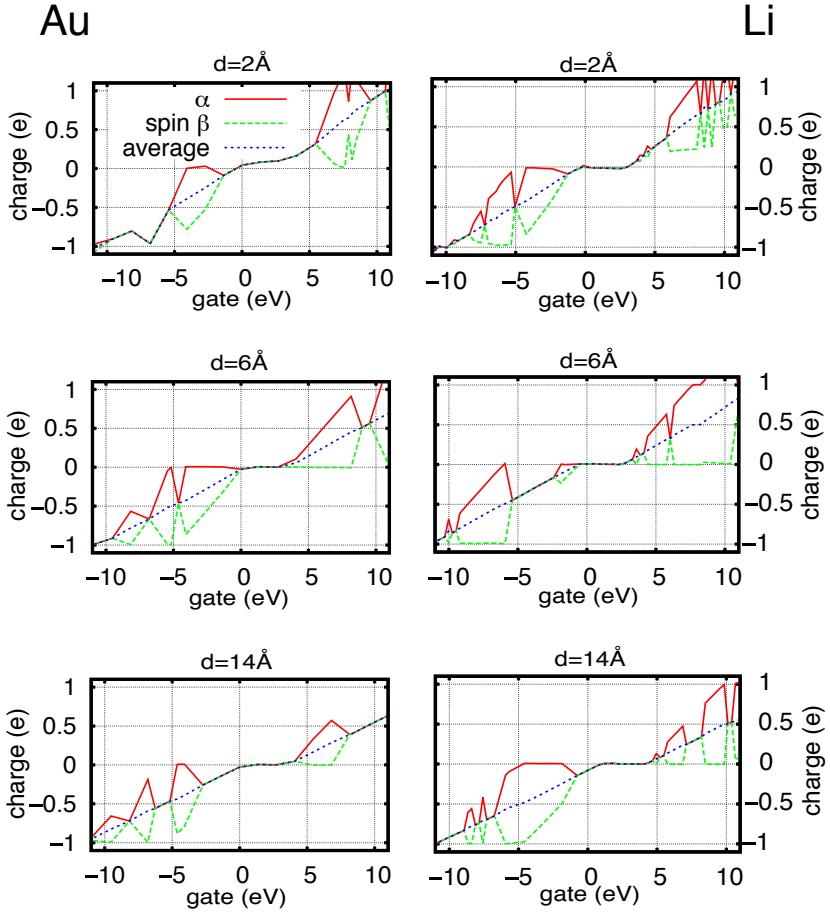

Figure 4.6: Spin resolved Hirshfeld charge excess in the 1,4 BDA as a function of the applied gate for a distance equal to 2 Å, 6 Å and 14 Å between the lead and the molecule, using a Au lead (left) and a Li lead (right).

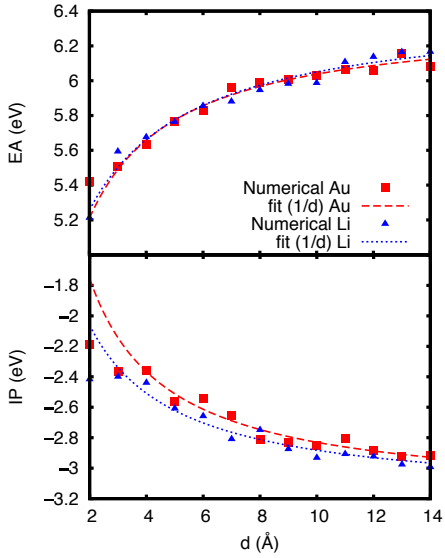

Figure 4.7: Ionization potential and electron affinity calculated in eV as a function of the distance between the 1,4 BDA and the lead in (Å) using **a)** gold lead and **b)** lithium lead.

Spin polarization is more prominent in this case as compared to the previous. This probably due to the fact that only few basis orbitals (of the amine group) couple to the gold instead of all the p_z orbitals of the carbon atoms in the previous case. This prominence of the plateaus makes it easier to identify the charge states in the weakly coupled and uncoupled cases than for the parallel configuration. It is important to note that the short distance configuration for benzene is artificial given that 2 Åis a distance shorter than the equilibrium position of the molecule over a substrate.

Our calculations show that image-charge effects contribute significantly to the distance-dependent renormalization of the molecular orbital levels with respect to the Fermi level of the electrode. For short distances, the energy values for the IP and the EA are different for the gold lead and the lithium lead. We attribute this difference to the anchoring group which is responsible for creating a bond between the lead and the molecule.

The values for the IP obtained in the long distance limit ($d \to \infty$) are 3.19 ± 0.13 eV and 3.20 ± 0.05 eV for gold and lithium respectively, and the EA values are 6.36 ± 0.07 eV for gold and 6.42 ± 0.08 eV for lithium. At this limit, the EA-IP gap obtained is very similar for both materials.

Comparing our results with those obtained previously by us [18], where the image charge effect for the same molecule is analyzed using a separate classical approximation based on atomic point charges, we observe similar asymmetric trends for the EA and the IP as a function of the distance. This effect is mainly due to the resident charge charge in the molecule and becomes more relevant for short distances.

Finally, at the distance where the formation of the chemical bond occurs, we observe a deviation of the calculated levels from the $\frac{1}{d}$ behavior. This occurs for d between 2 and 3 Å.

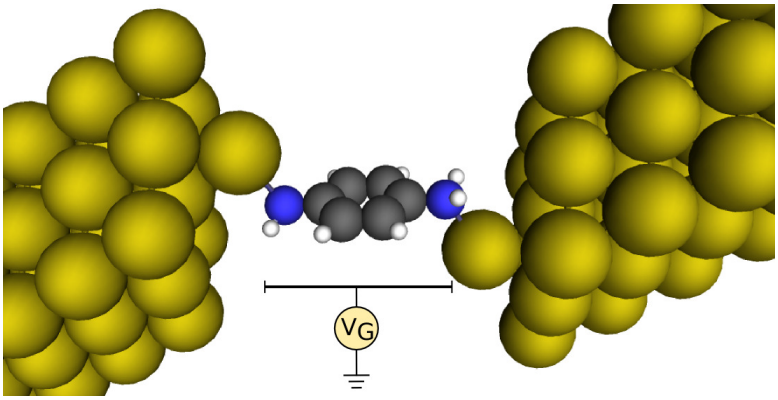

Figure 4.8: Scheme showing the Au-BDA-Au junction and the Gate applied on the molecule.

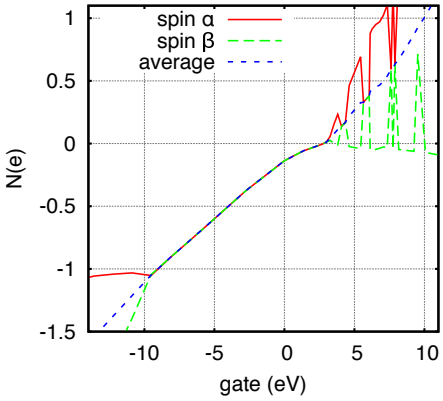

Figure 4.9: Number of electrons per spin in the molecule as a function of the applied gate.

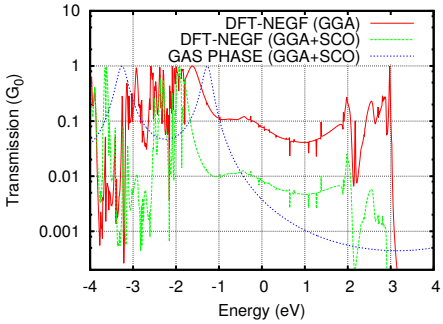

Figure 4.10: Transmission for the Au-BDA-Au junction using full SCF DFT-NEGF calculations without (dashed blue) and with (solid red) the scissor operator correction. The green dotted line was calculated for the molecules in gas phase attached to wide band limit electrodes using $\Gamma = 0.5$.

4.5. AU-BDA-AU JUNCTION AND SCISSORS OPERATOR

In the previous section we considered the molecular level alignment of a molecule near a metal surface, we now extend our model to a single molecule junction, in which we consider a 1,4 BDA molecule in between two gold electrodes. We consider a junction of type (I,I) according to Quek et al.[4] (see Fig. 4.8).

For the molecule in the junction, we relax the geometry. We then apply a gate over the molecule in order to find the IP and EA values. The molecule in the junction, at zero gate for the relaxed geometry, has a positive charge of 0.274. We find that in order to remove one electron from the molecule, we have to apply a gate -2.86 eV and to put an extra electron corresponds to 3.82 eV (see Fig. 4.9). These values that are in agreement with those presented in section 4.4.

Having a reliable value of the ionization and addition levels, we now shift the DFT eigenvalues of the molecule to the desired energies by means of a scissors operator (SCO) [4, 5, 50, 51], that has been proven to improve the conductance compared with experimental results [4]. It should be emphasized that our procedure doe not use gas-phase levels and corrections. Instead, our implementation directly uses values obtained from the molecule in the junction. First, the Hamiltonian and overlap matrix of the molecule (H^0_{mol}, S^0_{mol}) are extracted from the complete system, and we obtain their eigenvalues and eigenvectors. Then, the corrections are applied to the eigenvalues, by shifting all the occupied levels down by a constant value ϕ_{occ} while the unoccupied levels are shifted up by ϕ_{unocc}. With the shifted eigenvalues, the eigenvectors and the overlap matrix, we calculate the scissors operator hamiltonian (H^S_{mol}), which will replace the H^0_{mol} in the full system Hamiltonian. The scissors operator procedure is applied in each cycle of the self-consistent DFT-NEGF procedure.

For our DFT-NEGF calculations we use the same basis sets that we used in the previous sections in addition to the GGA PBE functional. Once convergence is reached, the transmission is calculated. In the limit of zero bias, we obtain the zero bias conductance from the Fisher-Lee relationship $G = G_0 T(E_F)$. In terms of $G_0 = \frac{2e^2}{h}$ the conductance quantum, the conductance value with the SCO correction is $0.0082 G_0$, which represents a significant reduction of one order of magnitude with respect to the value of $0.077 G_0$ obtained without the SCO correction. This is in good agreement with the experimental conductance $0.0064 G_0$ reported [4, 52, 53].

Considering the molecule in gas phase, the scissors operator can be applied to correct the transmission of the molecule attached to wide band electrodes, giving as a result a conductance equal to $0.007 G_0$. However, with this approximation the result is arbitrary given that the coupling strength is selected by hand to adjust the results.

It is important to remark that in our calculations as the IP and EA for the molecule are calculated in the junction, the scissors operator correction takes into account the image charge effect and the HOMO LUMO gap renormalization due to the presence of the electrodes.

4.6. CONCLUSIONS

In summary we have presented a method where we use DFT-NEGF calculations together with spin unrestricted calculations that allows us to calculate the IP and the EA of a

molecule in front of a metallic lead. Our method allows us to use different kinds of materials for the lead and predicts the IP-EA gap renormalization as a function of the distance between the lead and the molecule. With this method, it is possible to correct the position of the HOMO and LUMO peaks in the transmission curves of molecular junctions obtained using DFT-NEGF giving as a result a better agreement between experiments and calculations.

REFERENCES

[1] J. A. C. Gil and J. M. Thijssen, *Transport gap renormalization at a metal-molecule interface using dft-negf and spin unrestricted calculations,* The Journal of Chemical Physics **147**, 084102 (2017), http://dx.doi.org/10.1063/1.4999469 .

[2] P. Politzer and F. Abu-Awwad, *A comparative analysis of hartree-fock and kohn-sham orbital energies,* Theoretical Chemistry Accounts **99**, 83 (1998).

[3] B. N. Plakhutin, E. V. Gorelik, and N. N. Breslavskaya, *Koopmans theorem in the rohf method: Canonical form for the hartree-fock hamiltonian,* The Journal of Chemical Physics **125**, 204110 (2006), http://dx.doi.org/10.1063/1.2393223 .

[4] S. Quek, L. Venkataraman, H. Choi, S. Louie, M. Hybertsen, and J. Neaton, *Amine–gold linked single-molecule circuits: Experiment and theory,* Nano Lett. **11**, 3477 (2007).

[5] D. J. Mowbray, G. Jones, and K. S. Thygesen, *Influence of functional groups on charge transport in molecular junctions,* J. Chem. Phys. **128**, 111103 (2008).

[6] K. Kaasbjerg and K. Flensberg, *Strong polarization-induced reduction of addition energies in single-molecule nanojunctions,* Nano Lett. **8**, 3809 (2008).

[7] H. Ishii, H. Oji, E. Ito, N. Hayashi, D. Yoshimura, and K. Seki, *Energy level alignment and band bending at model interfaces of organic electroluminescent devices,* J. Lumin. **87-89**, 61 (2000).

[8] A. J. Cohen, P. Mori-Sánchez, and W. Yang, *Fractional charge perspective on the band gap in density-functional theory,* Phys. Rev. B **77**, 115123 (2008).

[9] A. J. Cohen, P. Mori-Sanchez, and W. Yang, *Insights into current limitations of density functional theory,* Science **321**, 792 (2008).

[10] A. J. Cohen, P. Mori-Sanchez, and W. Yang, *Fractional spins and static correlation error in density functional theory,* J. Chem. Phys. **129**, 121104 (2008).

[11] A. J. Cohen, P. Mori-Sanchez, and W. Yang, *Development of exchange-correlation functionals with minimal many-electron self-interaction error,* J. Chem. Phys. **126**, 191109 (2007).

[12] R. Hesper, L. H. Tjeng, and G. A. Sawatzky, *Strongly reduced band gap in a correlated insulator in close proximity to a metal,* EPL (Europhysics Letters) **40**, 177 (1997).

[13] J. Repp, G. Meyer, S. M. Stojković, A. Gourdon, and C. Joachim, *Molecules on insulating films: Scanning-tunneling microscopy imaging of individual molecular orbitals,* Phys. Rev. Lett. **94**, 026803 (2005).

[14] M. T. Greiner, M. G. Helander, W.-M. Tang, Z.-B. Wang, J. Qiu, and Z.-H. Lu, *Universal energy-level alignment of molecules on metal oxides,* Nat Mater **11**, 76 (2012).

[15] M. L. Perrin, C. J. O. Verzijl, C. A. Martin, A. J. Shaikh, R. Eelkema, van EschJan H., J. M. van Ruitenbeek, J. M. Thijssen, H. S. J. van der Zant, and D. Dulić, *Large tunable image-charge effects in single-molecule junctions,* Nat Nano **8**, 282 (2013).

[16] J. B. Neaton, M. S. Hybertsen, and S. G. Louie, *Renormalization of molecular electronic levels at metal-molecule interfaces,* Phys. Rev. Lett. **97**, 216405 (2006).

[17] K. Kaasbjerg and K. Flensberg, *Image charge effects in single-molecule junctions: Breaking of symmetries and negative-differential resistance in a benzene single-electron transistor,* Phys. Rev. B **84**, 115457 (2011).

[18] C. J. O. Verzijl, J. A. Celis Gil, M. L. Perrin, D. Dulić, H. S. J. van der Zant, and J. M. Thijssen, *Image effects in transport at metal-molecule interfaces,* The Journal of Chemical Physics **143**, 174106 (2015), http://dx.doi.org/10.1063/1.4934882.

[19] P. Hohenberg and W. Kohn, *Inhomogeneous electron gas,* Phys. Rev. **136**, B864 (1964).

[20] W. Kohn and L. J. Sham, *Self-consistent equations including exchange and correlation effects,* Phys. Rev. **140**, A1133 (1965).

[21] C. D. Pemmaraju, T. Archer, D. Sánchez-Portal, and S. Sanvito, *Atomic-orbital-based approximate self-interaction correction scheme for molecules and solids,* Phys. Rev. B **75**, 045101 (2007).

[22] A. Filippetti, C. D. Pemmaraju, S. Sanvito, P. Delugas, D. Puggioni, and V. Fiorentini, *Variational pseudo-self-interaction-corrected density functional approach to the ab initio description of correlated solids and molecules,* Phys. Rev. B **84**, 195127 (2011).

[23] J. C. Inkson, *Many-body effect at metal-semiconductor junctions. ii. the self energy and band structure distortion,* Journal of Physics C: Solid State Physics **6**, 1350 (1973).

[24] M. S. Hybertsen and S. G. Louie, *Electron correlation in semiconductors and insulators: Band gaps and quasiparticle energies,* Phys. Rev. B **34**, 5390 (1986).

[25] G. Onida, L. Reining, and A. Rubio, *Electronic excitations: density-functional versus many-body green's-function approaches,* Rev. Mod. Phys. **74**, 601 (2002).

[26] J. M. Garcia-Lastra and K. S. Thygesen, *Renormalization of optical excitations in molecules near a metal surface,* Phys. Rev. Lett. **106**, 187402 (2011).

[27] J. M. Garcia-Lastra, C. Rostgaard, A. Rubio, and K. S. Thygesen, *Polarization-induced renormalization of molecular levels at metallic and semiconducting surfaces,* Phys. Rev. B **80**, 245427 (2009).

[28] I. Tamblyn, P. Darancet, S. Y. Quek, S. A. Bonev, and J. B. Neaton, *Electronic energy level alignment at metal-molecule interfaces with a gw approach,* Phys. Rev. B **84**, 201402 (2011).

[29] G.-M. Rignanese, X. Blase, and S. G. Louie, *Quasiparticle effects on tunneling currents: A study of C_2H_4 adsorbed on the* Si(001)- (2×1) *surface,* Phys. Rev. Lett. **86**, 2110 (2001).

[30] M. Strange and K. S. Thygesen, *Image-charge-induced localization of molecular orbitals at metal-molecule interfaces: Self-consistent gw calculations,* Phys. Rev. B **86**, 195121 (2012).

[31] Sharifzadeh, S., Tamblyn, I., Doak, P., Darancet, P.T., and Neaton, J.B., *Quantitative molecular orbital energies within a g0w0 approximation,* Eur. Phys. J. B **85**, 323 (2012).

[32] A. M. Souza, I. Rungger, C. D. Pemmaraju, U. Schwingenschloegl, and S. Sanvito, *Constrained-dft method for accurate energy-level alignment of metal/molecule interfaces,* Phys. Rev. B **88**, 165112 (2013).

[33] R. Stadler, V. Geskin, and J. Cornil, *Towards a theoretical description of molecular junctions in the coulomb blockade regime based on density functional theory,* Phys. Rev. B **78**, 113402 (2008).

[34] R. Stadler, V. Geskin, and J. Cornil, *Screening effects in a density functional theory based description of molecular junctions in the coulomb blockade regime,* Phys. Rev. B **79**, 113408 (2009).

[35] C. J. O. Verzijl and J. M. Thijssen, *A DFT-based molecular transport implementation in ADF/BAND,* J. Phys. Chem. C **116**, 24393 (2012).

[36] C. R. Jacob and M. Reiher, *Spin in density-functional theory,* International Journal of Quantum Chemistry **112**, 3661 (2012).

[37] J. P. Perdew, R. G. Parr, M. Levy, and J. L. Balduz, *Density-functional theory for fractional particle number: Derivative discontinuities of the energy,* Phys. Rev. Lett. **49**, 1691 (1982).

[38] K. Burke, *Perspective on density functional theory,* J. Chem. Phys. **136**, 150901 (2012).

[39] Z.-F. Liu, J. P. Bergfield, K. Burke, and C. A. Stafford, *Accuracy of density functionals for molecular electronics: The anderson junction,* Phys. Rev. B **85**, 155117 (2012).

[40] J. P. Bergfield, Z.-F. Liu, K. Burke, and C. A. Stafford, *Bethe ansatz approach to the kondo effect within density-functional theory,* Phys. Rev. Lett. **108**, 066801 (2012).

[41] Z.-F. Liu and K. Burke, *Density functional description of coulomb blockade: Adiabatic versus dynamic exchange correlation,* Phys. Rev. B **91**, 245158 (2015).

[42] K. S. Thygesen and A. Rubio, *Renormalization of molecular quasiparticle levels at metal-molecule interfaces: Trends across binding regimes,* Phys. Rev. Lett. **102**, 046802 (2009).

[43] Q. Wu and T. Van Voorhis, *Direct optimization method to study constrained systems within density-functional theory,* Phys. Rev. A **72**, 024502 (2005).

[44] Q. Wu and T. Van Voorhis, *Constrained density functional theory and its application in long-range electron transfer,* Journal of Chemical Theory and Computation **2**, 765 (2006), pMID: 26626681, http://dx.doi.org/10.1021/ct0503163 .

[45] B. Kaduk, T. Kowalczyk, and T. Van Voorhis, *Constrained density functional theory,* Chemical Reviews **112**, 321 (2012), pMID: 22077560, http://dx.doi.org/10.1021/cr200148b .

[46] G. te Velde and E. J. Baerends, *Precise density-functional method for periodic structures,* Phys. Rev. B **44**, 7888 (1991).

[47] G. Wiesenekker and E. J. Baerends, *Quadratic integration over the three-dimensional brillouin zone,* J. Phys.: Condens. Matter **3**, 6721 (1991).

[48] *S.g. lias, in nist chemistry webbook, nist standard reference database number 69, edited by p. linstrom, w. mallartd (national institute of standards and technology, gaithersburg, md, 2012),* `http://webbook.nist.gov`.

[49] P. D. Burrow, J. A. Michejda, and K. D. Jordan, *Electron transmission study of the temporary negative ion states of selected benzenoid and conjugated aromatic hydrocarbons,* The Journal of Chemical Physics **86**, 9 (1987).

[50] V. M. García-Suárez and C. J. Lambert, *First-principles scheme for spectral adjustment in nanoscale transport,* New Journal of Physics **13**, 053026 (2011).

[51] S. Y. Quek, H. J. Choi, S. G. Louie, and J. B. Neaton, *Length dependence of conductance in aromatic single-molecule junctions,* Nano Lett. **9**, 3949 (2009).

[52] L. Venkataraman, J. E. Klare, C. Nuckolls, M. S. Hybertsen, and M. L. Steigerwald, *Dependence of single-molecule junction conductance on molecular conformation,* Nature **442**, 904 (2006).

[53] M. Kiguchi, S. Miura, T. Takahashi, K. Hara, M. Sawamura, and K. Murakoshi, *Conductance of single 1,4-benzenediamine molecule bridging between au and pt electrodes,* The Journal of Physical Chemistry C **112**, 13349 (2008), http://dx.doi.org/10.1021/jp806129u .

5

HYBRID FUNCTIONALS FOR TRANSPORT PROPERTIES CALCULATIONS USING DFT+NEGF

An idea is like a virus. Resilient. Highly contagious.
And even the smallest seed of an idea can grow.
It can grow to define or destroy you.

Cobb
Inception, Dir. C Nolan, CA: Warner Home Video, 2010

We present transport calculations using hybrid functionals in the fully self-consistent DFT-NEGF approach in molecular junctions with amine-anchored molecules of the OPE family. We investigate differences in band gaps and conductance between semi-local functionals like the generalized gradient approximation (GGA) and the Coulomb attenuated method using the Yukawa potential over hybrid functionals. We show that when implemented in transport calculations of single-molecule junctions, hybrid functionals show improvements with respect to the GGA in terms of consistent agreement with theoretical and experimental results found in literature.

5.1. INTRODUCTION

Electronic structure calculations have taken on a compelling role in the investigation of chemical and physical properties of molecules and materials. A common issue that still remains in the area of molecular electronics is the difficulty to find quantitative agreement between theoretical and experimental results. This makes the design of molecular electronic devices and correct predictability of their functioning difficult to achieve. Establishing a reliable theoretical model for transport calculations of molecular electronic devices is important for improving the understanding of experiments in this field.

The inconsistency between results obtained in theory and experiments can be related to the difficulties in determining the energy levels of a molecular system. Hartree Fock theory (HF) systematically overestimates the energy of the system [1], while Density Functional Theory (DFT) underestimate it [2].

An isolated molecule (gas phase) has well-defined energy levels, two of which correspond to the orbitals that play a major role in charge transport: the highest occupied molecular orbital (HOMO) and the lowest unoccupied molecular orbital (LUMO). When the molecule is brought in close contact with a metallic surface to form a junction, these levels are effected, more specifically, the energy gap between the HOMO and LUMO is reduced with respect to that which of the gas phase [3–8]. This is in part due to the image-charge effect (ICE) [6, 7, 9–11], it is the result of the Coulomb interaction between the charges on the molecule and the electrons in the electrodes, and it becomes stronger with decreasing molecule-metal sparation. Due to their local nature, standard approximations to the XC potential in DFT such as the Local Density Approximation (LDA) and the Generalized Gradient Approximation (GGA) do not fully capture the consequences of the image charge effect, and this is a source of discrepancies between theory and experiments [12–15].

Some corrections to the molecular orbital energy levels have been implemented [6, 7, 9–11], showing a better agreement in conductance results with the experiments. However, as these corrections are applied only to the molecule (or in some cases to the molecule and a few atoms in the electrodes), the interfacial orbitals are neglected.

Within the HF approximation, Koopmans' theorem provides a simple and natural connection between orbital energies and ionization potentials. It states that the energy needed to remove one electron from an isolated molecule, known as Ionization Potential (IP), is equal to the energy difference between HOMO and vacuum level. Similarly, the energy needed to add an extra electron to the molecule, known as the Electron Affinity (EA), is the energy difference between the LUMO and the vacuum level [16, 17]. However, by assuming a non-interacting many-particle solution to the Schrödinger Equation, HF theory neglects electron correlation, leading to an overestimation of the energy levels of an arbitrary molecular system with respect to the experimental values.

Koopmans' theorem is not fully satisfied in the approximated Kohn-Sham (KS) DFT method. Janack's theorem predicts the HOMO in an analogous way, but there, orbital relaxation effects make this theorem unusable in small systems, or large systems with weak polarization [18, 19].

In its nature, DFT is an exact theory, however in practice it is far from perfect due to the absence of a reliable XC functional. LDA [13, 20] has been successfully used in solid state systems for quite some time and, while the advent of functionals based on the gen-

eralized gradient approximation (GGA) [21] show an improvement in the HOMO-LUMO gap prediction of molecular devices, discrepancies between theory and experiments are still considerable. The development of Hybrid density functionals [22, 23], which include a part of the exact HF exchange, has boosted the accuracy further. Hybrids have shown excellent results in static calculations; nevertheless, so far no research has systematically studied the use of hybrids in fully self consistent non-equilibrium transport calculations.

In this chapter, we present transport calculations on single molecule junctions using hybrid density functionals. We compare our results with those obtained using standard GGA-PBE functional, as well as with results obtained using scissors operator (SCO) and image charges effect (ICE) corrections (see chapter 4).

In section 5.2, we introduce the hybrid functionals and we explain how they may contribute to the improvement of the transport calculations. In section 5.4 we use the fully self consistent DFT-NEFG method to calculate the zero bias transmission through a single molecule junction. We consider the BDA and the OPE3-diamine molecules which are molecules that have been widely studied. Finally we compare our results with those obtained using other functionals and, ICE and scissors operator (SCO) corrections (see chapter 7).

5.2. MODEL

We perform transport calculations on single molecule junctions using the DFT+NEGF scheme. For this we consider different hybrid functionals which are expected to predict the transport properties of the system in better approximation with respect to the experiments.

In this section we introduce the hybrid functionals that we use for our calculations. We explain the IP-EA determination method and the SCO as we applied for the molecule in the junction.

5.2.1. HYBRID FUNCTIONALS

Hybrid functionals mix the exact exchange energy calculated within the Hartree Fock approximation with the one calculated with a GGA functional. By mixing in a fraction of exact exchange, it is possible to mimic the effects of static correlation and produce an accurate functional [22]. This is more costly to compute because exact exchange is non-local, depending not only on the electron density but also on the density matrix. Specifically, the exchange and correlation (xc) energy used has the form:

$$E_{xc} = c_0 E_x^{HF} + c_1 E_{xc}^{GGA}, \tag{5.1}$$

c_0 and c_1 are mixing parameters.

Further progress in DFT has led to the development of hundreds of hybrid functionals. In our work we mainly use the following: B3LYP [24, 25], HSE [26] and CAMY-B3LYP [27, 28].

B3LYP (BECKE, 3-PARAMETERS, LEE-YANG-PARR)

Due to good results, the B3LYP hybrid functional is extremely popular in the applications of molecular structure calculations. The exchange and correlation is modeled as

$$E_{xc}^{\text{B3LYP}} = (1-a_0)E_x^{LDA} + a_0 E_x^{HF} + a_x E_x^{B88} + a_c E_c^{LYP} + (1-a_c)E_c^{VWN} \tag{5.2}$$

with $a_0 = 0.20$, $a_x = 0.72$ and $a_c = 0.81$. Here ΔE_x^{B88} and E_c^{LYP} are Becke's gradient correction to the exchange and the Lee, Yang and Parr correlations respectively. E_c^{VWN} is the Vosko, Wilk and Nusair correlation functional.

HSE (HEYD-SCUSERIA-ERNZERHOF)

These functionals, called range separated, use a separation between long range (LR) and short range (SR) Coulomb interactions according to Eq. 5.3. It was first proposed by Tawada et at. [29].

$$\frac{1}{r} = \underbrace{\frac{1-\text{erf}(\omega r)}{r}}_{SR} + \underbrace{\frac{\text{erf}(\omega r)}{r}}_{LR}, \tag{5.3}$$

The key in these range-separated hybrids is that the short range exchange energy is dominated by DFT exchange, while at long range the exchange energy is dominated by the HF exchange integral. These hybrids have shown better agreement in modeling the actual exchange potential in the short and long range limits.

5

$$E_{xc}^{\text{HSE}} = \alpha E_x^{\text{HF,SR}}(\omega) + (1-\alpha)E_x^{\text{PBE,SR}}(\omega) + E_x^{\text{PBE,LR}} + E_c^{\text{PBE}} \tag{5.4}$$

E_x^{PBE} and E_c^{PBE} are the Perdew, Burke, Ernzerhof exchange and correlation energies. Standard values for α and ω are $\alpha = 0.25$ and $0.1 < \omega < 0.2$. The purpose of ω is a mixing parameter between the pure DFT energy calculation ($\omega = 0$) and pure standard HF energy calculation ($\omega = \infty$).

CAMY-B3LYP (YUKAWA POTENTIAL)

Coulomb attenuated methods were first proposed by Gill and colleagues [30]. The CAM-B3LYP combines the strengths of B3LYP with a range separation

$$\frac{1}{r} = \underbrace{\frac{1-[\alpha+\beta\text{erf}(\omega r)]}{r}}_{SR} + \underbrace{\frac{[\alpha+\beta\text{erf}(\omega r)]}{r}}_{LR}, \tag{5.5}$$

with $\alpha = 0.19$ and $\beta = 0.46$. The CAM-B3LYP applies this coulomb attenuated correction to the B3LYP exchange functional.

This functional implementation uses the Yukawa potential $e^{(-\gamma r)}/r$ to realize the long range interactions, replacing the range separation function $\text{erfc}(\omega r)$ by the Slater function $e^{(-\gamma r)}$.

5.2.2. IP-EA DETERMINATION

DFT is designed to obtain the ground state properties of a system. It is therefore not straightforward to find a method for determining the energies of excited states using DFT. For a molecule in gas phase, Janak proved that the variation of the total Kohn Sham energy with respect to the occupation number of a given orbital is equal to the eigenvalue of that orbital [31]:

$$\frac{dE}{dn_i} = \epsilon_i, \tag{5.6}$$

where $0 < n_i < 1$ is the fractional occupation of the orbital. Considering the ground state energies of a system with N electrons we find:

$$E_N - E_{N-1} = \int_0^1 \epsilon_N(n)dn \tag{5.7}$$

Following a similar procedure to the one developed in chapter 4, we determine the IP and EA of a molecule connected to two leads.

Over a junction at zero bias, we apply a gate potential, which is constant across the molecule, and we obtain the electronic configuration of the system after the self consistent procedure within the DFT-NEGF framework, so that the gate needed to remove one electron from the molecule corresponds to the IP_{mol}, similarly the gate needed to add one corresponds to the EA_{mol}.

5.2.3. SCISSORS OPERATOR

With reliable values obtained for the energies of the HOMO and LUMO in 5.2.2, we shift the DFT molecule eigenvalues to lie at these energies by means of a SCO method.

For a single molecule junction, the Hamiltonian and overlap matrices of the molecule (H^0_{mol} and S^0_{mol}) are extracted from the full system KS-Hamiltonian and overlap matrices (H^{KS} and S^{KS}). By solving the corresponding eigenvalue problem, $H^0_{mol}\psi = \epsilon S^0_{mol}\psi$, we obtain the eigenvalues, $\epsilon_{n=1,...,M}$ and eigenvectors $\psi_{n=1,...,M}$, where M is the number of orbitals on the molecule. The corrections are applied to the eigenvalues, where all the occupied levels are shifted rigidly by a constant value ϕ_{occ}, while the unoccupied levels are shifted by the constant ϕ_{unocc}, the new H^{SCO}_{mol} is calculated. In the full Hamiltonian matrix we replace the sub-block H^0_{mol} with H^{SCO}_{mol}.

This SCO procedure is applied self-consistently and has two contributions. First, the correction to the HOMO-LUMO gap, which is too small when compared to the difference between the Electron Affinity and Ionization Potential. Secondly, the renormalization of the energy levels, when the molecule is close to metal surfaces (Image charge effect).

5.3. SINGLE MOLECULE JUNCTION CU-BDA-CU

Initially we consider the BDA molecule, which is a standard molecule for this kind of calculations. For the molecule in gas phase, we perform DFT calculations to optimize the geometry and obtain the molecular orbitals

Table 5.1: HOMO-LUMO gap of the BDA molecule in gas phase obtained using different functionals.

Functional	HOMO-LUMO gap (eV)
HF	10.531
LDA	3.129
GGA(PBE)	3.186
CAMY-B3LYP	6.805
ΔSCF	8.040

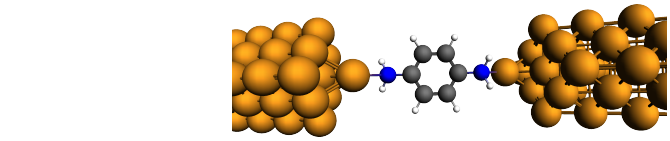

a) Geometry

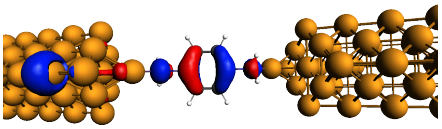

GGA(PBE) −2.043 *eV*
CAMY-B3LYP −3.102 *eV*

b) HOMO-A

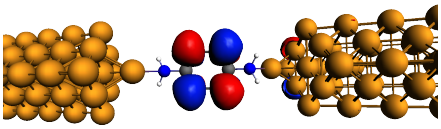

GGA(PBE) 1.600 *eV*
CAMY-B3LYP 4.030 *eV*

c) LUMO-A

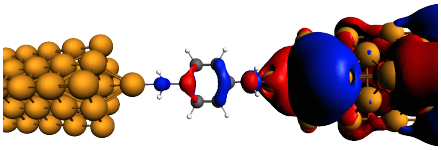

GGA(PBE) −2.201 *eV*
CAMY-B3LYP −2.745 *eV*

d) HOMO-B

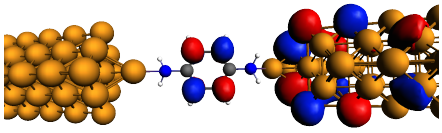

GGA(PBE) 1.845 *eV*
CAMY-B3LYP 4.089 *eV*

e) LUMO-B

Figure 5.1: a) Geometry of the single Cu-BDA-Cu molecule junction and the orbitals. b) and d) show two HOMO like orbitals with their energies with respect to the Fermi energy of the electrodes calculated with the GGA(PBE) and the CAMY-B3LYP functionals. c) and e) show two LUMO like orbitals with their respective energies.

We study the effect of the exchange correlation functionals on the transport gap. Using different functionals, we compare the HOMO-LUMO gap with the one obtained by using the ΔSCF approach (see table 5.1). As can be seen, HF overestimates the HOMO-LUMO gap and, LDA and GGA underestimate it. By the other side CAMY-B3LYP show better agreement with respect to the ΔSCF results.

To analyze the electronic transport through a molecular junction, we perform DFT calculations within the NEGF formalism. We attach the BDA molecule to the FCC (111) surface 5.1 of copper leads. We consider copper for the electrodes due to its high conductivity and sensitivity to the screening effect over the molecule. Furthermore this kind of leads result less expensive computationally compared to gold or silver.

We consider a junction of type (I,I) according to the Quek et al. classification [5], which consists of a copper atom on top of the (111) surface plane attaching the molecule to the lead. We relax the geometry to find the minimum energy configuration. For the leads, we use a scattering region that contains 27 atoms arranged in a FCC lattice, where the atoms are fixed at the crystal lattice positions ($a = 4.6149$ Å).

We use a DZ-basis of numerical atomic orbitals on the molecule and a SZ-basis of

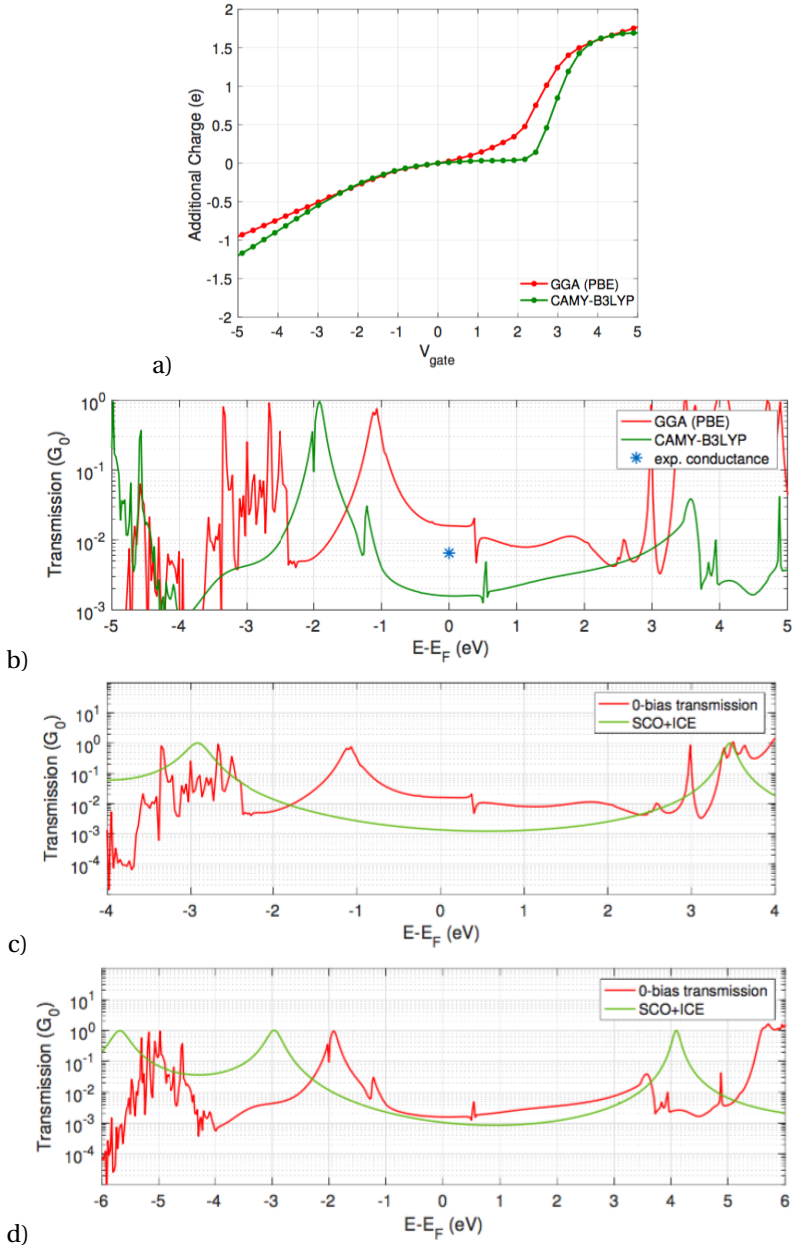

Figure 5.2: a)Excess of electrons in the molecule as a function of an applied gate for the Cu-BDA-Cu junction. b) Conductance obtained experimentally compared to the values obtained from zero bias transport calculations for GGA PBE and CAMY-B3LYP. Corrected zero bias transmissions compared with results obtained from SCO+ICE methods for XC functional c) GGA PBE. d) CAMY-B3LYP.

numerical atomic orbitals on the metal atoms. We do not use any frozen core for the atoms; the electronic configuration is calculated for all the electrons in the system.

We use as a reference calculation the PBE parametrization of the Generalized Gradient Approximation (GGA) functional [21] and we compare it with the CAMY-B3LYP functional to show the extra features due to hybrid functionals in our implementation of NEGF-based transport in the Amsterdam Density Functional (ADF)/band quantum chemistry package [32–34].

When the molecule is connected to the leads, the molecular orbitals hybridize with orbitals from the leads giving as a result extra channels for transmission through the system as can be seen in figure 5.1. The HOMO-LUMO gap of the molecule in the junction in figure 5.1 is 3.64 eV using GGA and 7.14 eV using CAMY-B3LYP. These values are close to the ones obtained for the molecule in gas phase.

Following the IP-EA determination procedure explained in section 5.2, we calculate the ionization potential and the electron affinity of the molecule in the junction using both functionals. Figure 5.2 a) shows the excess of electrons in the molecule as a function of an applied gate. For the GGA, the excess of electrons at zero gate is taken as the reference while for the CAMY-B3LYP zero excess of electrons is the reference. The IP-EA gap obtained for the GGA(PBE) and the CAMY-B3LYP functionals are 4.83 eV and 5.79 eV respectively. While for the GGA the IP-EA gap is bigger than the HOMO-LUMO gap obtained in gas phase, it is smaller in the case of the CAMY-B3LYP functional. These equilibrium calculations for both functionals correct the HOMO-LUMO and take the screening due to the copper into account.

We analyze the transmission through the system in the zero bias limit (see Fig. 5.2). The peaks in the transmission spectra reveal the presence of molecular orbitals involved in transport (see Fig. 5.1). The blue line, which corresponds to the transmission calculated by using the CAMY-B3LYP functional shows a value at 0 eV one order of magnitude smaller than the results obtained with GGA and GGA+SCO. Using the Fisher Lee relationship $G = G_0 T(E_F)$ with $G_0 = \frac{2e^2}{h}$, the zero bias conductance obtained with the CAMY-B3LYP is 0.0012 G_0. On the other hand, the conductance obtained with the GGA+SCO is 0.013 G_0. These values are in the same range of the experimental conductance 0.0064 G_0 reported for the same molecule with gold leads [5, 35, 36]. The peaks at 0.5 eV and -1 eV can be tracked from the density of states of the copper nanowire.

5.4. SINGLE MOLECULE JUNCTION CU-OPE3-CU

We now proceed to the OPE3-diamine molecule, which is a molecule that recently has been studied experimentally [37–41]. We first perform DFT calculations for the molecule in gas phase to optimize its geometry and determine the molecular orbitals.

Using different hybrid functionals, we compare the energies of the HOMO and the LUMO with those obtained by using ΔSCF approximation as can be seen in table 5.2.

From table 5.2, the functional showing the best agreement with the ΔSCF calculation is again the CAMY-B3LYP.

We consider a single molecule junction formed by an OPE3-diamine molecule in between two copper electrodes. In figure 5.3 we show the most stable configuration of the molecule in the junction using the (I,I) type junction according to Quek et. al. [5] for the

Table 5.2: List of functionals and their HOMO-LUMO gap for the OPE3-diamine molecule in gas phase

Functional	HOMO-LUMO gap (eV)
HF	8.472
LDA	2.268
GGA(PBE)	2.300
CAMY-B3LYP	5.284
ΔSCF	5.437

coupling between the copper and the amine groups, together with the HOMO like and LUMO like orbitals.

For the OPE3, the HOMO-LUMO gap from the orbitals in figure 5.3 is 2.51 eV using GGA and 5.14 eV using CAMY-B3LYP. We see that these values are comparable with those ones obtained for the molecule in gas phase.

We calculate the ionization potential and the electron affinity of the molecule in the junction. In Figure 5.4 a), we show the excess of electrons in the molecule as a function of an applied gate. This procedure is done for the GGA(PBE) and the Hybrid(CAMY-B3LYP) functionals. For the GGA, the excess of electrons at zero gate is taken as the reference while for the CAMY-B3LYP zero excess of electrons is the reference.

For the GGA functional, with the calculated values for the IP and the EA, we correct the position of the HOMO and LUMO peaks by using the SCO over the DFT-NEGF calculations. This corrects the underestimation of the HOMO-LUMO gap, which is typical of this functional, and takes into account the image charge effect according to the results shown in chapter 4.

The IP-EA gap obtained for the CAMY-B3LYP is very close to the HOMO-LUMO gap with the same functional obtained for the molecule in gas phase. Furthermore, the locations of the IP and EA with respect to the Fermi energy coincide with the HOMO and LUMO peaks in the transmission respectively. This suggests that the image charge effect does not play an important role for this molecule. To clarify this point, we calculate the shift of the energy levels due to the image charge effect using classical electrostatics following the method of reference [11]. We calculate the shift of the energy levels for a distance equal to 3.0 Å between the last (first) atom in the molecule and the image plane. The values obtained are equal to 0.23 eV for the occupied levels and -0.119 eV for the unoccupied levels. As we can see these values are small compared to the HOMO-LUMO gap. By shifting the energy levels, we recalculate the transmission taking into account the image charge correction.

In Figure 5.4, we compare the transmission obtained with the GGA and CAMY-B3LYP functionals and, the SCO and ICE corrections respectively.

The CAMY-B3LYP is a functional that provides better results in comparison to the ones obtained by using generalized gradient approximation, given that the hybrid functional corrects the HOMO-LUMO gap underestimation inherent of the semi-local approaches. Furthermore, with this functional, the IP (EA) value obtained from figure 5.4 coincides in good agreement with the HOMO (LUMO) from the DFT calculations of the molecule in the junction. This indicates that CAMY-B3LYP functional does good pre-

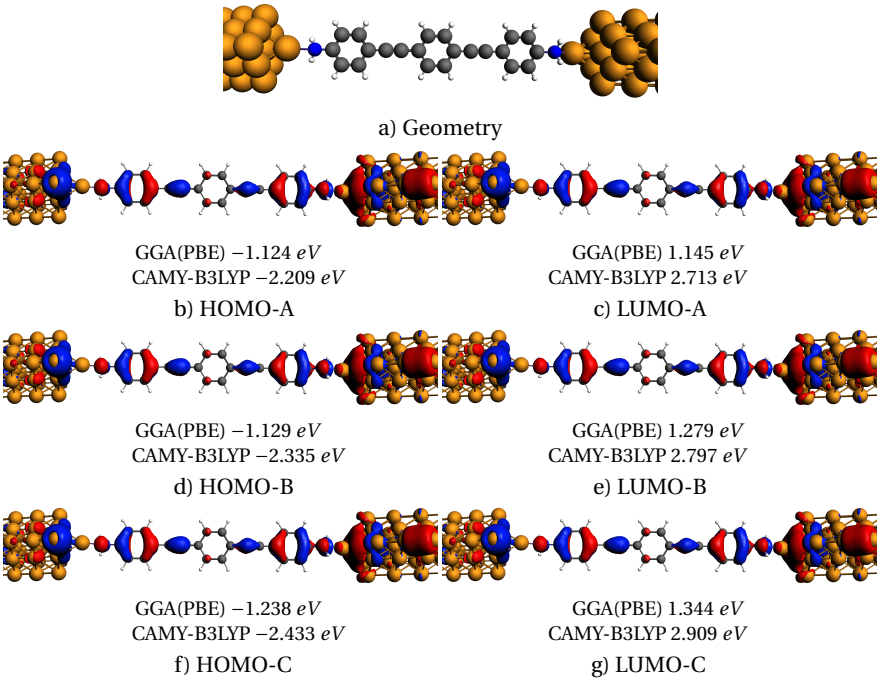

Figure 5.3: Geometry of the single molecule junction with the orbitals of the molecule in the junction. b), d) and f) show the HOMO like orbitals and their energy calculated with respect to the Fermi energy of the electrodes. c), e) and g) show the LUMO like orbitals and their energies.

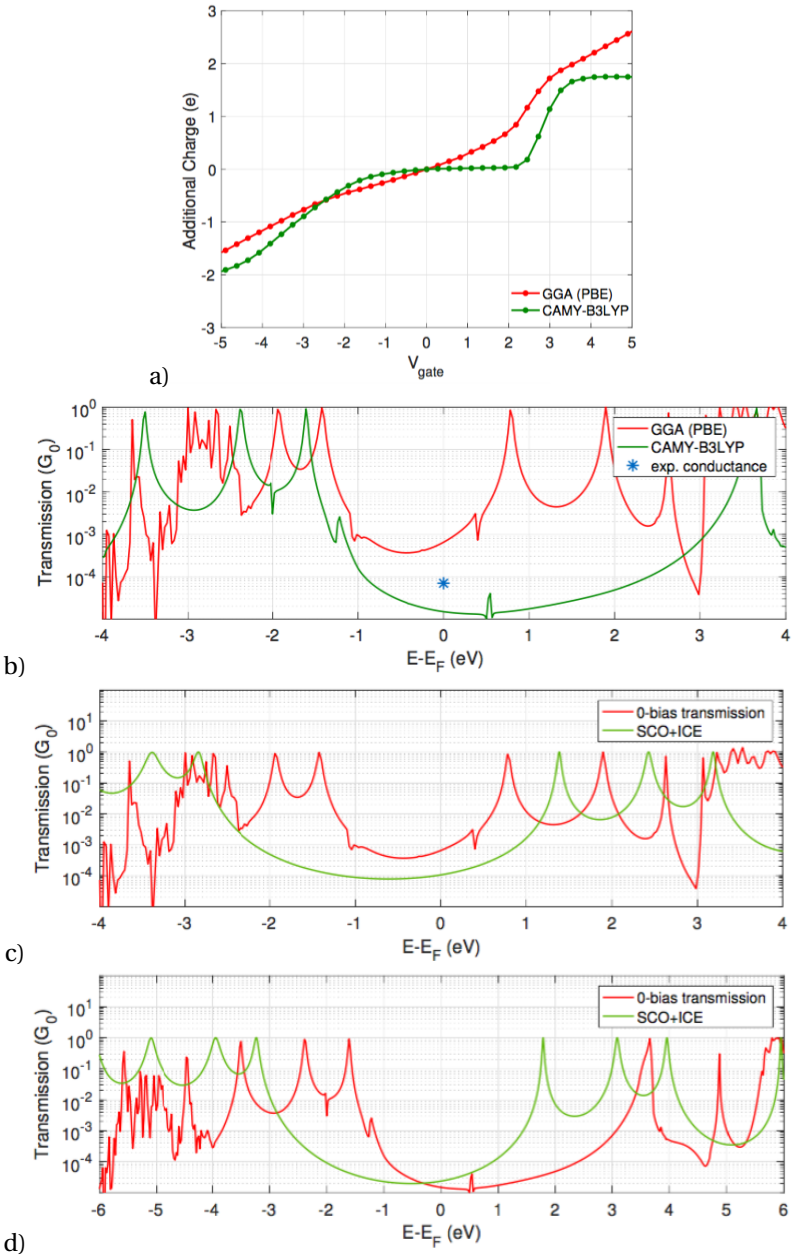

Figure 5.4: a) Excess of electrons in the molecule as a function of an applied gate for the Cu-OPE3-Cu molecule. b) Calculated transmission for the Cu-OPE3-Cu single molecule junction using GGA(PBE) and CAMY-B3LYP functionals. Corrected zero bias transmissions compared with results obtained from SCO+ICE methods for XC functional b) GGA PBE. c) CAMY-B3LYP.

dictions of the excited states of systems where the screening effect of the electrodes is weak.

5.5. CONCLUSIONS

In summary, we have presented full self consistent DFT+NEGF calculations on two single molecule junctions using hybrid functionals. We compare the results with those obtained using semi-local functionals. We calculated the HOMO-LUMO gap of the two molecules in gas phase and we contrast it with the calculated IP-EA gap in the junction.

Finally, we conclude that the CAMY-B3LYP can potentially provide better results in comparison to the ones obtained by using just the generalized gradient approximation. This is due to the fact that this functional includes the correction of the HOMO-LUMO gap underestimation proper of the semi-local functionals. Furthermore, with this functional the IP (EA) coincides in better agreement with the HOMO (LUMO) in systems where the screening effect of the electrodes is weak, which leads to better predictions of the molecular orbitals.

REFERENCES

[1] J. P. Perdew and K. Schmidt, *Jacobs ladder of density functional approximations for the exchange-correlation energy,* AIP Conference Proceedings **577**, 1 (2001), http://aip.scitation.org/doi/pdf/10.1063/1.1390175 .

[2] M. Levy, *Universal variational functionals of electron densities, first-order density matrices, and natural spin-orbitals and solution of the v-representability problem,* Proceedings of the National Academy of Sciences **76**, 6062 (1979), http://www.pnas.org/content/76/12/6062.full.pdf .

[3] P. Politzer and F. Abu-Awwad, *A comparative analysis of hartree-fock and kohn-sham orbital energies,* Theoretical Chemistry Accounts **99**, 83 (1998).

[4] B. N. Plakhutin, E. V. Gorelik, and N. N. Breslavskaya, *Koopmans theorem in the rohf method: Canonical form for the hartree-fock hamiltonian,* The Journal of Chemical Physics **125**, 204110 (2006), http://dx.doi.org/10.1063/1.2393223 .

[5] S. Quek, L. Venkataraman, H. Choi, S. Louie, M. Hybertsen, and J. Neaton, *Amine–gold linked single-molecule circuits: Experiment and theory,* Nano Lett. **11**, 3477 (2007).

[6] D. J. Mowbray, G. Jones, and K. S. Thygesen, *Influence of functional groups on charge transport in molecular junctions,* J. Chem. Phys. **128**, 111103 (2008).

[7] K. Kaasbjerg and K. Flensberg, *Strong polarization-induced reduction of addition energies in single-molecule nanojunctions,* Nano Lett. **8**, 3809 (2008).

[8] H. Ishii, H. Oji, E. Ito, N. Hayashi, D. Yoshimura, and K. Seki, *Energy level alignment and band bending at model interfaces of organic electroluminescent devices,* J. Lumin. **87-89**, 61 (2000).

[9] J. B. Neaton, M. S. Hybertsen, and S. G. Louie, *Renormalization of molecular electronic levels at metal-molecule interfaces,* Phys. Rev. Lett. **97**, 216405 (2006).

[10] K. Kaasbjerg and K. Flensberg, *Image charge effects in single-molecule junctions: Breaking of symmetries and negative-differential resistance in a benzene single-electron transistor,* Phys. Rev. B **84**, 115457 (2011).

[11] C. J. O. Verzijl, J. A. Celis Gil, M. L. Perrin, D. Dulić, H. S. J. van der Zant, and J. M. Thijssen, *Image effects in transport at metal-molecule interfaces,* The Journal of Chemical Physics **143**, 174106 (2015), http://dx.doi.org/10.1063/1.4934882.

[12] P. Hohenberg and W. Kohn, *Inhomogeneous electron gas,* Phys. Rev. **136**, B864 (1964).

[13] W. Kohn and L. J. Sham, *Self-consistent equations including exchange and correlation effects,* Phys. Rev. **140**, A1133 (1965).

[14] C. D. Pemmaraju, T. Archer, D. Sánchez-Portal, and S. Sanvito, *Atomic-orbital-based approximate self-interaction correction scheme for molecules and solids,* Phys. Rev. B **75**, 045101 (2007).

[15] A. Filippetti, C. D. Pemmaraju, S. Sanvito, P. Delugas, D. Puggioni, and V. Fiorentini, *Variational pseudo-self-interaction-corrected density functional approach to the ab initio description of correlated solids and molecules,* Phys. Rev. B **84**, 195127 (2011).

[16] A. J. Cohen, P. Mori-Sánchez, and W. Yang, *Fractional charge perspective on the band gap in density-functional theory,* Phys. Rev. B **77**, 115123 (2008).

[17] A. J. Cohen, P. Mori-Sanchez, and W. Yang, *Insights into current limitations of density functional theory,* Science **321**, 792 (2008).

[18] A. J. Cohen, P. Mori-Sanchez, and W. Yang, *Fractional spins and static correlation error in density functional theory,* J. Chem. Phys. **129**, 121104 (2008).

[19] A. J. Cohen, P. Mori-Sanchez, and W. Yang, *Development of exchange-correlation functionals with minimal many-electron self-interaction error,* J. Chem. Phys. **126**, 191109 (2007).

[20] S. H. Vosko, L. Wilk, and M. Nusair, *Accurate spin-dependent electron liquid correlation energies for local spin density calculations: a critical analysis,* Canadian Journal of Physics **58**, 1200 (1980), https://doi.org/10.1139/p80-159 .

[21] J. P. Perdew, K. Burke, and M. Ernzerhof, *Generalized gradient approximation made simple,* Phys. Rev. Lett. **77**, 3865 (1996), pBE.

[22] A. D. Becke, *A new mixing of hartree–fock and local density-functional theories,* J. Chem. Phys. **98**, 1372 (1993).

[23] C. Lee, W. Yang, and R. G. Parr, *Development of the colle-salvetti correlation-energy formula into a functional of the electron density,* Phys. Rev. B **37**, 785 (1988).

[24] K. Kim and K. D. Jordan, *Comparison of density functional and mp2 calculations on the water monomer and dimer,* The Journal of Physical Chemistry **98**, 10089 (1994), http://dx.doi.org/10.1021/j100091a024 .

[25] P. J. Stephens, F. J. Devlin, C. F. Chabalowski, and M. J. Frisch, *Ab initio calculation of vibrational absorption and circular dichroism spectra using density functional force fields,* The Journal of Physical Chemistry **98**, 11623 (1994), http://dx.doi.org/10.1021/j100096a001 .

[26] J. Heyd, G. E. Scuseria, and M. Ernzerhof, *Hybrid functionals based on a screened coulomb potential,* The Journal of Chemical Physics **118**, 8207 (2003), http://dx.doi.org/10.1063/1.1564060 .

[27] T. Yanai, D. P. Tew, and N. C. Handy, *A new hybrid exchange–correlation functional using the coulomb-attenuating method (cam-b3lyp),* Chemical Physics Letters **393**, 51 (2004).

[28] Y. Akinaga and S. Ten-no, *Range-separation by the yukawa potential in long-range corrected density functional theory with gaussian-type basis functions,* Chemical Physics Letters **462**, 348 (2008).

[29] Y. Tawada, T. Tsuneda, S. Yanagisawa, T. Yanai, and K. Hirao, *A long-range-corrected time-dependent density functional theory,* The Journal of Chemical Physics **120**, 8425 (2004), http://dx.doi.org/10.1063/1.1688752 .

[30] P. M. W. GILL, R. D. ADAMSON, and J. A. POPLE, *Coulomb-attenuated exchange energy density functionals,* Molecular Physics **88**, 1005 (1996), http://dx.doi.org/10.1080/00268979609484488 .

[31] J. F. Janak, *Proof that $\partial e/\partial ni = \epsilon$ in density-functional theory,* Phys. Rev. B **18**, 7165 (1978).

[32] C. Fonseca Guerra, J. G. Snijders, G. te Velde, and E. J. Baerends, *Towards an order-n dft method,* Theoretical Chemistry Accounts **99**, 391 (1998).

[33] G. te Velde and E. J. Baerends, *Precise density-functional method for periodic structures,* Phys. Rev. B **44**, 7888 (1991).

[34] G. te Velde, F. Bickelhaupt, S. van Gisbergen, C. Fonseca Guerra, E. Baerends, J. Snijders, and T. Ziegler, *Chemistry with ADF,* J. Comput. Chem. **22**, 931 (2001).

[35] L. Venkataraman, J. E. Klare, C. Nuckolls, M. S. Hybertsen, and M. L. Steigerwald, *Dependence of single-molecule junction conductance on molecular conformation,* Nature **442**, 904 (2006).

[36] M. Kiguchi, S. Miura, T. Takahashi, K. Hara, M. Sawamura, and K. Murakoshi, *Conductance of single 1,4-benzenediamine molecule bridging between au and pt electrodes,* The Journal of Physical Chemistry C **112**, 13349 (2008), http://dx.doi.org/10.1021/jp806129u .

[37] R. Frisenda, M. L. Perrin, H. Valkenier, J. C. Hummelen, and H. S. J. van der Zant, *Statistical analysis of single-molecule breaking traces,* physica status solidi (b) **250**, 2431 (2013).

[38] R. Frisenda, S. Tarkuç, E. Galán, M. L. Perrin, R. Eelkema, F. C. Grozema, and H. S. J. van der Zant, *Electrical properties and mechanical stability of anchoring groups for single-molecule electronics,* Beilstein Journal of Nanotechnology **6**, 1558 (2015).

[39] R. Frisenda, M. L. Perrin, and H. S. J. van der Zant, *Probing the local environment of a single ope3 molecule using inelastic tunneling electron spectroscopy,* Beilstein Journal of Nanotechnology **6**, 2477 (2015).

[40] C. R. Arroyo, R. Frisenda, K. Moth-Poulsen, J. S. Seldenthuis, T. Bjørnholm, and H. S. van der Zant, *Quantum interference effects at room temperature in opv-based single-molecule junctions,* Nanoscale Research Letters **8**, 234 (2013).

[41] R. Frisenda and H. S. J. van der Zant, *Transition from strong to weak electronic coupling in a single-molecule junction,* Phys. Rev. Lett. **117**, 126804 (2016).

6

Stretching-Induced Conductance Increase in a Spin-Crossover Molecule

Sooner or later you're going to realize just as I did
that there's a difference between knowing the path and walking the path.

Morpheus
The Matrix. Dir. L. Wachowski and Lil. Wachowski. CA: Warner Home Video, 1999.

We investigate transport through mechanically triggered single-molecule switches that are based on the coordination sphere dependent spin state of Fe^{II}-species. In these molecules, in certain junction configurations the relative arrangement of two terpyridine ligands within homoleptic Fe^{II}-complexes can be mechanically controlled. Mechanical pulling may thus distort the Fe^{II} coordination sphere and eventually modify their spin state. DFT calculations are predict a stretching-induced spin transition in the Fe^{II}-complex and a larger transmission for the high-spin configuration.

Parts of this chapter have been published in Nano Letters **16**, 4733 (2016) [1].

6.1. INTRODUCTION

Control over the molecular conductance by means of an external stimulus is an interesting concept in molecular scale electronics and different single-molecule switches are known in literature[2–5]. In the most common design, the molecule contains chemical groups that can switch between two or more stable configurations, like dithienylethene or azobenzene groups[6–10]. Depending on the system, the conductance can be tuned by means of light[11, 12], mechanical manipulation[13–16], electrochemical gating[17, 18], the applied bias voltage[19] or by the current[7, 20].

The spin-crossover (SCO) phenomenon [21–23] can lead to bistability, as was observed recently in some metal-containing molecules and compounds[24–26]. A spin-crossover molecule exhibits two different ground states, each of them stable under certain conditions and characterized by different values of the molecular spin. Among the various metal atoms, the complexes of iron(II) are the most investigated ones[27]. When the iron atom is surrounded by an octahedral ligand environment (ligand field), its five spin-degenerate 3d levels split into a doublet and a triplet, as shown in Figure 1b. The filling order of these levels with the six electrons of Fe^{II} depends on the ratio between the ligand field energy (ELF), and the spin exchange energy (EEXC). If ELF»EEXC, the electrons are all paired up and the triplet is completely filled, giving a total spin S = 0. In the opposite case, EEXC»ELF, the levels are filled according to Hund's rule and the spin is maximized reaching a value S = 2. The first case is defined as the low-spin (LS) state and the second one as the high-spin (HS) state. Different stimuli, like pressure or temperature, have been used to vary the ratio EEXC/ELF to control the SCO state. Apart from the total spin, the LS and HS states present differences in geometry, electronic structure, and highest occupied molecular orbital-lowest unoccupied molecular orbital (HOMO-LUMO) gap energy. According to theoretical predictions [28] and low-temperature scanning tunnel microscopy (STM) experiments[24, 25], the HS state is more conducting than the LS state.

In this chapter, we propose to modify the spin state of Fe^{II} terpyridine complexes mechanically. The concept and the molecular design are displayed in Figure 6.1 The SCO active center is the Fe^{II} complex 1, consisting of two terpyridine (tpy) ligands that are further phenyl functionalized. For each ligand, one of both phenyl rings is decorated with a thiol group in the para position as anchor group that is known to have considerable mechanical stability on gold electrodes[29–31]. In certain junction arrangements, the geometry of the coordination sphere provided by the two terpyridine ligands should depend on the electrodes spacing and thus become tunable by mechanical manipulation.

6.2. MODEL

The intended SCO-based switching mechanism is sketched in Figure 6.1. When the tpy ligands are arranged perpendicularly, the complex is in the LS state. Upon increasing the electrode separation, the ligands are pulled further apart and the distortion of the perpendicular arrangement of the two tpy ligands leads to a reduction of ELF. For large enough distortion, the exchange energy will dominate over the ligand field energy thereby triggering the switch from the LS to the HS state. With both ligands bearing the

thiol anchor group in the para position with respect to the coordinating pyridine nitrogen, the coordinated central ion is part of the current path, and alterations in its spin state are expected to be reflected in the junctions transport characteristics[24, 25, 32].

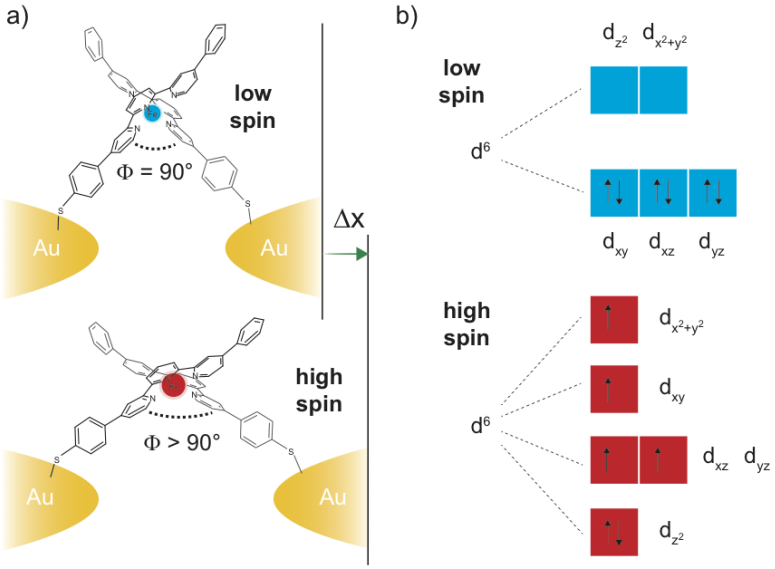

Figure 6.1: Two-terminal mechanically controlled single-molecule junction. a) Sketch of the Fe^{II}-based SCO molecular junction and the LS and HS switch triggered by separating the electrodes by Δx. b) Iron II 3d levels involved in the spin-crossover phenomenon.

6.3. EXPERIMENTAL SETUP

The experimental setup used for the measurements done reported by Frisenda et. al. [1], consist of a mechanically controlled break junction (MCBJ), which provides two gold nanoelectrodes of adjustable distance (Fig. 6.1).

Briefly, a MCBJ sample consists of a gold wire deposited on top of a flexible substrate. Bending the substrate results in the thinning of the wire until its rupture, which leaves two sharp gold extremities facing each other. The two tips can be used as nanoelectrodes and eventually a molecule can bridge the gap; for specific junction arrangements, the geometry of the complexes can be changed by separating the electrodes until the rupture of the molecular junction. During the stretching of the wire, current-voltage (I-V) characteristics are measured. By pushing the electrodes together the wire is reformed and a new breaking experiment can start by repeating the procedure.

After the rupture of the gold wire in the presence of molecule in 84% of the traces (525 out of 624), the conductance decays exponentially as a function of displacement. This behavior, typical of vacuum tunneling, indicates that no molecule bridges the electrodes. In the remaining 16% of the traces (99 traces), the presence of plateaus and steps and the absence of an exponential and monotonous decrease in the conductance versus

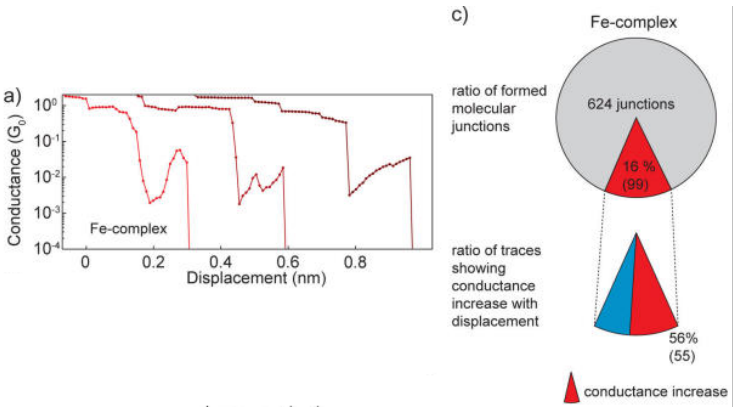

Figure 6.2: a) Conductance measurements of three examples of conductance traces as a function of electrode displacement measured respectively in the presence of the FeII-complex. b) Junction-formation statistics and percentage of molecular junctions showing a conductance increase.

distance indicate that a molecule is bridging the electrodes. Plots of the conductance versus electrode displacement often show an increase in the molecular conductance during the stretching; a few examples are shown in Figure 6.2 a). Among the 99 molecular junctions, 55 traces show a conductance increase while stretching, corresponding to 56% of the molecular junctions.

6.4. DFT CALCULATIONS

We study the transition from the LS state to the HS state theoretically using density functional theory (DFT) calculations. For both states individually, we perform a geometrical relaxation of the Fe^{II} complex in gas phase. Then we stretch or compress the molecule by changing the distance between the sulfur atoms, perform a geometric relaxation, and calculate the energies. For this calculation, we use the ADF quantum chemistry package with a TZP-basis of atomic orbitals and the B3LYP functional. In Figure 6.3a), we plot the energy for the low-spin and high-spin states as a function of the separation between the sulfur atoms. We define the separation of 16.03 Å as the zero, corresponding to an angle of 90 between the two tpy-subunits. For short stretching distances up to 3 Å, the LS state is more favorable. At a stretching of 3.5 Å, a crossover to a regime where the HS state is the stable one occurs. The relaxed molecular geometries for both states are shown in Figure 6.3b) for a sulfur-sulfur separation, respectively, of 16.03 Å (LS) and 20.52 Å (HS). The angle between the two tpy central units is equal to 90 and 101, respectively.

To analyze the transport properties of the two states, we perform self-consistent DFT-NEGF calculations for the molecules attached to a face-centered cubic (111) gold surface. For our calculations, we use a TZP-basis of numerical atomic orbitals on the molecule, a SZ-basis of numerical atomic orbitals on the gold atoms and the GGA PBE functional in our implementation of the NEGF-based transport in the ADF/ band quantum chemistry package. Figure 6.4c) compares the mean transmissions for the LS and HS states as a function of the energy, with the Fermi energy at 0 eV. In the region of

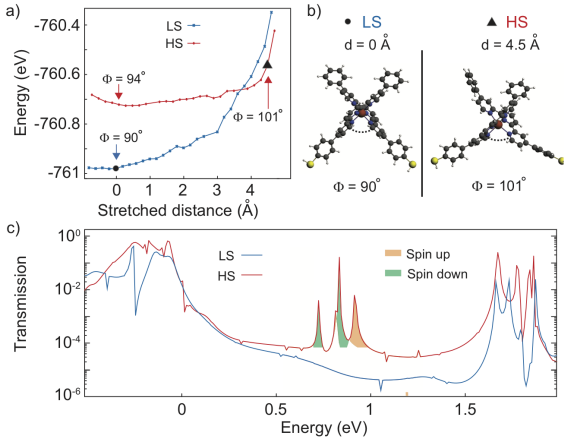

Figure 6.3: DFT calculations. a) Energy of the LS and HS states as a function of stretching distance found from DFT calculations. b) Relaxed geometries of the LS and HS states at the stretching distance of 0 Åand 4.5 Åre-spectively. c) Total transmission of the LS and HS geometries shown in (b) in a metal-molecule-metal configu-ration calculated with self-consistent DFT-NEGF. The shaded areas correspond to spin polarized transmission for up (orange) or down (green) spin electrons.

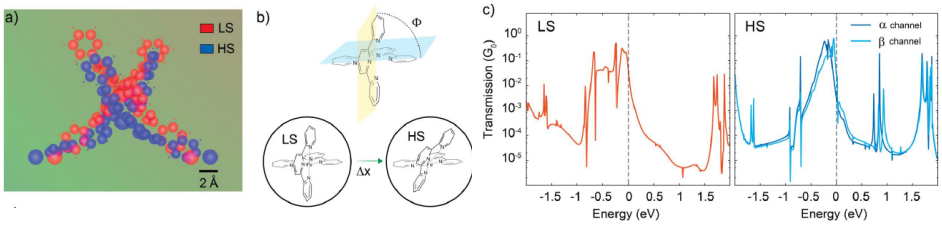

Figure 6.4: a) Comparison of the geometries of the FeII-complex in the low spin and high spin states. b) Schematic drawing of the two central terpyridine ligands. c) Spin resolved projected transmission spectra, in logarithmic scale, calculated for a junction containing the molecule in between gold leads for the LS and HS configurations. In the case of LS, the transmission is degenerate for the two polarizations.

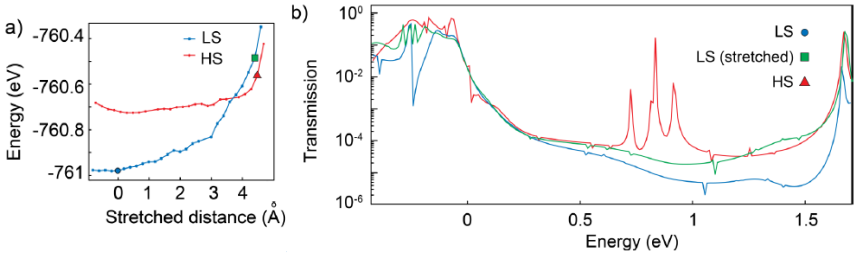

Figure 6.5: DFT calculations. a) Energy of the LS and HS states as a function of stretching distance found from DFT calculations. b) Total transmission of the LS, LS stretched and HS geometries in a metal-molecule-metal configuration calculated with self-consistent DFT-NEGF. The Fermi energy of the contacts is at 0 eV.

the HOMO-LUMO gap, between 0 and 1.5 eV, the HS state shows a larger transmission than the LS state. We further notice that the HS state transmission shows a certain degree of spin- polarization, evidenced in Figure 6.4b), this can also be seen in Figure 6.6 which shows the spin polarization of the molecule, while the LS transmission is not spin-polarized. Thus, the calculations predict for the Fe^{II} complex the presence of a stretching-induced SCO transition that is accompanied by an increase in conductance when going from the LS to the HS state.

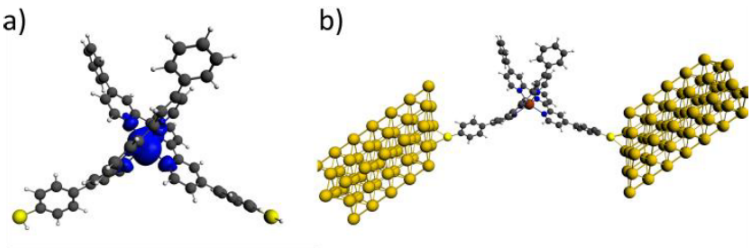

Figure 6.6: Geometry configuration of the molecule in the HS state a) for the molecule in gas phase and b) for the molecule in the junction. The blue cloud surrounding the iron atom shows the spin polarization of the system.

Apart from the HS-LS transition, predicted in the case of the FeII complex, other mechanisms can increase the conductance of a molecular junction while stretching the electrodes [33, 34]. Bruot et al. [16] found that even simple molecules like benzene dithiol immobilized in molecular junctions formed with gold electrodes at low temperature can show a conductance increase while stretching. This conductance modulation is attributed to a stretching-induced better alignment of the HOMO with the Fermi energy of the electrodes. If this more favorable level alignment compensates the decrease in electronic coupling, the conductance will increase for larger displacement. Although we cannot exclude that this mechanism may also play a role here, we expect that the level shifts are smaller in our more extended molecules.

Alternatively, in the molecules studied here, the tpy ligands may also be important for charge transport from one electrode to the other. Specifically, the angle ϕ between the two flat tpy groups (indicated in Figure 6.1a) can influence the transport through the molecule. [35, 36] Considering the overlap of the two tpy π-systems, in a first approximation the closer the angle is to 90° the smaller the conductance of the molecule [37], independently from the central metal atom species.

Figure 6.5 shows the transmission calculated for the Fe^{II} complex in a stretched configuration (stretching distance of 4.5 Å, see Figure 6.5a). These calculations indicate that the transmission of the low-spin complex increases as the molecule is stretched. Thus, this mechanism can occur, irrespective of the SCO transition, with the central metal ion acting exclusively as a mechanical joint between both tpy ligands and not as a charge transport channel.

Using mechanically controllable gold nano-electrodes, the zero-bias conductance can be monitorized while stretching the electrodes. Experiments on Fe^{II}, show that an increment in conductance is observed while the electrodes are stretched, that increment

can reach 2 orders of magnitude. The same procedure a Ru^{II} ion, for which a SCO transition is not expected to occur, an increase in conductance versus stretching is obtained but on average it is smaller than the obtained for the Fe^{II} case. The comparison between the two metal centers suggests that small conductance increases can be induced by stretching these molecules independently from the central atom type but that the inclusion of the SCO-active Fe^{II} ion gives larger and more frequent conductance increases.

6.5. CONCLUSIONS

In summary, we have studied transport through mechanically switchable Fe^{II} spin crossover molecules. Using DFT calculations that indicate that the SCO transition can be triggered by pulling on the terminal sulfur atoms of the Fe^{II} complex and that the high-spin state, energetically more favorable in the stretched molecule, has a larger zero-bias conductance than the low-spin state.

REFERENCES

[1] R. Frisenda, G. D. Harzmann, J. A. Celis Gil, J. M. Thijssen, M. Mayor, and H. S. J. van der Zant, *Stretching-induced conductance increase in a spin-crossover molecule,* Nano Letters **16**, 4733 (2016), pMID: 27088578, http://dx.doi.org/10.1021/acs.nanolett.5b04899 .

[2] A. S. Lukas and M. R. Wasielewski, *Approaches to a molecular switch using photoinduced electron and energy transfer,* in *Molecular Switches* (Wiley-VCH Verlag GmbH, 2001) pp. 1–35.

[3] N. Weibel, S. Grunder, and M. Mayor, *Functional molecules in electronic circuits,* Org. Biomol. Chem. **5**, 2343 (2007).

[4] S. J. van der Molen and P. Liljeroth, *Charge transport through molecular switches,* J. Phys.: Condens. Matter **22**, 133001 (2010).

[5] L. Sun, Y. A. Diaz-Fernandez, T. A. Gschneidtner, F. Westerlund, S. Lara-Avila, and K. Moth-Poulsen, *Single-molecule electronics: from chemical design to functional devices,* Chem. Soc. Rev. **43**, 7378 (2014).

[6] M. Irie, *Diarylethenes for memories and switches,* Chemical Reviews **100**, 1685 (2000), pMID: 11777416, http://dx.doi.org/10.1021/cr980069d .

[7] B.-Y. Choi, S.-J. Kahng, S. Kim, H. Kim, H. W. Kim, Y. J. Song, J. Ihm, and Y. Kuk, *Conformational molecular switch of the azobenzene molecule: A scanning tunneling microscopy study,* Phys. Rev. Lett. **96**, 156106 (2006).

[8] N. Henningsen, K. J. Franke, I. F. Torrente, G. Schulze, B. Priewisch, K. Rck-Braun, J. Doki, T. Klamroth, P. Saalfrank, and J. I. Pascual, *Inducing the rotation of a single phenyl ring with tunneling electrons,* The Journal of Physical Chemistry C **111**, 14843 (2007), http://dx.doi.org/10.1021/jp0741861 .

[9] E. S. Tam, J. J. Parks, W. W. Shum, Y.-W. Zhong, M. B. Santiago-Berros, X. Zheng, W. Yang, G. K.-L. Chan, H. D. Abrua, and D. C. Ralph, *Single-molecule conductance of pyridine-terminated dithienylethene switch molecules,* ACS Nano **5**, 5115 (2011), pMID: 21574612, http://dx.doi.org/10.1021/nn201199b .

[10] Y. Kim, T. J. Hellmuth, D. Sysoiev, F. Pauly, T. Pietsch, J. Wolf, A. Erbe, T. Huhn, U. Groth, U. E. Steiner, and E. Scheer, *Charge transport characteristics of diarylethene photoswitching single-molecule junctions,* Nano Letters **12**, 3736 (2012), pMID: 22734823, http://dx.doi.org/10.1021/nl3015523 .

[11] J. Hwang, M. Pototschnig, R. Lettow, G. Zumofen, A. Renn, S. Gotzinger, and V. Sandoghdar, *A single-molecule optical transistor,* Nature **460**, 76 (2009).

[12] S. Lara-Avila, A. V. Danilov, S. E. Kubatkin, S. L. Broman, C. R. Parker, and M. B. Nielsen, *Light-triggered conductance switching in single-molecule dihydroazulene/vinylheptafulvene junctions,* The Journal of Physical Chemistry C **115**, 18372 (2011), http://dx.doi.org/10.1021/jp205638b .

[13] S. Y. Quek, M. Kamenetska, M. L. Steigerwald, H. J. Choi, S. G. Louie, M. S. Hybertsen, N. B., and VenkataramanLatha, *Mechanically controlled binary conductance switching of a single-molecule junction,* Nat Nano **4**, 230 (2009).

[14] Y. Kim, H. Song, F. Strigl, H.-F. Pernau, T. Lee, and E. Scheer, *Conductance and vibrational states of single-molecule junctions controlled by mechanical stretching and material variation,* Phys. Rev. Lett. **106**, 196804 (2011).

[15] J. S. Meisner, M. Kamenetska, M. Krikorian, M. L. Steigerwald, L. Venkataraman, and C. Nuckolls, *A single-molecule potentiometer,* Nano Letters **11**, 1575 (2011), pMID: 21413779, http://dx.doi.org/10.1021/nl104411f .

[16] C. Bruot, J. Hihath, and N. Tao, *Mechanically controlled molecular orbital alignment in single molecule junctions,* Nat. Nano **7**, 35 (2012).

[17] N. Darwish, I. Dez-Prez, S. Guo, N. Tao, J. J. Gooding, and M. N. Paddon-Row, *Single molecular switches: Electrochemical gating of a single anthraquinone-based norbornylogous bridge molecule,* The Journal of Physical Chemistry C **116**, 21093 (2012), http://dx.doi.org/10.1021/jp3066458 .

[18] M. Baghernejad, X. Zhao, K. Barul rns, M. Feg, P. Moreno-Garca, A. V. Rudnev, V. Kaliginedi, S. Vesztergom, C. Huang, W. Hong, P. Broekmann, T. Wandlowski, K. S. Thygesen, and M. R. Bryce, *Electrochemical control of single-molecule conductance by fermi-level tuning and conjugation switching,* Journal of the American Chemical Society **136**, 17922 (2014), pMID: 25494539, http://dx.doi.org/10.1021/ja510335z .

[19] X. H. Qiu, G. V. Nazin, and W. Ho, *Mechanisms of reversible conformational transitions in a single molecule,* Phys. Rev. Lett. **93**, 196806 (2004).

[20] P. Liljeroth, J. Repp, and G. Meyer, *Current-induced hydrogen tautomerization and conductance switching of naphthalocyanine molecules,* Science **317**, 1203 (2007), http://science.sciencemag.org/content/317/5842/1203.full.pdf .

[21] L. Cambi and L. Szeg, *ber die magnetische susceptibilitt der komplexen verbindungen,* Berichte der deutschen chemischen Gesellschaft (A and B Series) **64**, 2591 (1931).

[22] P. Gtlich, *Spin crossover quo vadis?* European Journal of Inorganic Chemistry **2013**, 581 (2013).

[23] E. Ruiz, *Charge transport properties of spin crossover systems,* Phys. Chem. Chem. Phys. **16**, 14 (2014).

[24] T. Miyamachi, M. Gruber, V. Davesne, M. Bowen, S. Boukari, L. Joly, F. Scheurer, G. Rogez, T. K. Yamada, P. Ohresser, E. Beaurepaire, and W. Wulfhekel, Nat. Commun. **3**, 938 (2012).

[25] T. G. Gopakumar, F. Matino, H. Naggert, A. Bannwarth, F. Tuczek, and R. Berndt, *Electron-induced spin crossover of single molecules in a bilayer on gold,* Angewandte Chemie International Edition **51**, 6262 (2012).

[26] G. D. Harzmann, R. Frisenda, H. S. J. van der Zant, and M. Mayor, *Single-molecule spin switch based on voltage-triggered distortion of the coordination sphere,* Angewandte Chemie International Edition **54**, 13425 (2015).

[27] P. Gütlich, A. B. Gaspar, and Y. Garcia, *Spin state switching in iron coordination compounds,* Beilstein Journal of Organic Chemistry **9**, 342 (2013).

[28] D. Aravena and E. Ruiz, J. Am. Chem. Soc. **134**, 777 (2012).

[29] H. Hakkinen, *The gold-sulfur interface at the nanoscale,* Nat Chem **4**, 443 (2012).

[30] W. Haiss, C. Wang, I. Grace, A. S. Batsanov, D. J. Schiffrin, S. J. Higgins, M. R. Bryce, C. J. Lambert, and R. Nichols, J. Nat. Mater. **5**, 995 (2006).

[31] R. Frisenda, S. Tarkuc, E. Galan, M. L. Perrin, R. Eelkema, F. C. Grozema, H. S. J. van der Zant, and J. Beilstein, Nanotechnol. **6**, 1558 (2015).

[32] M. Gruber, V. Davesne, M. Bowen, S. Boukari, E. Beaurepaire, W. Wulfhekel, and T. Miyamachi, Phys. Rev. B: Condens. Matter Mater. Phys. **89**, 195415 (2014).

[33] D. Q. Andrews, R. Cohen, R. P. V. Duyne, and M. A. Ratner, *Single molecule electron transport junctions: Charging and geometric effects on conductance,* J. Chem. Phys. **125**, 174718 (2006).

[34] M. Kamenetska, M. Koentopp, A. C. Whalley, Y. S. Park, M. L. Steigerwald, C. Nuckolls, M. S. Hybertsen, and L. Venkataraman, *Formation and evolution of single-molecule junctions,* Phys. Rev. Lett. **102**, 126803 (2009).

[35] G. C. Solomon, D. Q. Andrews, R. P. V. Duyne, and M. A. Ratner, *Electron transport through conjugated molecules: When the pi system only tells part of the story,* ChemPhysChem **10**, 257 (2009).

[36] L. Venkataraman, J. E. Klare, C. Nuckolls, M. S. Hybertsen, and M. L. Steigerwald, *Dependence of single-molecule junction conductance on molecular conformation,* Nature **442**, 904 (2006).

[37] S. Woitellier, J. P. Launay, and C. Joachim, Chem. Phys. **131**, 481 (1989).

7

SWITCHABLE RECTIFICATION OF RUTHENIUM-COMPLEX MOLECULAR JUNCTIONS

Hope, it is the quintessential human delusion,
simultaneously the source of your greatest strength,
and your greatest weakness.

The Architect
The matrix reloaded, Dir. L. Wachowski, Lil. Wachowski, CA: Warner Home Video, 2003

We investigate electronic transport trough a molecular device that combines rectification with switchability. We show that the current-voltage characteristics change from symmetric to asymmetric if the relative humidity of the surrounding is increased. We discuss this change, which is fully reversible within a coherent transport model by using two weakly coupled sites.

Parts of this chapter will be published in Nat. Nano.

7.1. INTRODUCTION

The molecular diode was the initial proposal that started the revolution of functional single-molecule devices [1]. The idea of this new device was based on the semi-conducting pn-junctions. As one side of the molecule was electron rich and the other electron poor, the current is favored in one direction above the other. Since that proposal, other theoretical predictions and models have been developed based on other mechanisms, such as asymmetric tunneling barriers[2, 3] or asymmetric charging [4].

Experimentally, rectification ratios (current ratio between the forward and reverse bias) as high as 100 have been reported in measurements on self-assembled monolayers(SAM) [5]. In this chapter, we present a model to describe the large rectification ratio measured in Leiden University laboratories on di-nuclear Ru-complex molecules. Together with that, we present an explanation for the switchability that the device presents depending on the humidity, that is, resistor for dry conditions and rectifier for humid conditions.

Our model is based on orbital resonances and demonstrates that this mechanism leads to rectification for this kind of systems. Using density functional theory (DFT) and the non-equilibrium Greens function (NEGF) formalism, we investigate how the presence of water molecules affects the system and why these trigger the rectification for certain Ru-complexes. Finally, we demonstrate that in order to achieve this rectification, a two site structure is essential.

7.2. EXPERIMENTAL SETUP

Recent measurements done by Atesci et. al., in a monolayer of di-nuclear Ru-complex molecules, have shown results that combine rectification with switchability. The current-voltage (I-V) characteristics changes from symmetric (resistor) to asymmetric (diode) if the relative humidity of the surrounding atmosphere is increased. In fact, the rectification ratio (RR) increases from near-unity, in 5% humidity, to 1000 in 50% humidity. This change was proved to be fully reversible.

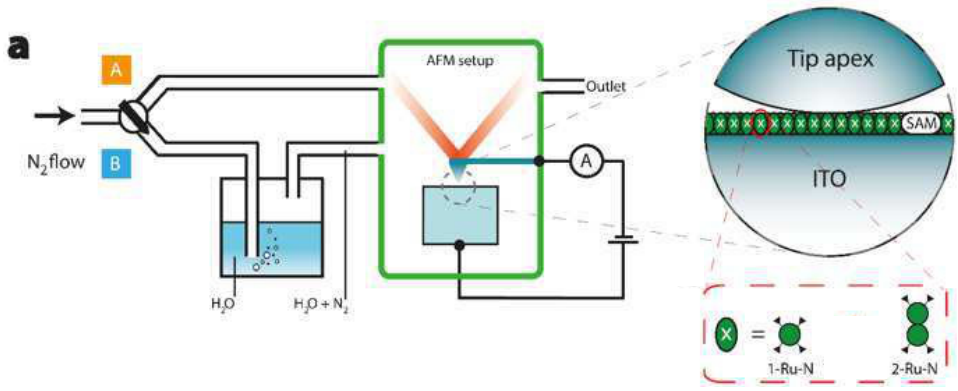

Figure 7.1: Schematic representation of the experimental setup and molecular systems studied.

Experimentally, a conductive-probe atomic force microscopy (C-AFM) [6–8] was employed to measure I-V characteristics of self-assembled monolayers (SAMs) of two types of Ru-complexes on indium-tin-oxide (ITO) (see Fig 7.1). The mono-nuclear 1-Ru-N and di-nuclear 2-Ru-N molecules contain tetrapodal phosphonic acid anchoring groups, symmetric on both sides, as can be seen in the Figure 7.2.

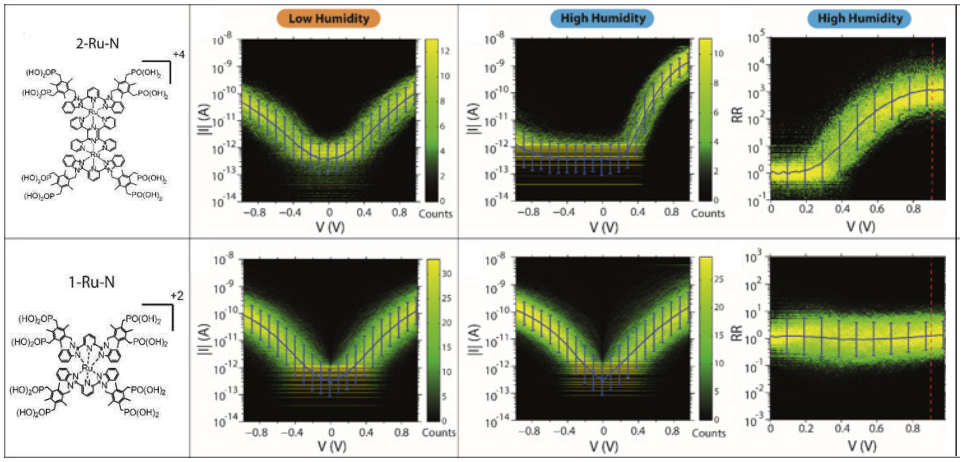

Figure 7.2: First column) Molecular structures and their charge of the Ru-complexes used in the experiments. Second column) I-V characteristics of the molecular junctions in low humidity conditions (5%). Third column) I-V characteristics and rectification ratio of the molecular junctions in high humidity conditions (60%).

On 2-Ru-N, humidity has a remarkable effect. The I-V characteristics recorded in dry conditions are nearly symmetric, while the high-humidity curves shows a diode-like behavior. Moreover, this remarkable effect is fully reversible. By the other side, 1-Ru-N shows I-V characteristics that does not change significantly between high and low humidity, and is nearly symmetric.

7.3. CALCULATIONS AND ANALYSIS

The fact that the 2-Ru complexes give rise to humidity-induced rectification, whereas the 1-Ru do not, establishes that something inherent to the molecule causes this change. We propose a two-site structure for transport mechanism to describe this increment in rectification.

Quantum chemistry calculations for the mono-nuclear Ru complex (1-Ru-N) show a significant energy difference between the HOMO and the orbitals below. This suggest that the HOMO is the main responsible for transport, which means, that a single level model would be sufficient to describe the I-V characteristics of this complex. By the other side, calculations for the gas-phase 2-Ru complex, show that the highest occupied molecular orbital (HOMO) and the orbital below it, the HOMO-1 show an anti-symmetric and symmetric structure respectively; moreover, these orbitals are nearly degenerate. Subtracting or adding these orbitals results into nearly localized molecular orbitals (LMO's), one centered around the ruthenium near the tip, and the other near the

substrate side. These LMO's define the two-site structure - for the molecule in gas phase, the two sites have approximately the same chemical potential - this is the so-called resonance condition.

Applying a voltage across the molecule, the chemical potentials of these two orbitals shift apart. Due to this breakdown of the resonance condition, the current drops. Such a drop was observed by Perrin et. al. [9] for a two-site di-hydro-anthracene molecule. This mechanism is represented in Figure 7.3 (upper panels).

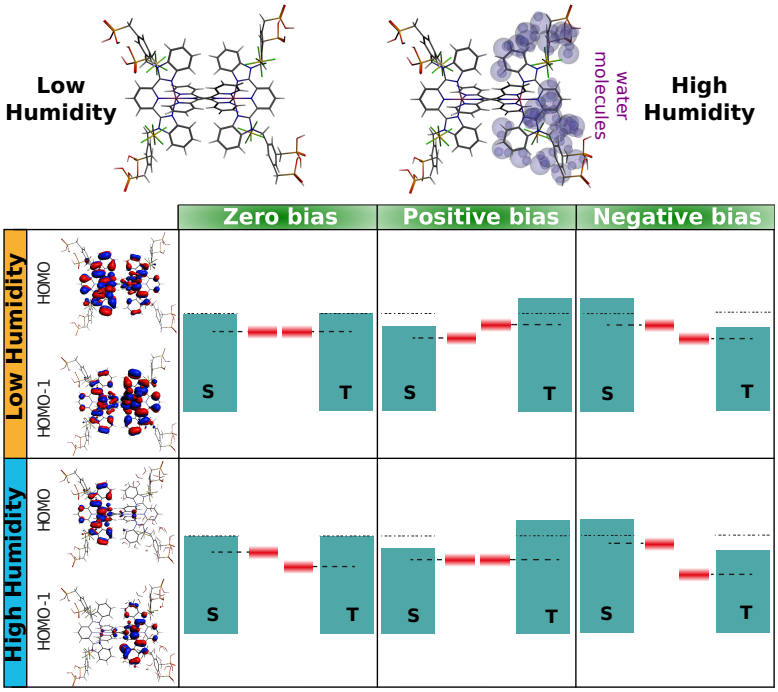

Figure 7.3: 2Ru-N complex in Dry conditions and Humid conditions. In the presence of an asymmetric water distribution, the HOMO and HOMO-1 are more strongly localized on the substrate side and tip side Ru centers respectively. Illustration of a two-level system between substrate and tip electrodes in dry conditions: The two LMOs are aligned at zero bias, which does not result in rectification as the current is equally suppressed for negative and positive bias. In humid conditions: the substrate side LMO has a relatively higher chemical potential compared to the tip counterpart due to an asymmetric gating effect caused by the displacement of the counter ions and the dipole effect by the water molecules. This results in rectification, due to current suppression when the levels are misaligned at negative bias, and relatively high current when, due to a positive bias, the levels come close to resonance.

For a rectifier, the symmetry between the two sites must be broken [10]. Indeed, we anticipate that the tip electrode will attract more water molecules than the surface, due to its enhanced capillarity. To find out how an enhanced water concentration on the tip side, affects the electrostatics, we have performed detailed quantum calculations of the ruthenium complex, including the phosphonic acid end groups, together with the counter-ions and 28 water molecules at the tip side. The calculations were performed using the Amsterdam Density Functional (ADF) [11, 12]; see 7.5.

The mere presence of the water shifts the chemical potential of the LMO located near the tip relative to that of the other LMO. The near-resonance condition of the two LMO's is then broken, and the transmission is therefore low. This situation is represented in Fig. 7.3 (second row, left figure).

The bias voltage was realized in the calculation by applying a homogeneous electric field directed along the tip-surface axis. For each field intensity and for several initial conformations of the 28 water molecules, a geometric optimization was performed. The calculations systematically show the same trend: for a positive bias (i.e. the substrate potential is lower than the tip potential), the counter ions move away from the tip towards the center of the molecule [13]. This changes the electrostatic environment of the LMO near the tip, moving its chemical potential towards (away from) that of the LMO near the surface for a positive (negative) bias. As a consequence, the current increases (decreases) for positive (negative) bias. This trend then explains the rectification observed upon introducing humidity – see the middle and right figure on the second row of figure 7.3.

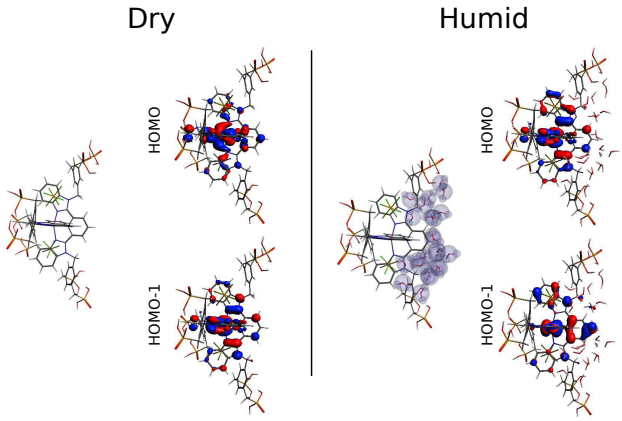

Figure 7.4: DFT-calculated distributions of the HOMO and HOMO-1 for the 1-Ru-N molecule (a) without and (b) with water molecules.

Taking into account these definitions for the location of the water molecules and the electrodes in Figure 7.3, we perform DFT calculations for the 1-Ru-N complex in dry and humid conditions, getting as a result that humidity has a limited effect on the number of energy levels that are involved in electronic transport.

To substantiate this analysis, we have performed transport calculations using the non-equilibrium Green's function method as implemented into ADF. To this end, the geometrically optimized molecules were coupled to wide band limit (WBL) electrodes, and the conductance for 110 bias voltages ranging from -1.1 to 1.1 Volts applied across the two electrodes, the current was calculated, both for dry (0 water molecules) and for humid (28 water molecules) conditions, for both the 1-Ru and 2-Ru complexes. The results are shown in Fig. 7.5. We see that for the 2-Ru-N, upon introduction of water molecules, rectification takes place, whereas this is absent in dry conditions. Also, for the 1-Ru-N, there is no rectification, in humid nor in dry condition, in line with the experimental

observations. A competing mechanism, which has been invoked successfully to explain rectification in [14, 15], is based purely on the difference in capacities to the leads induced by the water (in that experiment, an ionic solution was used). The result is that the transport level (which does not necessarily possess a composite two-site structure) is pinned near the Fermi energy of the nearest electrode. In our case, this would lead to a rectification in both the 1-Ru and 2-Ru complexes. The fact that this was not observed experimentally suggests that in our experiment, the two-site structure is essential [10].

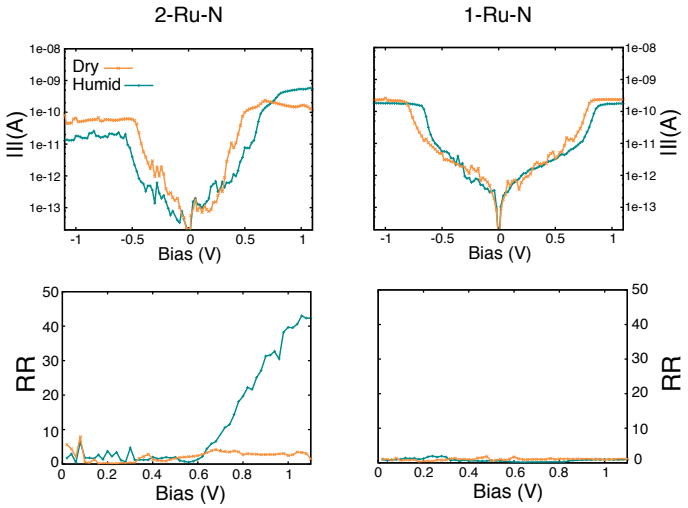

Figure 7.5: Current (Top) and RR (Bottom) calculated for the 2-Ru-N (left) and the 1-Ru-N (right) complex with and without water. In the latter case, energy splitting of the LMOs leads to asymmetric I-Vs, as in Fig. 5 indicates. See also Computational details under Methods for more details.

Although DFT calculations for transport not always give accurate predictions for the current levels, they can be used to reproduce experimental trends. In our calculations, we have included only 28 water molecules due to hardware restrictions, and there are many different conformations possible for these. However, for two independent starting conformations, we have observed very similar motion for the counter-ions upon applying a bias voltage. We emphasize that a dynamical treatment, in which the water molecules and the counter-ions are allowed to move in order to find their relaxed positions for every applied field, is essential for explaining the experimental results (See Fig. 7.6b)).

For the 2Ru-N complex in humid conditions, the electrostatic interaction between the water molecules and the counter ions induces a displacement in the latter. Figure 7.6a) shows the distance between the ions at the tip side and Ru Center as a function of the magnitude of an external electric field orientated along the X-axis. Comparing the Ru-ions distance at zero external electric field in dry conditions with the distance for humid conditions, it is clear that due to the presence of the water molecules, the ions are displaced from their original position. This displacement which is close to 0.25 Å removes the degeneracy between the HOMO and HOMO-1 giving rise to the rectification seen in Figure 7.5.

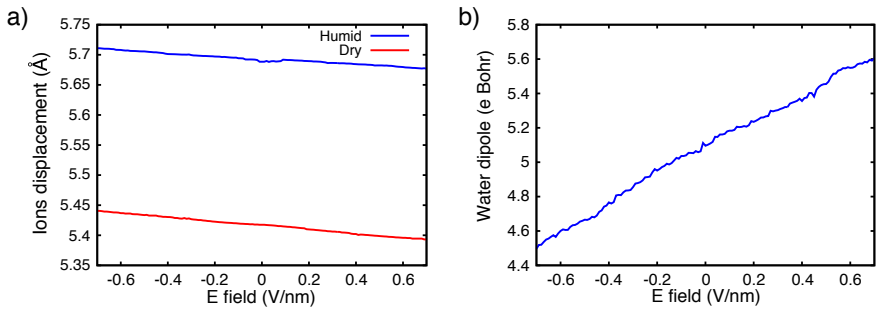

Figure 7.6: a) Ion displacement as a function of the external electric field in dry and humid conditions. It can be seen that for humid conditions and zero external electric field, the ions are already displaced with respect their positions at dry conditions. b) Total dipole moment of the water molecules as a function of the external electric field.

The displacement of the ions at the tip side in the presence of water removes the degeneracy between the LMO's. In order to disentangle the effect of the mere displacement of the counter ions, and that of the water molecules being present, we have analyzed how the LMO's change with the displacement of the counter ions, with the water molecules removed from the system.

In Figure 7.7, we show how the main orbitals involved in transport change upon moving ions away from the Ru centers along the axis connecting these centers. It can be seen that for an ion displacement of 0.5 Å, the HOMO and HOMO-1 orbitals are not degenerate, which leads to a significant rectification. Furthermore, for $d = 1.0$ Å there are many energy levels in between the left LMO and the right LMO.

Using NEGF we perform transport calculations for ten different ions-Ru distances between 0.0 Å and 1.0 Å. In Figure 7.10, we show the current and the rectification for the three distances used in figure 7.7 in the absence of water.

A detailed analysis of the rectification ratio calculated at 1 V as a function of the ion displacement shows that the maximum rectification is close to 40 and it is achieved at 0.6 Å, for distances larger than 0.6 Å the rectification decays because the energy difference between the left LMO and right LMO requires higher voltages to achieve a sizable current (See Figure 7.9). In addition, some orbitals localized on the ions or the phosphonic acids with energies in between the two LMOs start influencing the conductance properties (See Figure 7.7 **c)**).

Including the water molecules (humid conditions), the calculations can be performed in two different ways. The first one is shown in Figure 7.10, which consist in freezing the positions of the water molecules and the counter ions for all magnitudes of the external electric field (static), and the second one which is shown in Figure 7.5 of the main text, where the positions of the counter ions and the water molecules are updated for every applied electric field (dynamic).

It is clear that the dynamic model shows an enhancement in the rectification as this is supposed to be closer to the experimental situation.

Finally, we analyze the temperature dependence of the 2-Ru-N complex conductance. For this, we use the results obtained from our quantum chemistry calculations

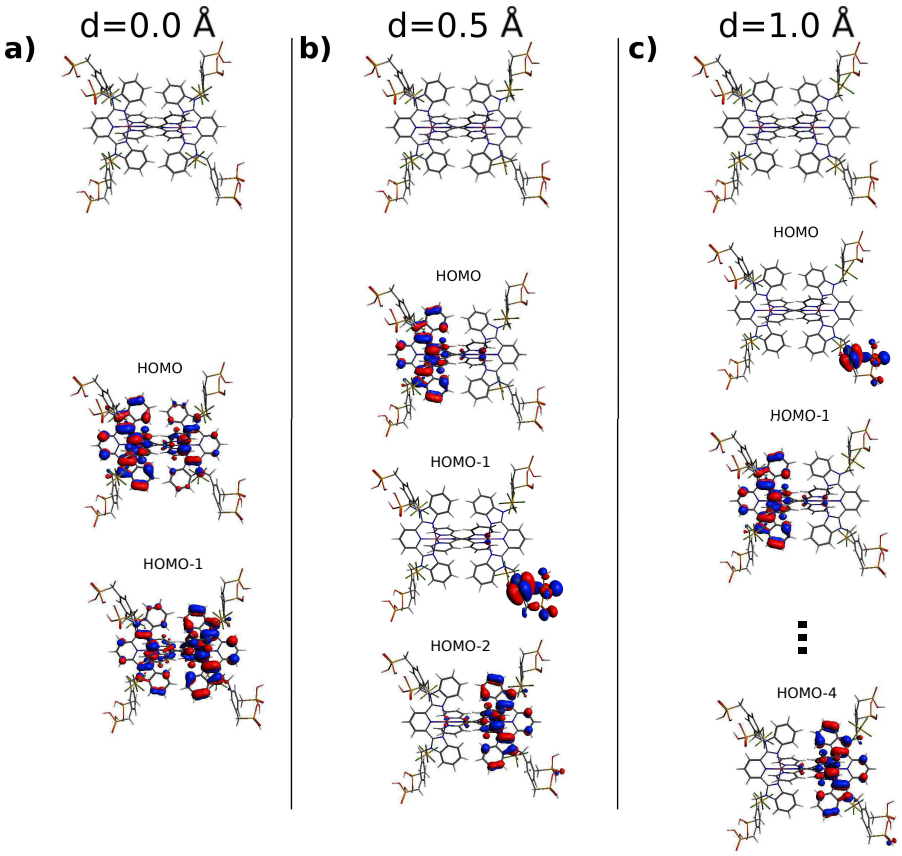

Figure 7.7: Comparison of the molecular orbitals of the 2Ru-N complex when the counter ions at the right side of the system are displaced a distance. **a)** 0.0 Å. **b)** 0.5 Å. **c)** 1.0 Å. These calculations were performed without considering water molecules. It is clear that when the counter ions are displaced, the HOMO and HOMO-1 energy levels are not degenerated anymore.

in dry conditions and the values normally used in the experiments. We have considered a two site model where the energy levels are positioned at an energy E_0, with respect to the chemical potential of the electrodes at V=0, with a broadening $\Gamma = \Gamma_R + \Gamma_L$, where $\Gamma_{R(L)}$ is the tunnel rate to the right (left) electrode. In this model the temperature is included by mean of the Fermi distribution function [16].

Figure 7.11 shows the results of the calculated current as a function of the inverse of the temperature at different bias voltages normalized to E_0. At low temperatures, the current is temperature-independent. As the temperature increases, the tails of the Fermi distributions of the electrochemical potentials start to overlap with the energy levels increasing exponentially with temperature.

Figure 7.11, right panel, shows how the conductance depends on the temperature for a two-site system, within a range between 285 K and 357 K for two different bias voltages 0.3 V and 0.6 V. As it can be seen, the conductance decays with the inverse of

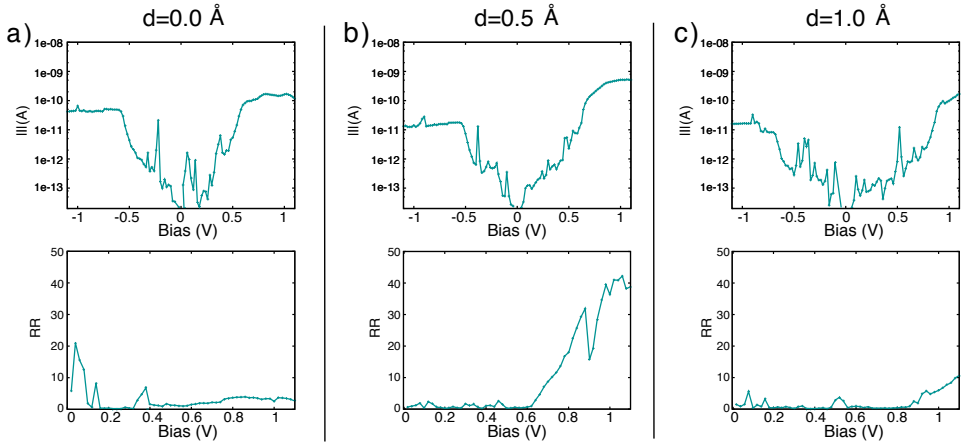

Figure 7.8: Comparison between the current and the rectification ratio calculated when the counter ions at the right side of the system are displaced a distance. **a)** 0.0 Å. **b)** 0.5 Å. **c)** 1.0 Å.

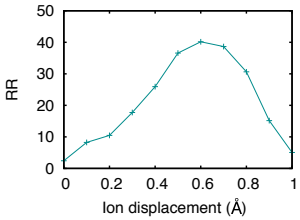

Figure 7.9: Rectification ratio as a function of the ions displacement calculated for a bias equal to 1.0 V. It can be seen how the rectification increases and achieve a maximum at 0.6 Å.

the temperature. This result support to the two-site model used for the 2-Ru-N, although it does not reproduce completely the magnitude of the experimental results, it explains in good agreement the trend

7.4. CONCLUSIONS

In summary, we have studied transport through switchable Ru complex rectifier. Using DFT calculations we show that the system behaves according to the two site model where the humidity introduces asymmetries to the system leading to rectification. Although modeling is challenging due to the complex composition of the system, a coherent tunneling picture with two LMOs in series is consistent with our experimental data. The highly sensitive 2-Ru-N SAMs offer new possibilities as nanoscale sensors or, vice versa, as smooth electrical switches, controlled by non-invasive parameters.

7.5. COMPUTATIONAL DETAILS

We use GGA (PBE) functional with a DZ-basis of atomic orbitals for the H, C and N atoms and DZP-basis of atomic orbitals for the Ru atoms. We adjust the Ru-complex

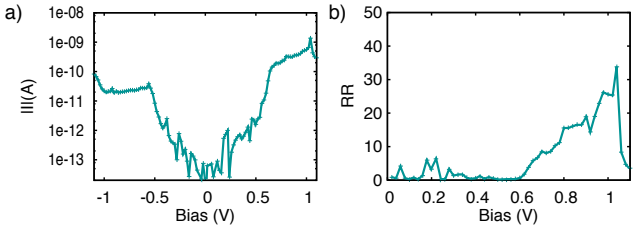

Figure 7.10: **a)** Electric current and **b)** rectification ratio as a function of the bias voltage for the 2Ru-N complex in humid conditions using a static model where the counter ions and the water molecules position are fixed during all the calculation. We use the Ions and water positions used in figure 7.5 at zero external electric field.

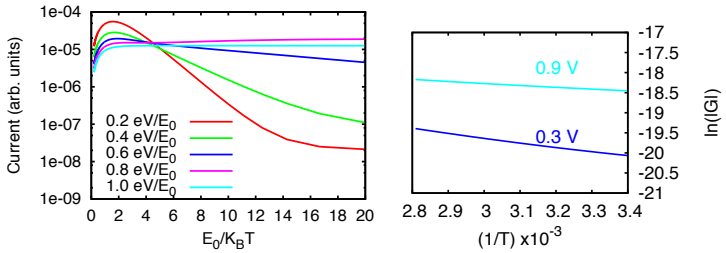

Figure 7.11: (left) Calculated current as a function of the inverse temperature for five different bias voltages for a broadening $\Gamma = 0.002E_0$. (right) Conductance calculated for a two-site model as a function of the inverse of the temperature.

7

energy levels using the scissors operator and the image charges correction [17, 18]. For the transport calculation we have considered the wide band limit (WBL). To simulate the solvent, we include explicit water molecules that were previously relaxed using the QMMM method within ADF [19]. We apply a bias voltage to the system by introducing an external uniform electric filed along the x-axis. Knowing the length of the Ru complexes it is possible to calculate the voltage. We perform geometry optimizations upon varying the magnitude of the external electric field. With our NEGF code, which reads the output files of the system, we calculate the transmission for every magnitude of the electric field. The electric current is calculated by using the Landauer formula.

REFERENCES

[1] A. Aviram and M. A. Ratner, *Molecular rectifiers,* Chem. Phys. Lett. **29**, 277 (1974).

[2] P. Kornilovitch, A. Bratkovsky, and R. Stanley Williams, *Current rectification by molecules with asymmetric tunneling barriers,* Phys. Rev. B **66**, 165436 (2002).

[3] J. Taylor, M. Brandbyge, and K. Stokbro, *Theory of rectification in tour wires: The role of electrode coupling,* Phys. Rev. Lett. **89**, 138301 (2002).

[4] M. Paulsson, F. Zahid, and S. Datta, *Handbook of nanoscience, engineering and technology,* (CRC Press, 2003) Chap. Resistance of a Molecule.

[5] C. A. Nijhuis, W. F. Reus, and G. M. Whitesides, *Molecular rectification in metalsam-metal oxidemetal junctions,* Journal of the American Chemical Society **131**, 17814 (2009), pMID: 19928851, http://dx.doi.org/10.1021/ja9048898 .

[6] C. M. Guedon, H. Valkenier, T. Markussen, K. S. Thygesen, J. C. Hummelen, and S. J. van der Molen, *Observation of quantum interference in molecular charge transport,* Nat Nano **7**, 305 (2012).

[7] D. J. Wold and C. D. Frisbie, *Fabrication and characterization of metal-moleculemetal junctions by conducting probe atomic force microscopy,* Journal of the American Chemical Society **123**, 5549 (2001), pMID: 11389638, http://dx.doi.org/10.1021/ja0101532 .

[8] S. Ho Choi, B. Kim, and C. D. Frisbie, *Electrical resistance of long conjugated molecular wires,* Science **320**, 1482 (2008), http://science.sciencemag.org/content/320/5882/1482.full.pdf .

[9] M. L. Perrin, R. Frisenda, M. Koole, J. S. Seldenthuis, J. A. Celis Gil, H. Valkenier, J. C. Hummelen, N. Renaud, F. C. Grozema, J. M. Thijssen, D. Dulić, and van der ZantHerre S. J., *Large negative differential conductance in single-molecule break junctions,* Nat Nano **9**, 830 (2014).

[10] M. L. Perrin, E. Galan, R. Eelkema, F. Grozema, J. M. Thijssen, and H. S. J. van der Zant, *Single-molecule resonant tunneling diode,* The Journal of Physical Chemistry C **119**, 5697 (2015), http://dx.doi.org/10.1021/jp512803s .

[11] G. te Velde, F. Bickelhaupt, S. van Gisbergen, C. Fonseca Guerra, E. Baerends, J. Snijders, and T. Ziegler, *Chemistry with ADF,* J. Comput. Chem. **22**, 931 (2001).

[12] C. Fonseca Guerra, J. G. Snijders, G. te Velde, and E. J. Baerends, *Towards an order-n dft method,* Theoretical Chemistry Accounts **99**, 391 (1998).

[13] V. Kaliginedi, H. Ozawa, A. Kuzume, S. Maharajan, I. V. Pobelov, N. H. Kwon, M. Mohos, P. Broekmann, K. M. Fromm, M.-a. Haga, and T. Wandlowski, *Layer-by-layer grown scalable redox-active ruthenium-based molecular multilayer thin films for electrochemical applications and beyond,* Nanoscale **7**, 17685 (2015).

[14] L. Yuan, R. Breuer, L. Jiang, M. Schmittel, and C. A. Nijhuis, *A molecular diode with a statistically robust rectification ratio of three orders of magnitude,* Nano Letters **15**, 5506 (2015), pMID: 26196854, http://dx.doi.org/10.1021/acs.nanolett.5b02014 .

[15] K. Cheung, X. Chen, T. Albrecht, and A. Kornyshev, *Principles of a single-molecule rectifier in electrolytic environment,* JOURNAL OF PHYSICAL CHEMISTRY C **120**, 3089 (2016).

[16] M. Poot, E. Osorio, K. O'Neill, J. M. Thijssen, D. Vanmaekelbergh, C. A. van Walree, L. W. Jenneskens, and H. S. J. van der Zant, *Temperature dependence of three-terminal molecular junctions with sulfur end-functionalized tercyclohexylidenes,* Nano Letters **6**, 1031 (2006), http://dx.doi.org/10.1021/nl0604513 .

[17] S. Quek, L. Venkataraman, H. Choi, S. Louie, M. Hybertsen, and J. Neaton, *Amine–gold linked single-molecule circuits: Experiment and theory,* Nano Lett. **11**, 3477 (2007).

[18] D. J. Mowbray, G. Jones, and K. S. Thygesen, *Influence of functional groups on charge transport in molecular junctions,* J. Chem. Phys. **128**, 111103 (2008).

[19] C. C. Pye, T. Ziegler, E. L. van Lenthe, and J. N. Louwen, *An implementation of the conductor-like screening model of solvation within the amsterdam density functional package — part ii. cosmo for real solvents,* Canadian Journal of Chemistry **87**, 790 (2009), http://dx.doi.org/10.1139/V09-008 .

ACKNOWLEDGEMENTS

This research was carried out with financial support from the Dutch Foundation for Fundamental Research on Matter (NWO FOM).

With respect to the professional aspect, I would like to thank Chris Verzijl, Riccardo Frisenda, Mickael Perrin, Diana Dulic, Husein Atesci, Sense Jan van der Molen, Herre van der Zant and Jos Thijssen for the interesting discussions and fruitful collaborations which lead to each of the papers which have come out of this work, of which we are co-authors.

I would like to thank SCM group for the useful software that you have developed all these years. Thanks Stan for the support and the fruitful talks about the releases year after year. I am particularly indebted to Pier Philipsen and Mirko Franchini, main developers of BAND software implementation for their assistance and guidance. Without their expertise the implementation work of the small functions that I developed would not be successful.

With respect to my personal life, there are many people who I would like to thank. To start Jos, thank you for offering me to do this PhD. I also want to thank you for this opportunity to learn, you taught me a lot about science, cooking, wines and how to prepare a good espresso.

When I started my PhD. in Delft, I arrived to a place where I did not know anybody but everybody was friendly and helpful. The first person that I met was Marcin, we shared office for a few moths, he graduated shortly after I arrived. He looked to be a serious man, but he was a very kind and polite person. Anton, Michael, Yaroslav and Yuli, members of the theory group, thanks to your projects, I met my nice friends. Sebastian, since the beginning we both know that play football with a tennis ball was not easy, trying to do 21 repetitions without letting the ball drop was a difficult goal, but as far as I remember we completed 10 repetitions, which is not a bad number. Joao thanks for teaching me expressions and words in Portuguese, it is a beautiful and complex language "Vou praticar por conta própria". Adriaanje, it was amazing to share office with you, we talk about everything sports, places, jobs, plans, etc., you are great listening, I still have problems to pronounce your last name, but I am practicing. Tómas, Doru, Pablo, Vincent, Bas, Vigdis I do not forget about you, it was nice to share with you the coffee, the lunch and the talks.

Rafal and Albert, thank you for these years, you have been nice friends, I wish you both the best in your life. Thank you for being with me the day of my wedding. When we started we made a promise, that we will try 100 different beer brands during the PhD., the Klooster and the Beepbop were really helpful. I have to be honest, Rafal is in another level, maybe he already tried 500 (maybe more) and he does not need a list (my list is at the end of this book). Albert, talking with you about latin music, dance, and daily life made feel in home.

To the MED group, thanks for the ideas, the discussions and the collaborations. Julien, Anastasia, Riccardo, Ignacio, Mathijs, Mickael, Max, Rocco, Davide, Diana and Herre. You gave me the opportunity to take a close view to the experiments and see how the devices behave in real life. With you I finally understood that the cow is not spheric.

I would like to express my sincerest appreciation to J. van der Maesen and J.de Boer for the fun, instructive and challenging chats we have had over the past few years.

To my friends and family in Colombia, I am so sorry if I did not talk to you very frequently, I never forget about you. Remember you gave me strength to continue every day.

There is a person who I want show how special she is for me, she is my support and my strength, Carmen, you are my Carmenitalbasauria, my bear and my love, you listened to me when I had doubts and you talked to me when I had no words, I am too realistic and talking with you always brings me to dream, thanks for stand my disorder and being with me.

A mis queridos mamasitalbasauria, taitasaurio y motalbasaurio, no me alcanzan las palabras para agradecerles, todo se lo debo a ustedes, todos los pasos que por pequeños o grandes que sean han sido guiados por sus enseñanzas. No puedo expresar lo afortunado que soy por haber nacido en el seno de esta familia. Mami, yo se que su merced me mira desde allá, gracias por sus oraciones, un picote y un abrazote. Este trabajo es para ustedes, no ha habido día en estos cuatro años en el que no los piense, esto es lo poquito que puedo dar para demostrarles cuanto los quiero.

Table 7.1: Beers list

- Hobgoblin
- Aname
- Grolsh
- Amstel
- Palm
- Latrape
- Krombacher
- Jupiler
- Westmalle
- Gouden Carolus
- hourlong chouffe
- pilsener
- desperados
- becks
- Schnoor Bräu (Bremen)
- Wicküler
- Bavaria
- St. Feuillien (rossa)
- Komes (poland)
- Brand
- Leffe
- Wieckse (rosé)
- Kasteel
- Hoegaarden Rosée
- Guinness
- Cobra India
- Paulaner
- SanBernardos
- De Blauwe Ijsbeer
- MagicStoneDog
- Brouwerij de Molen
- Alfa
- Grimberger
- Emelisse
- BBC
- Shorts Brewing Co.
- American Nitro Porter, Gonzo's Biggdogg Brewing (Kalamazoo, MI)
- Dos Equis
- Dragon's Milk. New Holland brewing
- Bitburger premium Pills
- schelde Brouwerij
- goldstar (Israel)
- De Klok
- De koninck
- Judas
- Brugse zot
- Holtland
- Warsteiner
- San Miguel
- Texel
- Brewdog
- Egils Pilsner
- Jillz
- Edelweiss
- Kwak
- Steenbrugge
- Rodenbach rosso
- Brugge
- Boon kriek
- Westvleteren
- Augustijn
- Klokke Roeland
- Celis White
- Zeezuiper
- Kolibrie
- Framboise Boon
- Jopen Adriaan wit
- Maneblusserk
- Leidsch Bier
- Neptunus bier
- De Koperen Kat
- Formidabel
- Spierkracht tripel
- Bier-Biére Export
- Vedett
- Maredsous Abbaye-Abdij
- Monteith's Southern pale ale New Zealand
- Dag & Dauw (Bergamot IPA)
- Budels pils
- Holger
- Birra Moretti
- Picon Biére
- Kanterbrãu
- Stella Artois
- LöwenWeisse Hefe-Weissbier
- Thornbridge Squatters pale ale
- London pride ale fullers
- lieffmans
- Fix Dark (griek)
- Seef Bier
- Piraat
- Hopus
- Troubadour MAGMA
- Brouwerij't IJ Zatte
- Ayinger, Bräuweisse Bayerisches bier
- Thai Thai (Oedipus)
- Urthel (Hop-It)
- Ciney blonde (cuvée)
- Hertog Jan
- Tempelier
- Gajes (leiden)
- Floreffe
- Niksicko (Montenegro)
- Löwenbräu

CURRICULUM VITÆ

Jose Arturo CELIS GIL

12-11-1985 Born in Bogotá, Colombia.

EDUCATION

1997–2002 Secondary School
Instituto San Bernardo de la Salle, Bogotá

2003–2008 Bachelor in Physics
Universidad Nacional de Colombia
Thesis: Molecular Dynamics of composed particles
Promotor: Dr. F. Fonseca
Cum Laude

2009–2011 Master in Sciences Physics
Universidad Nacional de Colombia
Thesis: Shot noise in superconducting systems
Promotor: Dr. William J. Herrera

2013–2017 PhD. Applied Physics
Delft University of Technology, The Neterlands
Thesis: Modeling level alignment at interfaces in molecular junctions.
Promotor: Prof. dr. ir. H.S.J. van der Zant
co-Promotor: Dr. J. M. Thijssen

LIST OF PUBLICATIONS

10. Huseyin Atesci, Veerabhadrarao Kaliginedi, **J. A. Celis Gil**, Hiroaki Ozawa, Joseph M. Thijssen, Peter Broekmann, Masa-aki Haga, Sense Jan van der Molen, *Humidity-sensitive properties of ruthenium complex molecular junctions*, In preparation for submission

9. J. van der Maesen, **J. A. Celis Gil**, Joseph M. Thijssen, *Hybrid functionals for transport calculations in single molecule junctions using DFT-NEGF*, In preparation for submission

8. Huseyin Atesci, Veerabhadrarao Kaliginedi, **J. A. Celis Gil**, Hiroaki Ozawa, Joseph M. Thijssen, Peter Broekmann, Masa-aki Haga, Sense Jan van der Molen, *Humidity-controlled rectification of ruthenium-complex molecular junctions*, Accepted for publication in Nature Nanotechnology

7. **J. A. Celis Gil**, J.M. Thijssen, *Transport gap renormalization at a metal-molecule interface using DFT-NEGF and spin unrestricted calculations*, The Journal of Chemical Physics **147**, 084102 (2017)

6. **J. A. Celis Gil**, S. Gomez P., William J. Herrera, *Noise cross-correlation and Cooper pair splitting efficiency in multi-terminal superconductor junctions*, Solid State Communications **258**, 25-32 (2017).

5. R. Frisenda, G. D. Harzmann, **J. A. Celis Gil**, J. M. Thijssen, M. Mayor, H. S. J. van der Zant, *Stretching-induced conductance increase in a spin-crossover molecule*, Nano Letters **16**, 4733 (2016).

4. C. J. O. Verzijl, **J. A. Celis Gil**, M. L. Perrin, D. Dulic , H. S. J. van der Zant, J. M. Thijssen, *Image effects in transport at metal-molecule interfaces*, The Journal of Chemical Physics **143**, 174106 (2015).

3. M. L. Perrin, R. Frisenda, M. Koole, J. S. Sendenthuis, **J. A. Celis Gil**, H. Valkenier, J. C. Hummelen, N. Reaud, F. C. Grozema, J. M. Thijssen, D. Dulic, H. S. J. van der Zant, *Large negative differential conductance in single-molecule break junctions*, Nature Nanotechnology **9**, 830 (2014).

2. **J. A. Celis G**, William J. Herrera, *Shot noise in HTc superconductor quantum point contact system*, Physica B: Condensed Matter **16**, 3081 (2012).

1. **J. A. Celis**, C. A. Martinez Barbosa, R. A. Casas, *Computation of initial conditions for a thin disc as an extension of Dehnen Algorithm*, RevMex AA **40**, 113 (2011).